



# Meteorological Model Performance for Annual 2022 Simulation WRF v4.4.2



EPA-454/R-24-001

March 2024

Meteorological Model Performance for Annual 2022 Simulation WRF v4.4.2

U.S. Environmental Protection Agency  
Office of Air Quality Planning and Standards  
Air Quality Assessment Division  
Research Triangle Park, NC

## **1. INTRODUCTION**

The Weather Research and Forecasting model (WRF) was applied for the entire year of 2022 to generate meteorological data to support emissions and photochemical modeling applications for the base and future years of the 2022 Modeling Platform. The WRF meteorological fields will be converted to air quality modeling input data and used to support assessments of ozone, PM2.5, visibility, and a variety of toxics.

The WRF model was applied to both the 36- and 12-km continental United States (36NOAM & 12US, respectively) scale domains, initialized directly from meteorological analysis data. Model parameterizations and options outlined in this document were chosen based on a series of sensitivity runs performed by U.S. Environmental Protection Agency (USEPA) Office of Research and Development that provided an optimal configuration based on temperature, mixing ratio, and wind field. All WRF simulations were done by General Dynamics Information Technology (GDIT) under contract to the USEPA.

## **2. MODEL CONFIGURATION**

Version 4.4.2 of the WRF model, Advanced Research WRF (ARW) core (Skamarock, 2008) was used for generating the 2022 simulation. Selected physics options include Pleim-Xiu land surface model, Asymmetric Convective Model version 2 planetary boundary layer scheme, Kain-Fritsch cumulus parameterization utilizing the moisture-advection trigger (Ma and Tan, 2009), Morrison double moment microphysics, and RRTMG longwave and shortwave radiation schemes (Gilliam and Pleim, 2010).

The 36-km North American domain (36NOAM) WRF model simulation was initialized using the 0.25-degree Global Forecast System (GFS) analysis and the 3-hour forecast from the 00Z, 06Z, 12Z, and 18Z simulations. The 12-km United States (12US) WRF model was initialized using the 12km North American Model (12NAM) analysis product provided by National Climatic Data Center (NCDC). Where 12NAM data were unavailable, the 40km Eta Data Assimilation System (EDAS) analysis (ds609.2) from the National Center for Atmospheric Research (NCAR) was used. Analysis nudging for temperature, wind, and moisture was applied above the boundary layer only. The model simulations were conducted continuously. The 'ipxwrf' program was used to initialize deep soil moisture at the start of the run using a 10-day spinup period (Gilliam and Pleim, 2010). Landuse and land cover data were based on the United States Geological Survey (USGS) for the 36NOAM simulation and the 2011 National Land Cover Database (NLCD 2011)<sup>1</sup>.

---

<sup>1</sup> The 2011 version of the NLCD is the most up-to-date landuse data that has been processed from satellite information and WRF-ready at the time these simulations were conducted.

Sea surface temperatures were ingested from the Group for High Resolution Sea Surface Temperatures (GHR SST) (Stammer et al., 2003) 1km SST data.

Additionally, lightning data assimilation was utilized in the 12US simulation to suppress (force) deep convection where lightning is absent (present) in observational data. This method is described by Heath et al. (2016) and was employed to help improve precipitation estimates generated by the model.

Figures 2.1 and 2.2 show the 36NOAM and 12US domain, which utilized a Lambert conformal projection centered at (-97,40) with true latitudes of 33 and 45 degrees north. The 36NOAM domain contains 184 cells in the X direction and 160 cells in the Y direction. The 12US domain contains 412 cells in the X direction and 372 cells in the Y direction. The atmosphere is resolved with 35 vertical layers up to 50 mb (see table 2.1), with the thinnest layers being nearest the surface to better resolve the planetary boundary layer (PBL).

<b>WRF Layer</b>	<b>Height (m)</b>	<b>Pressure (mb)</b>	<b>Sigma</b>
35	17,556	50.0	0.000
34	14,780	97.5	0.050
33	12,822	145.0	0.100
32	11,282	192.5	0.150
31	10,002	240.0	0.200
30	8,901	287.5	0.250
29	7,932	335.0	0.300
28	7,064	382.5	0.350
27	6,275	430.0	0.400
26	5,553	477.5	0.450
25	4,885	525.0	0.500
24	4,264	572.5	0.550
23	3,683	620.0	0.600
22	3,136	667.5	0.650
21	2,619	715.0	0.700
20	2,226	753.0	0.740
19	1,941	781.5	0.770
18	1,665	810.0	0.800
17	1,485	829.0	0.820
16	1,308	848.0	0.840
15	1,134	867.0	0.860
14	964	886.0	0.880
13	797	905.0	0.900
12	714	914.5	0.910
11	632	924.0	0.920
10	551	933.0	0.930
9	470	943.0	0.940
8	390	952.5	0.950
7	311	962.0	0.960

6	232	971.5	0.970
5	154	981.0	0.980
4	115	985.75	0.985
3	77	990.5	0.990
2	38	995.25	0.995
1	19	997.63	0.9975
Surface	0	1000.0	1.000

**Table 2.1** WRF layers and their approximate height above ground level along with their respective sigma and pressure levels.

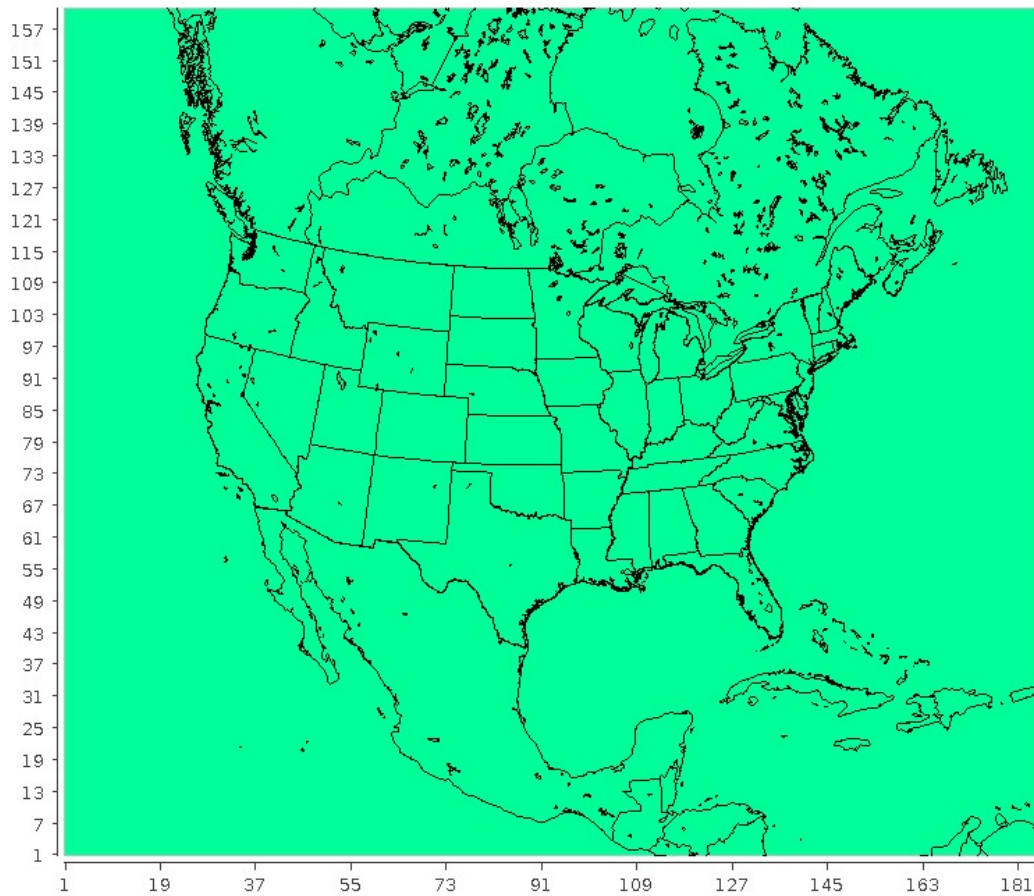


**Figure 2.1.** Map of the WRF model domain: 36NOAM.

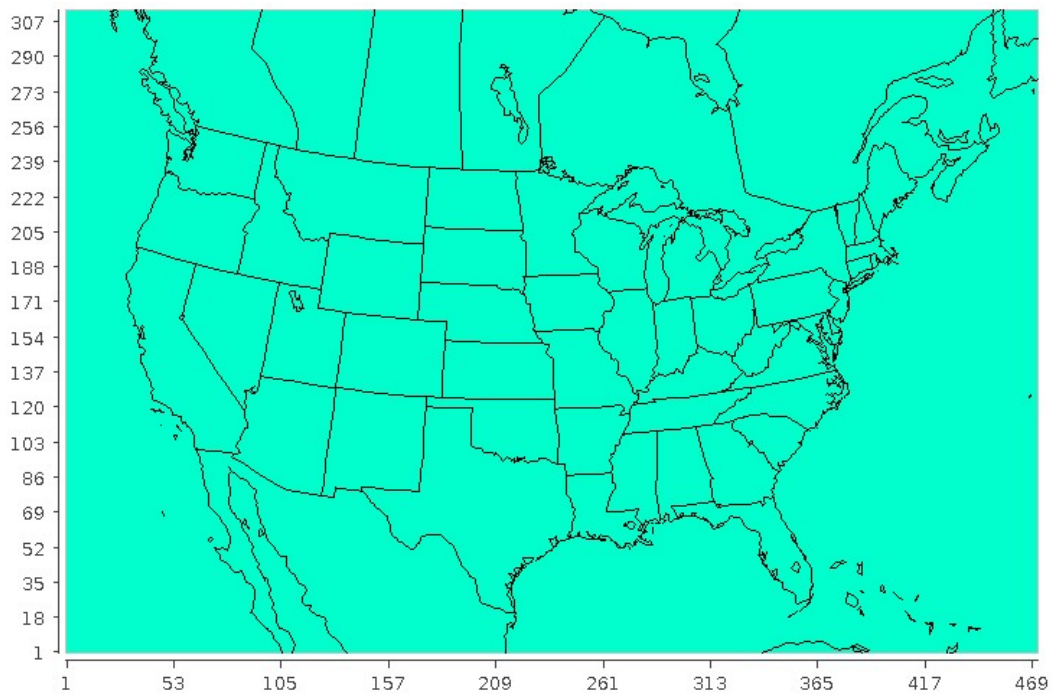


**Figure 2.2** Map of WRF model domain: 12US.

### **3 MODEL PERFORMANCE DESCRIPTION**

The WRF model simulations were evaluated to determine whether the output fields represent a reasonable representation of the actual meteorology that occurred during the modeling period. Identifying and quantifying these output fields allows for a downstream assessment of how the air quality modeling results are impacted by the meteorological data. For the purposes of this assessment, 2-meter temperature and mixing ratio, 10-meter wind speed and direction, and downward shortwave radiation at the surface are compared to the corresponding measured data. As described below, the evaluation of precipitation includes both a qualitative and quantitative comparison between measured and modeled data.

The observation database for surface-based temperature, wind speed and direction, and mixing ratio is based on measurements made at United States (i.e., National Weather Service) and Canadian (i.e., Environment Canada) airports. The observational dataset (ds472 network) is available from NCAR<sup>2</sup>. Monitors used for evaluation are shown in Figure 3.1.

---

<sup>2</sup> <https://rda.ucar.edu/datasets/ds472.0/>

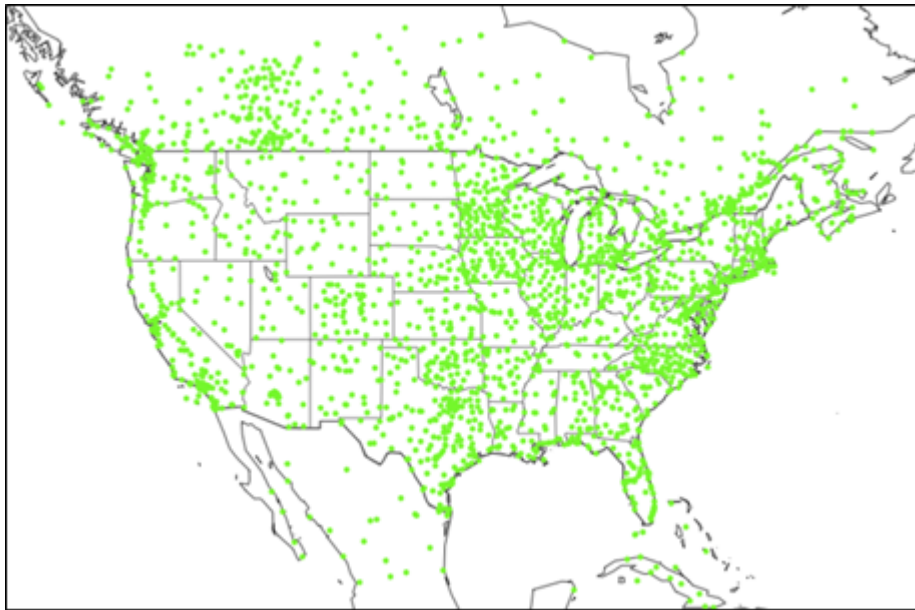


**Figure 3.1** Stations used for model performance: ds472 network.

Shortwave downward radiation measurements are taken at surface-based monitor locations and these data are obtained from the Baseline Surface Radiation Network (BSRN, <https://bsrn.awi.de/>). This network is global and a map of the locations used in this evaluation is shown below (see Figure 3.2).

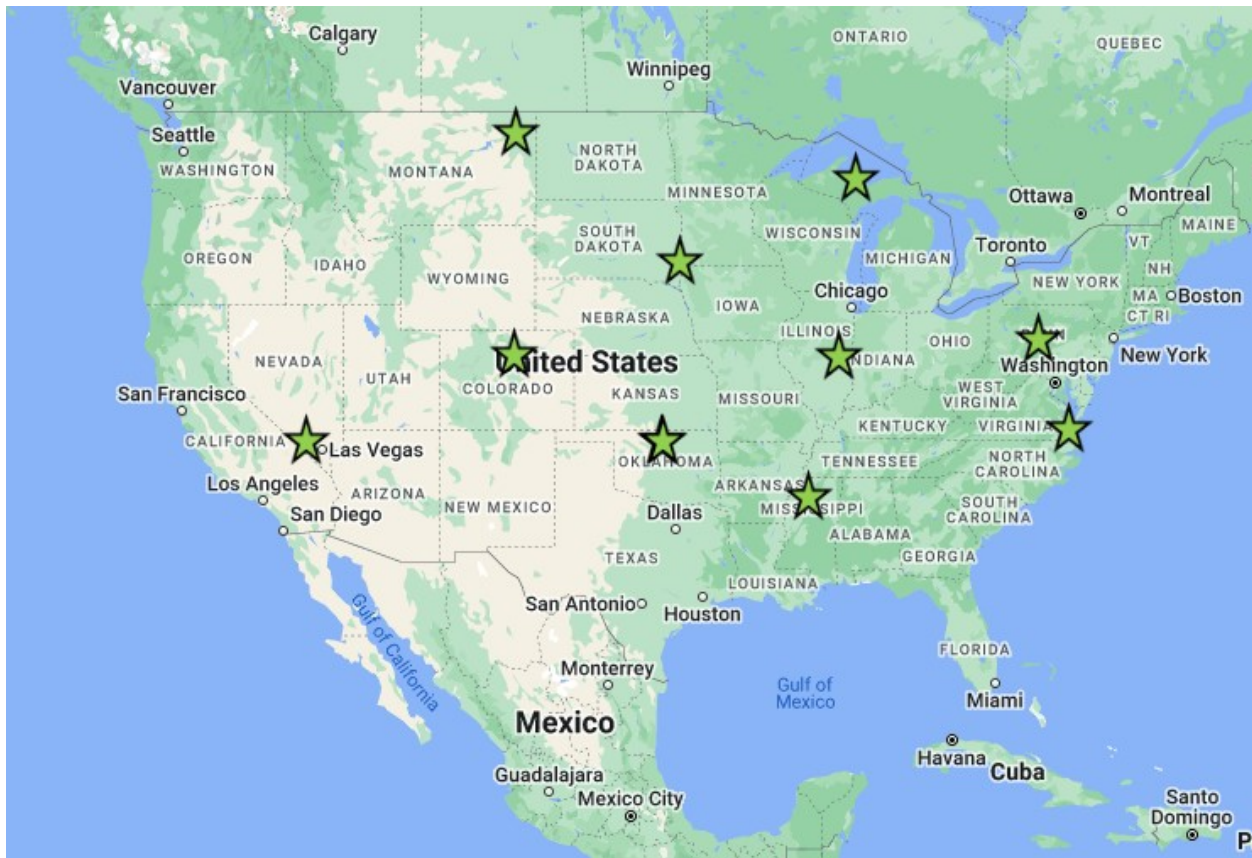


**Figure 3.2.** Location of radiation monitors.

Rainfall observations are estimated by the Parameter-elevation Relationships on Independent Slopes Model (PRISM) model<sup>3</sup>, which uses an elevation-based regression model to analyze precipitation. PRISM's horizontal resolution is approximately 2 to 4 km and is re-projected to the WRF modeling domain for direct comparison to model estimates. The rainfall analysis is limited to the contiguous United States as the model utilizes elevation and measured precipitation data at automated weather stations.

Model performance (for temperature, wind speed, and water vapor mixing ratio) is described using quantitative metrics: mean bias, mean (gross) error, fractional bias, and fractional error (Boylan and Russell, 2006). These metrics are useful because they quantify model performance in the units of the measured meteorological variable and as a normalized percentage. Since wind direction is reported in compass degrees, estimating performance metrics for wind direction is problematic as modeled and observed northerly winds may be similar but differences would result in a very large artificial bias. For example, the absolute difference in a northerly wind direction measured in compass degrees of 1° and 359° is 358° when the actual difference is only 2°. To address this issue, wind field displacement, or the difference in the U

<sup>3</sup> <https://prism.oregonstate.edu/>

and V vectors between modeled (M) and observed (O) values, is used to assess wind vector performance (Equation 1). Performance is best when these metrics approach 0.

$$(1) \quad \text{Wind displacement (km)} = (\mathbf{U}_M - \mathbf{U}_O + \mathbf{V}_M - \mathbf{V}_O) * (1 \text{ km}/1000 \text{ m}) * (3600 \text{ s}/\text{hr}) * (1 \text{ hr})$$

Rainfall performance is examined spatially using side-by-side comparisons of monthly total rainfall plots and statistically using monthly domain-wide biases. The WRF model outputs predictions approximately 15 meters above the surface while observations are at 10 meters. WRF generates output at near instantaneous values (90 second time step) as opposed to longer averaging times taken at monitor stations. This should be considered when interpreting model performance metrics.

### 3.1 Model Performance for Winds

WRF-predicted wind speed estimates are compared to surface-based measurements made in the ds472 network described earlier and shown below for the 36NOAM (Figure 3.1.1) and 12US (Figure 3.1.2) domains. Regional<sup>4</sup> analysis of statistical metrics for wind speed performance by quarter<sup>5</sup> is shown in Table 3.1.1 for the 12US domain only. Monthly spatial biases across all hours are shown for the 36NOAM (Figures 3.1.3-3.1.6) and 12US (Figures 3.1.7-3.1.10) domains. Monthly spatial biases across daytime hours only are shown for the 36NOAM (3.1.11-3.1.14) and 12US (3.1.15-3.1.18) domains. The hourly distribution of the observed and predicted wind speeds by each Climate Region and quarter is shown in Figure 3.1.19 for the 12US domain.

There is a noticeable overprediction of wind speeds in the eastern US across all hours and daytime hours only in both the 36NOAM and 12US simulations. That overprediction is coupled with a general underprediction of wind speeds in the western US, except in areas of exceedingly complex terrain (e.g., Rocky Mountains). There appears to be no significant difference when analyzing the biases during daytime hours or all hours of the day.

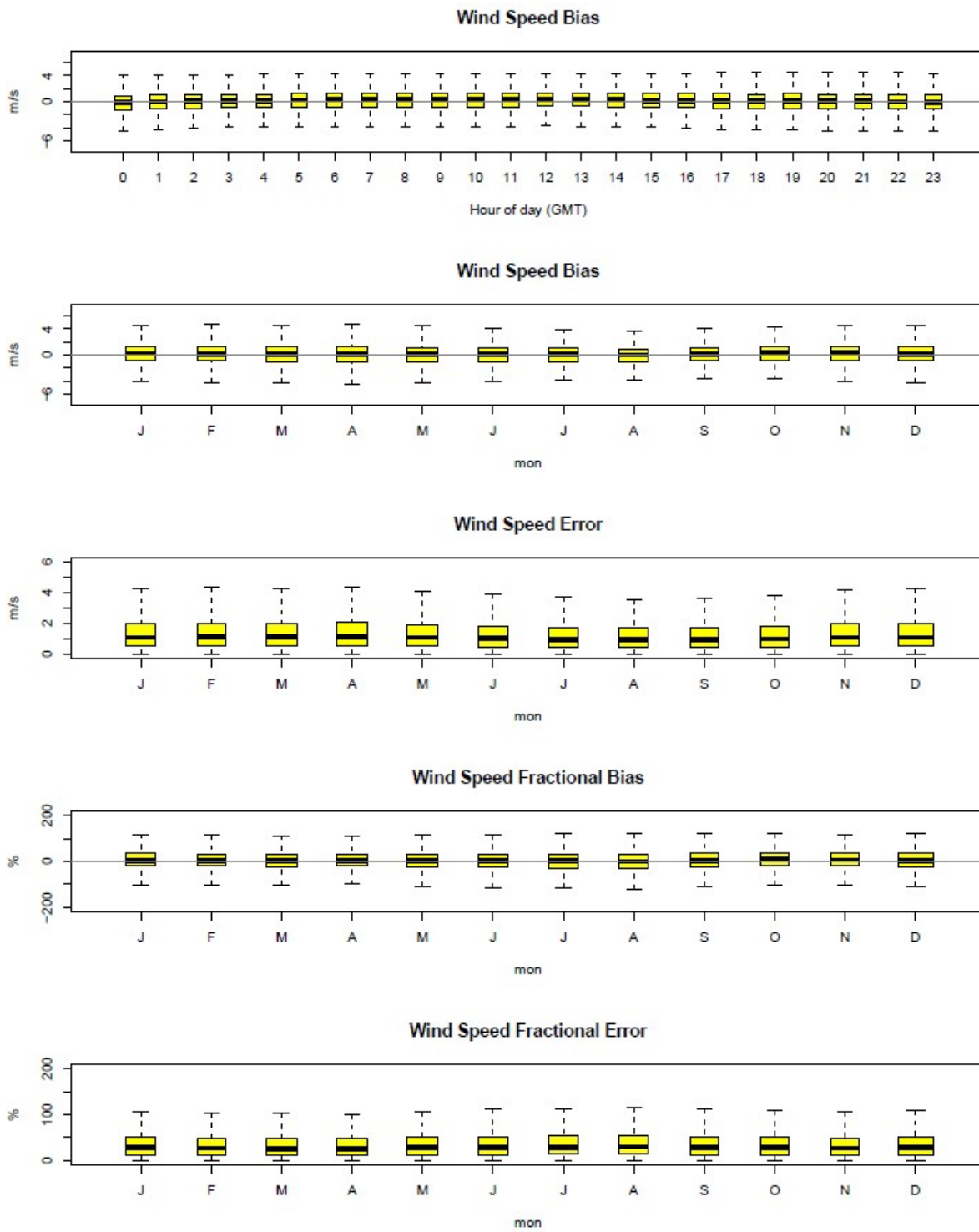
Statistically, the mean bias across most regions and seasons is generally within +/- 0.5 m/s. The underprediction in the western portions of the country noted above is less than -0.75 m/s on average across all hours of the year.

---

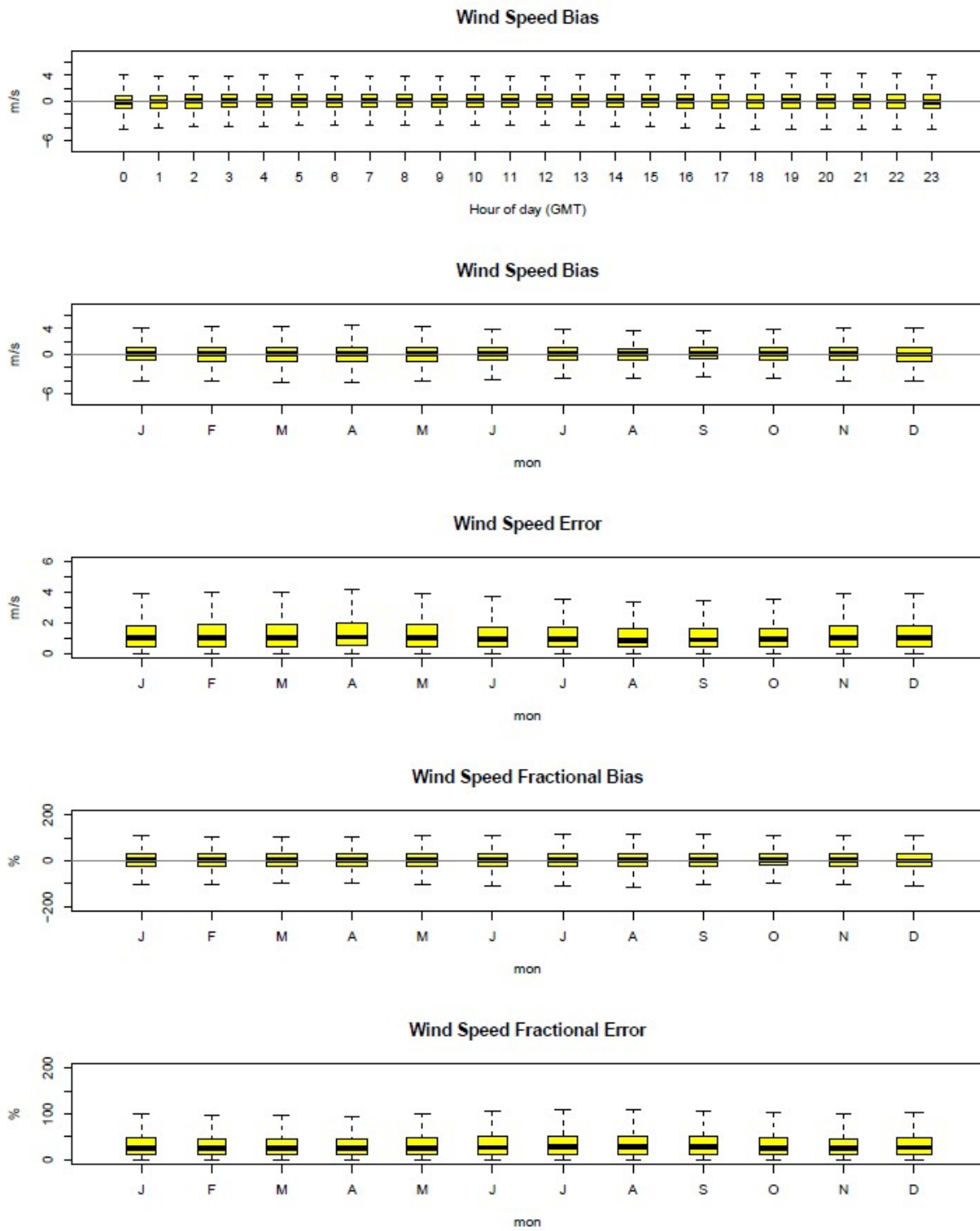
<sup>4</sup> Regions used are the NOAA Climate Regions outlined here:

<https://www.ncei.noaa.gov/access/monitoring/reference-maps/us-climate-regions>

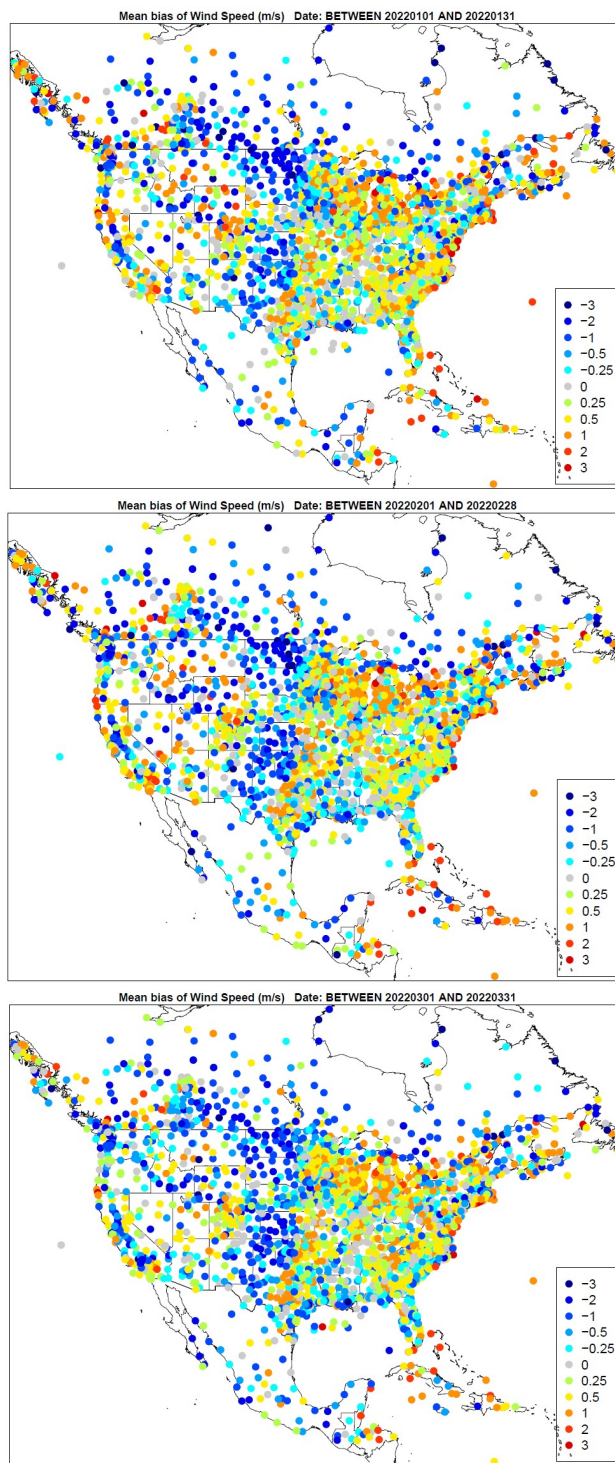
<sup>5</sup> Quarters are Q1 (January, February, March), Q2 (April, May, June), Q3 (July, August, September), and Q4 (October, November, December).



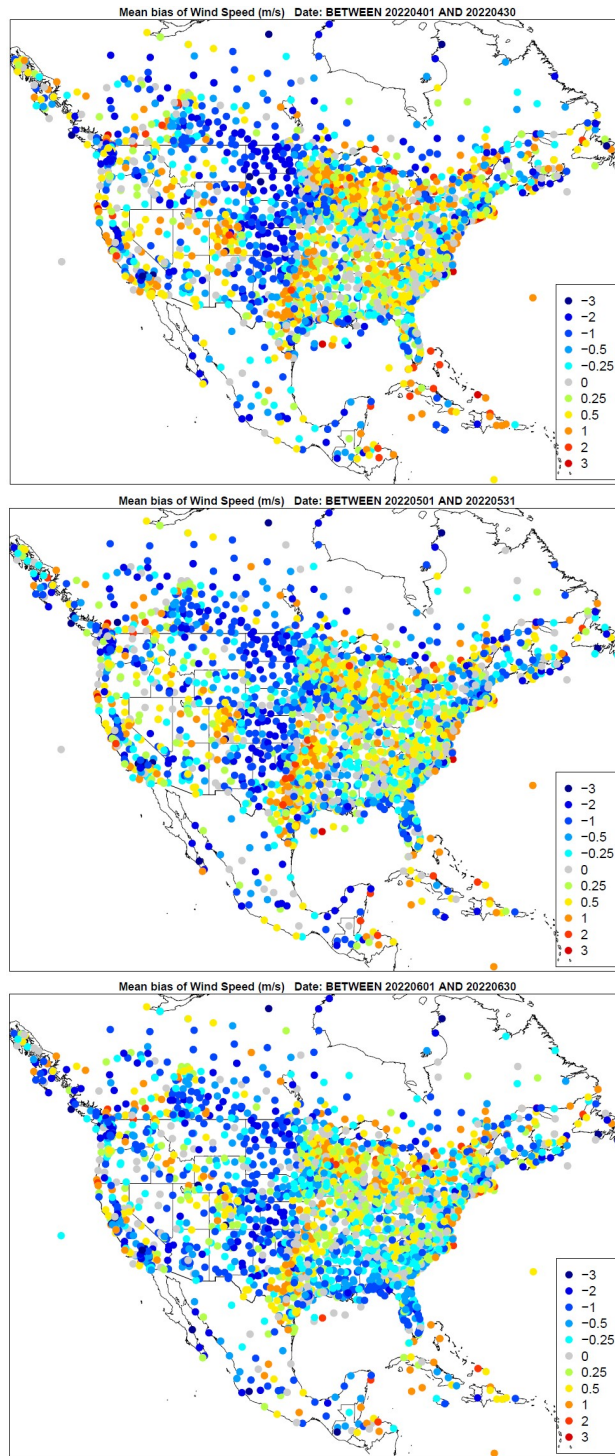
**Figure 3.1.1.** Distribution of hourly bias by hour and hourly bias, error, fractional bias, and fractional error for wind speed by month for 36NOAM domain.



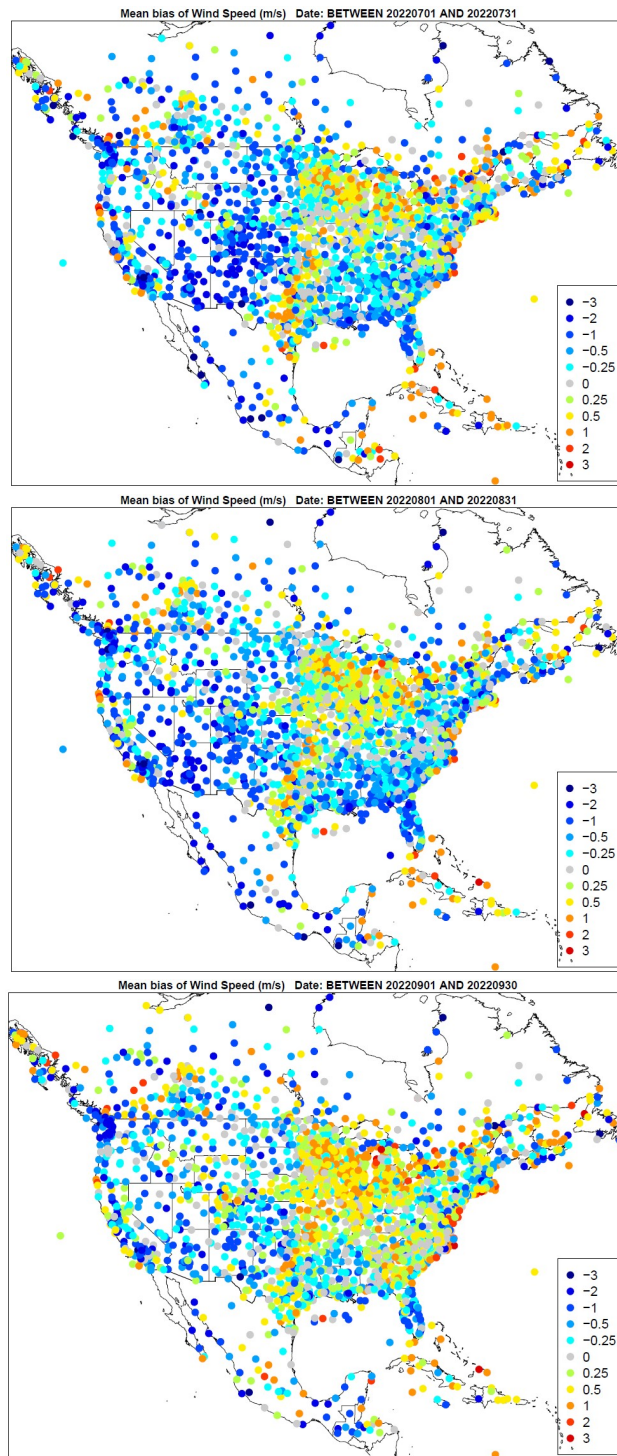
**Figure 3.1.2.** Distribution of hourly bias by hour and hourly bias, error, fractional bias, and fractional error for wind speed by month for 12US domain.



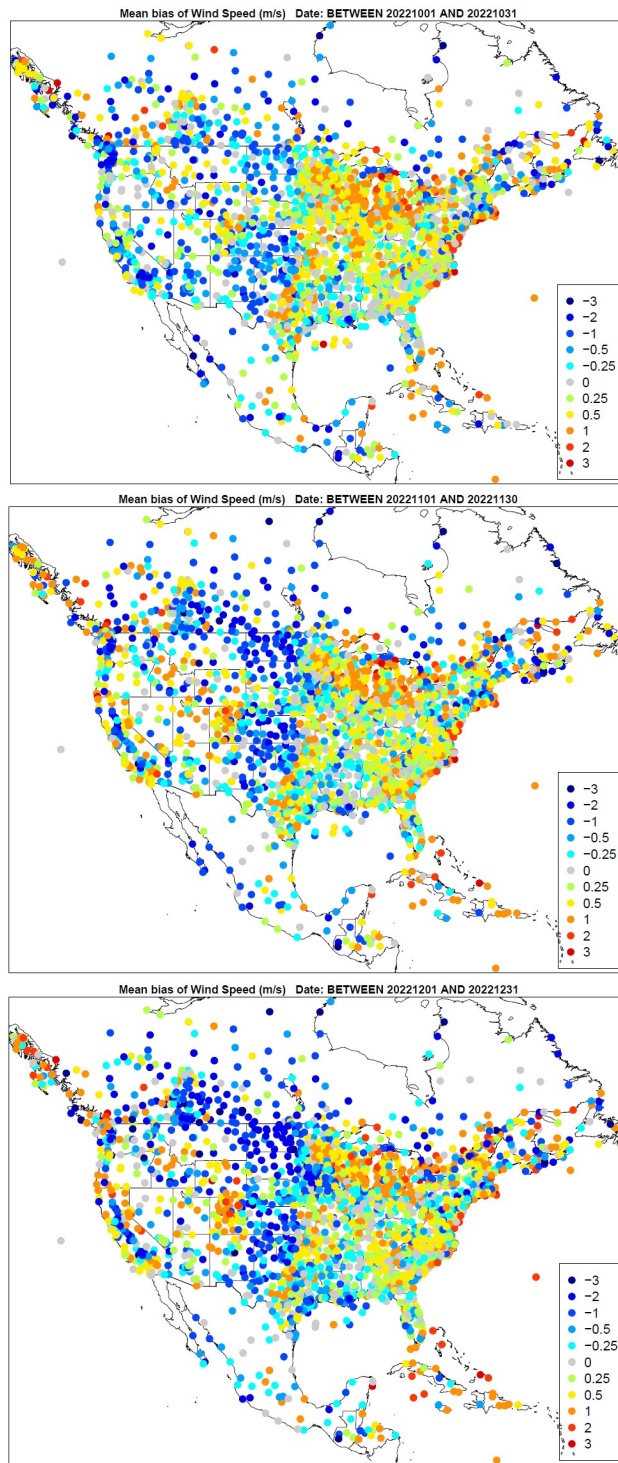
**Figure 3.1.3.** Spatial distribution of wind speed bias (m/s) across all hours for the months of January, February, and March (top to bottom) for the 36NOAM domain.



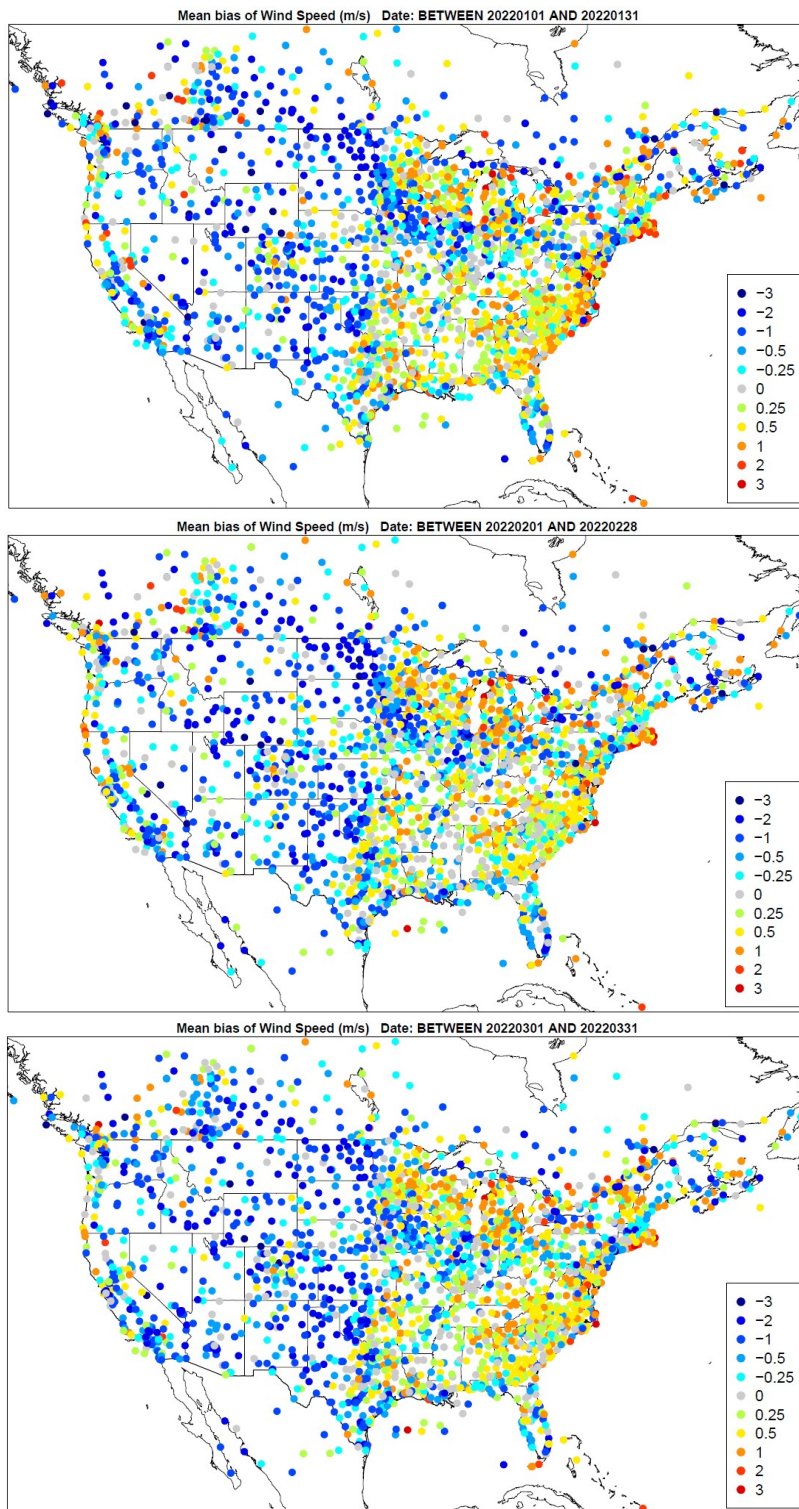
**Figure 3.1.4.** Spatial distribution of wind speed bias (m/s) across all hours for the months of April, May, and June (top to bottom) for the 36NOAM domain.



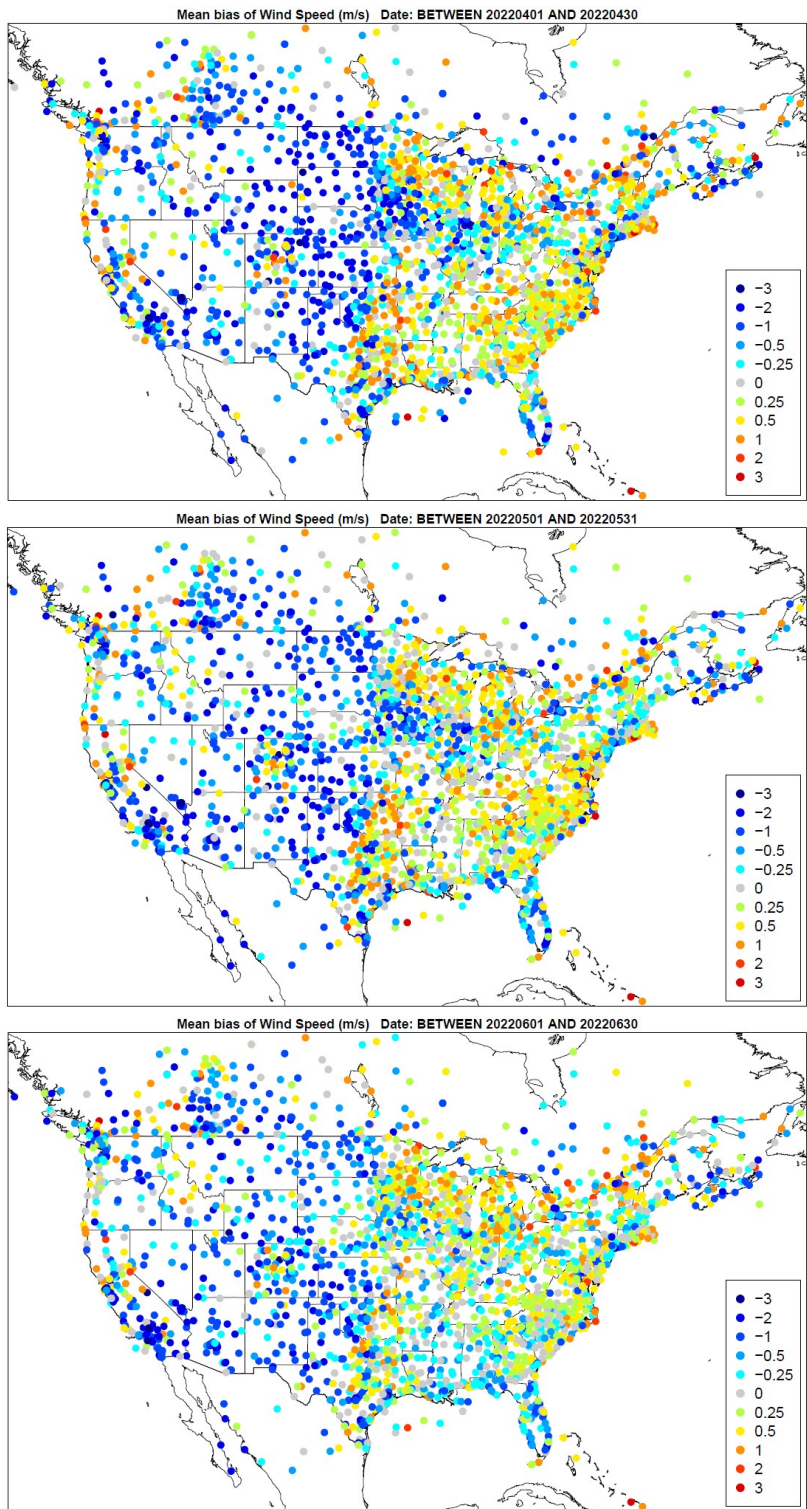
**Figure 3.1.5.** Spatial distribution of wind speed bias (m/s) across all hours for the months of July, August, and September (top to bottom) for the 36NOAM domain.



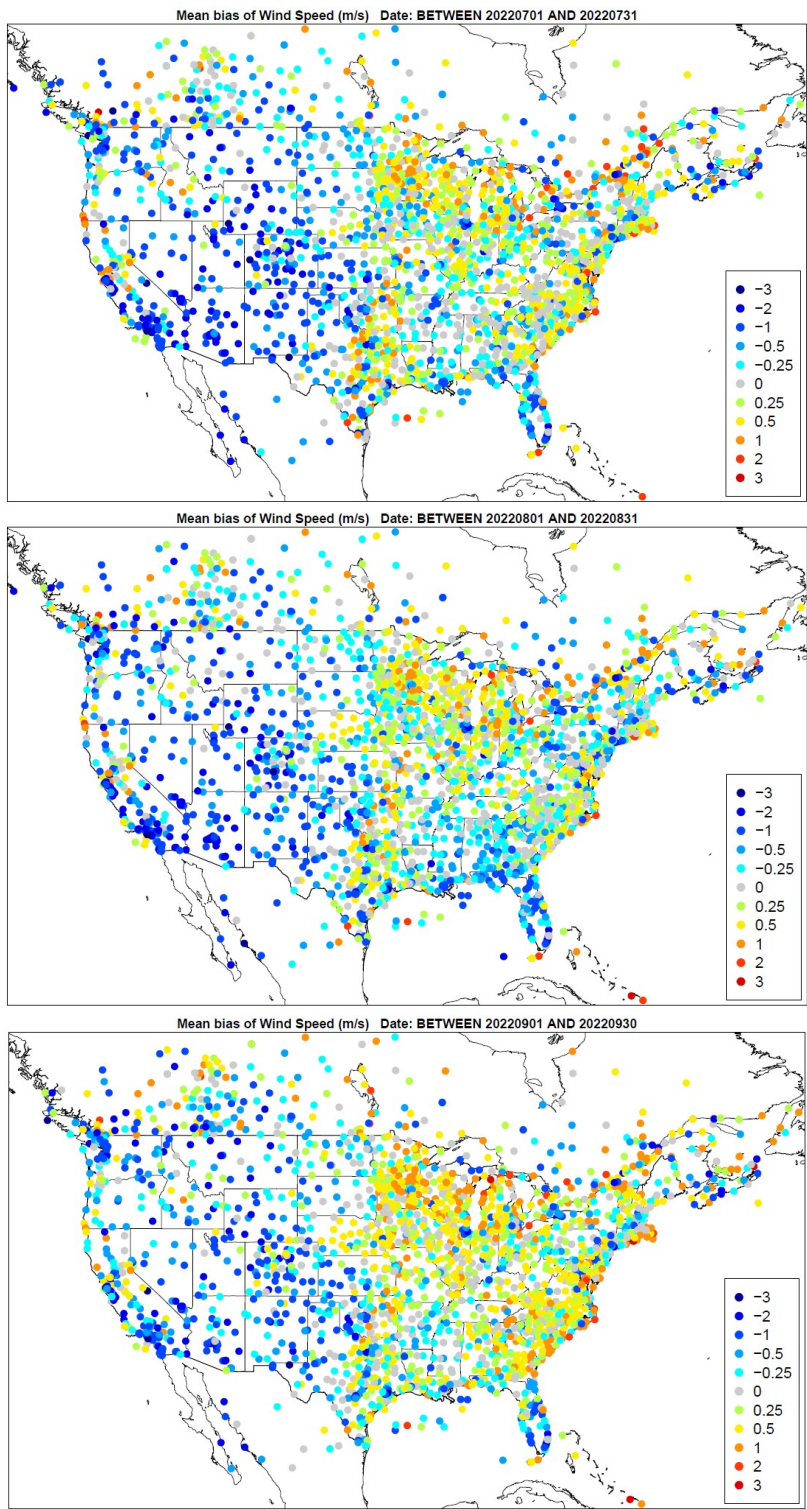
**Figure 3.1.6.** Spatial distribution of wind speed bias (m/s) across all hours for the months of October, November, and December (top to bottom) for the 36NOAM domain.



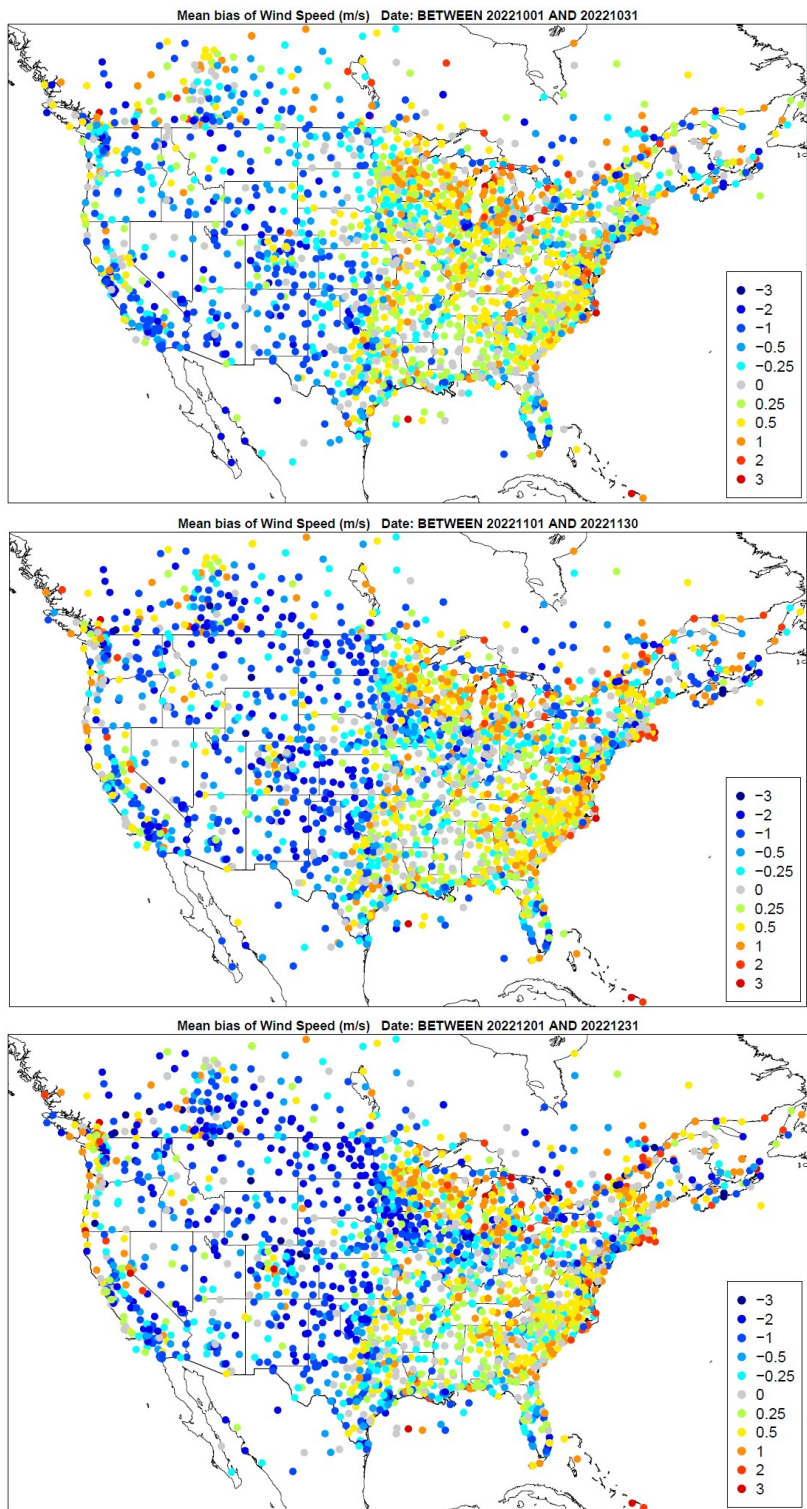
**Figure 3.1.7.** Spatial distribution of wind speed bias (m/s) across all hours for the months of January, February, and March (top to bottom) for the 12US domain.



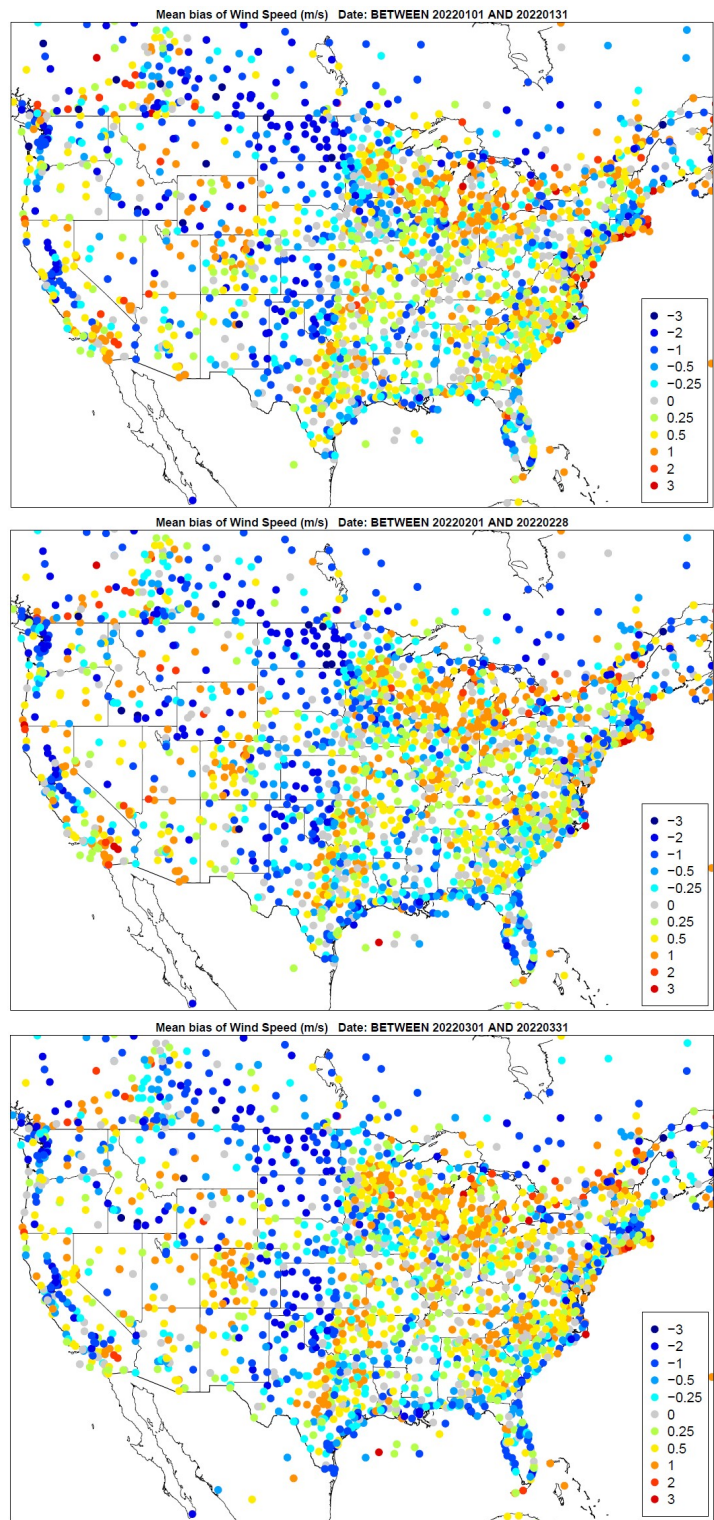
**Figure 3.1.8.** Spatial distribution of wind speed bias (m/s) across all hours for the months of April, May, and June (top to bottom) for the 12US domain.



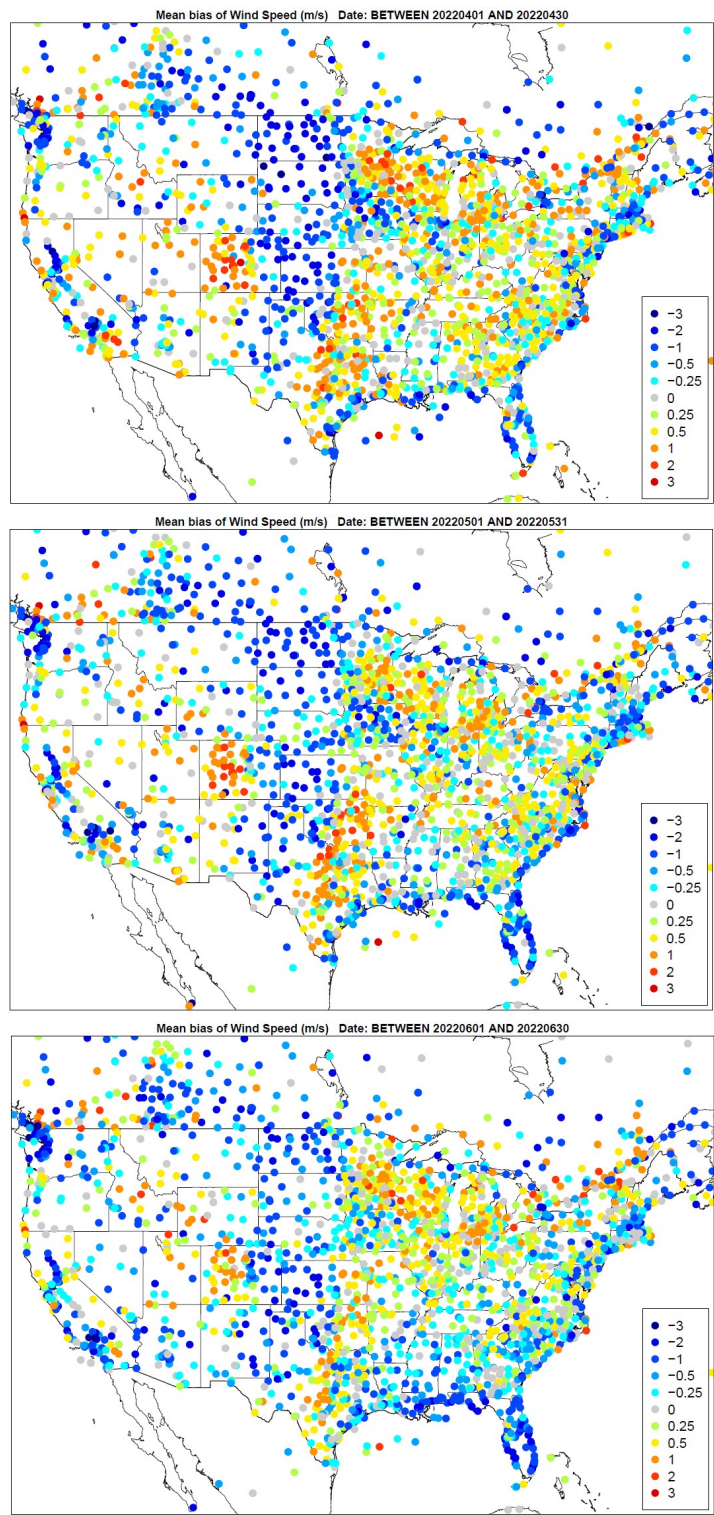
**Figure 3.1.9.** Spatial distribution of wind speed bias (m/s) across all hours for the months of July, August, and September (top to bottom) for the 12US domain.



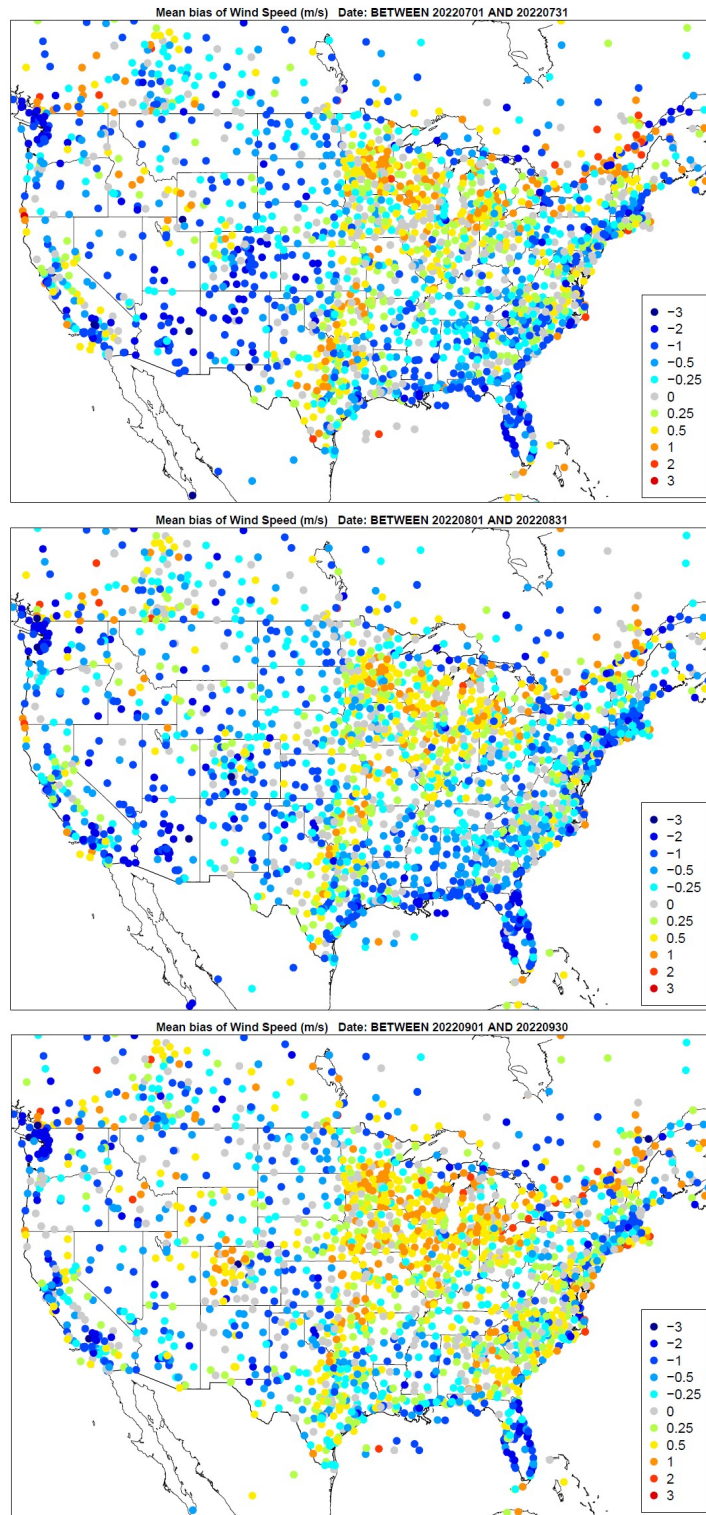
**Figure 3.1.10.** Spatial distribution of wind speed bias (m/s) across all hours for the months of October, November, and December (top to bottom) for the 12US domain.



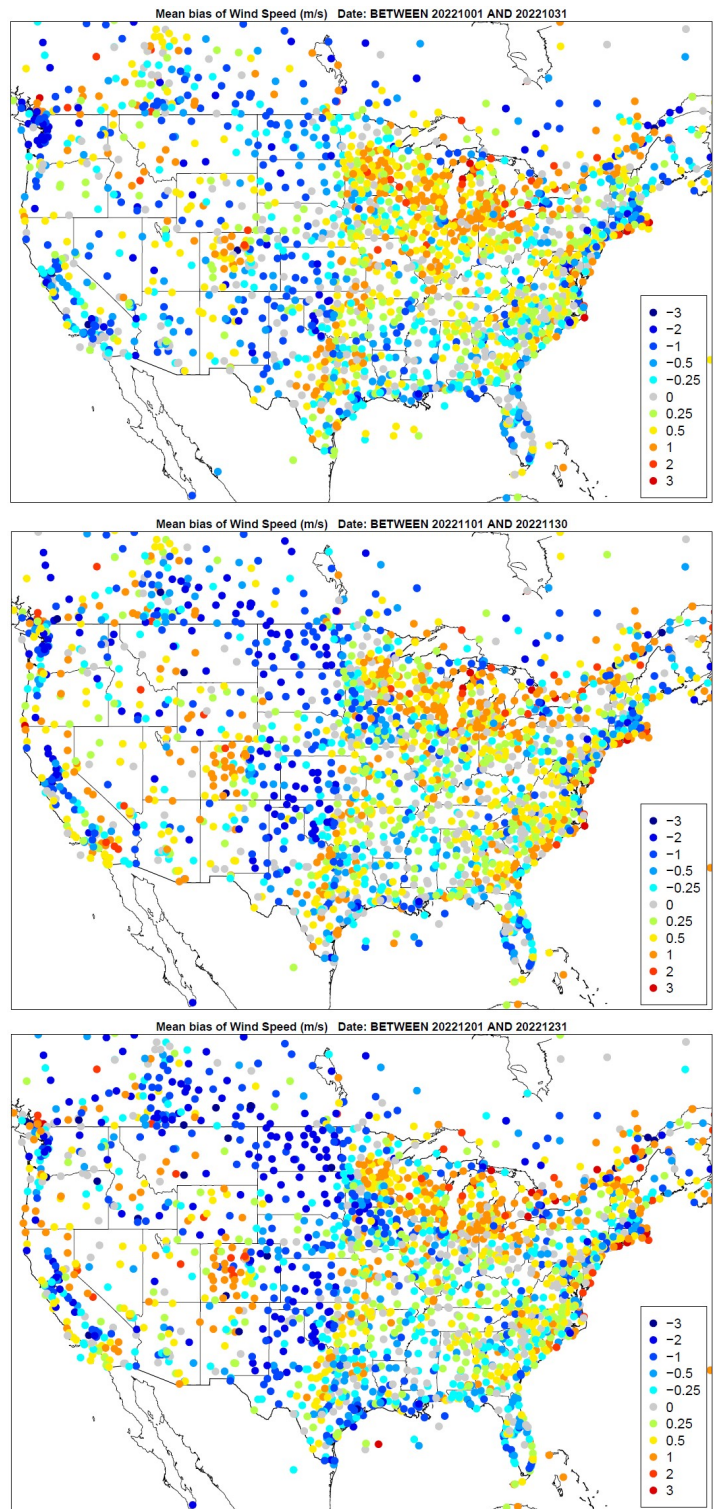
**Figure 3.1.11.** Spatial distribution of wind speed bias (m/s) across daytime hours for the months of January, February, and March (top to bottom) for the 36NOAM domain.



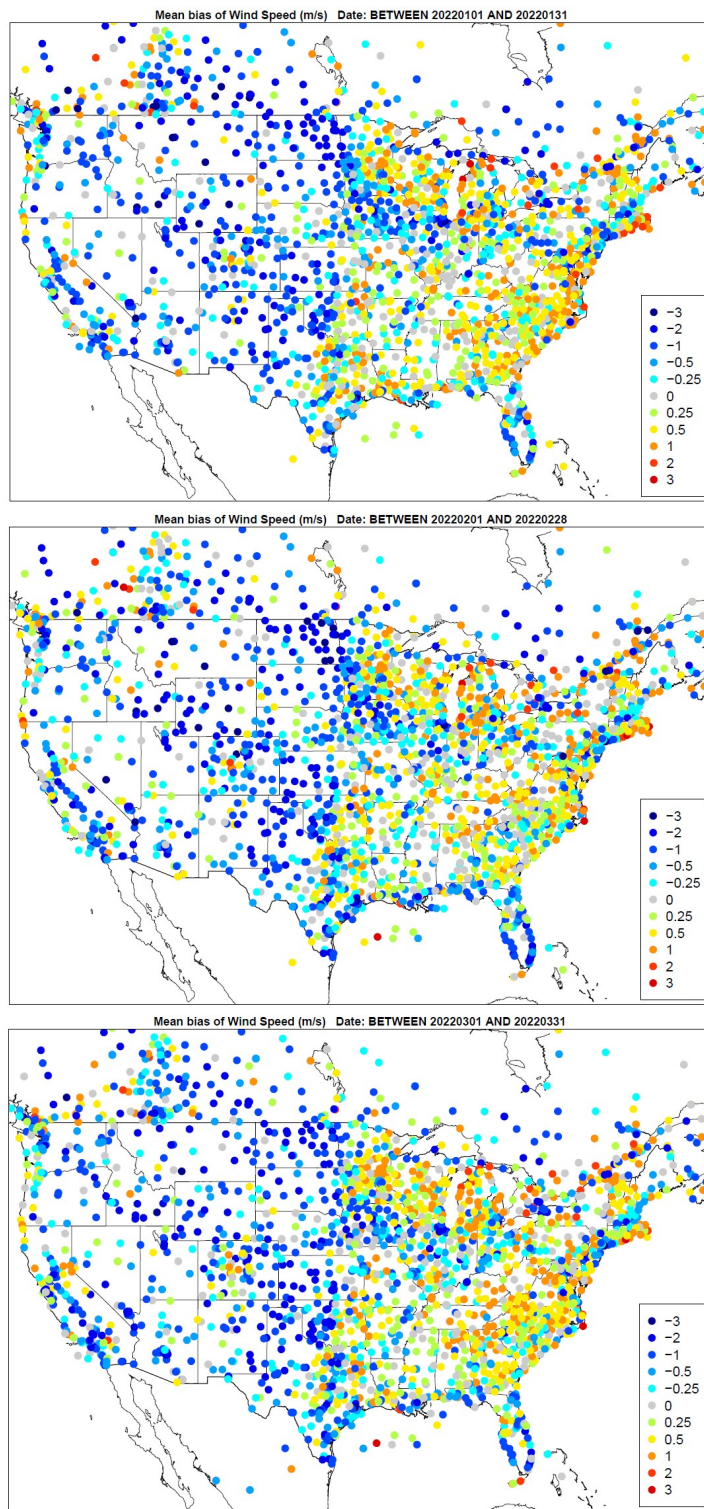
**Figure 3.1.12.** Spatial distribution of wind speed bias (m/s) across daytime hours for the months of April, May, and June (top to bottom) for the 36NOAM domain.



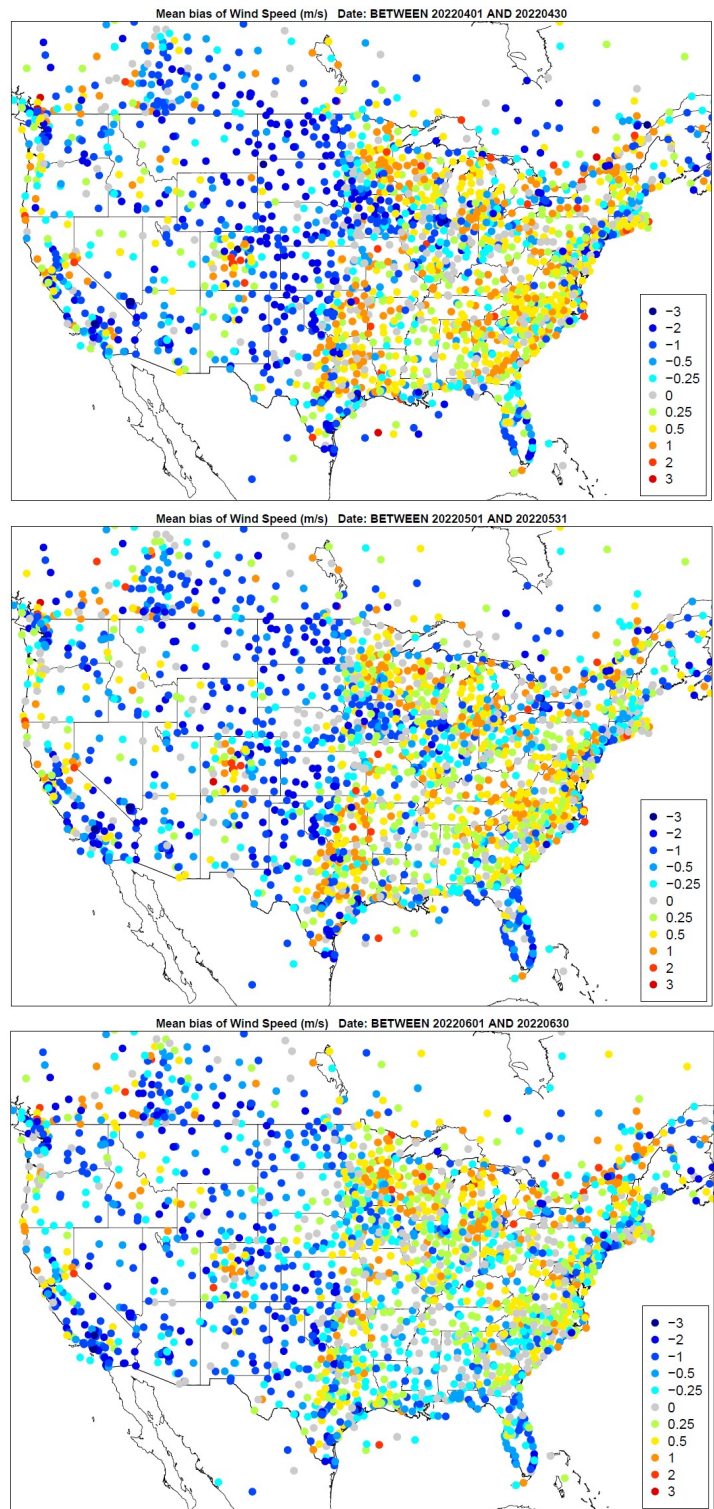
**Figure 3.1.13.** Spatial distribution of wind speed bias (m/s) across daytime hours for the months of July, August, and September (top to bottom) for the 36NOAM domain.



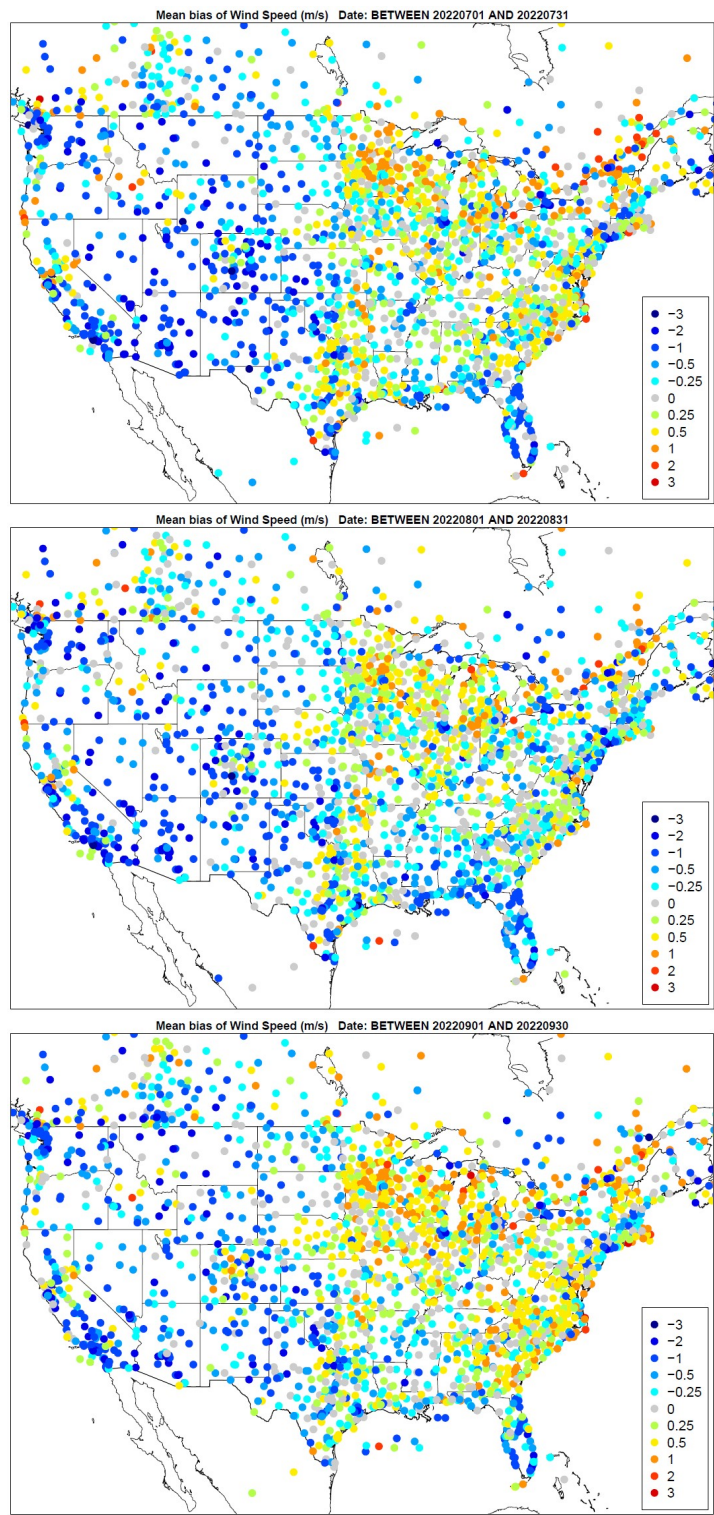
**Figure 3.1.14.** Spatial distribution of wind speed bias (m/s) across daytime hours for the months of October, November, and December (top to bottom) for the 36NOAM domain.



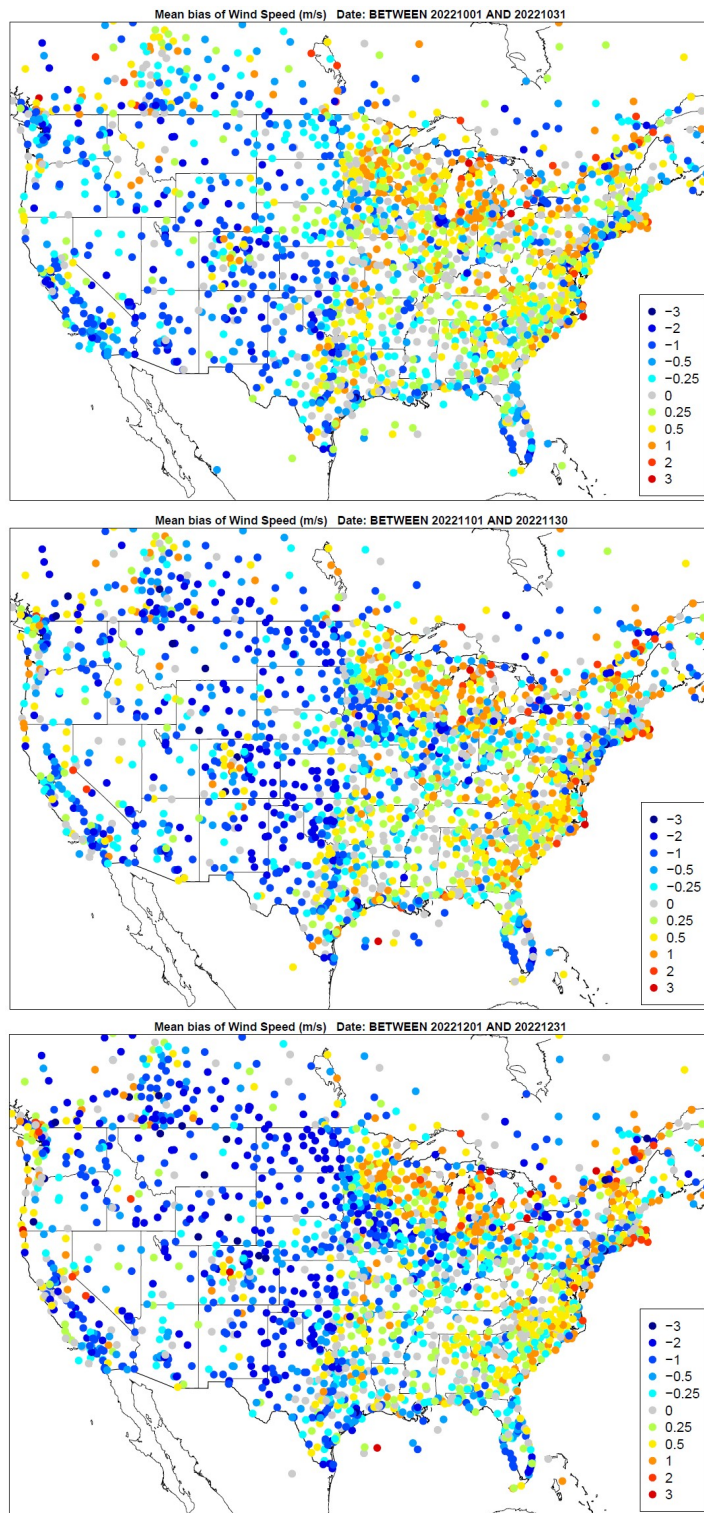
**Figure 3.1.15.** Spatial distribution of wind speed bias (m/s) across daytime hours for the months of January, February, and March (top to bottom) for the 12US domain.



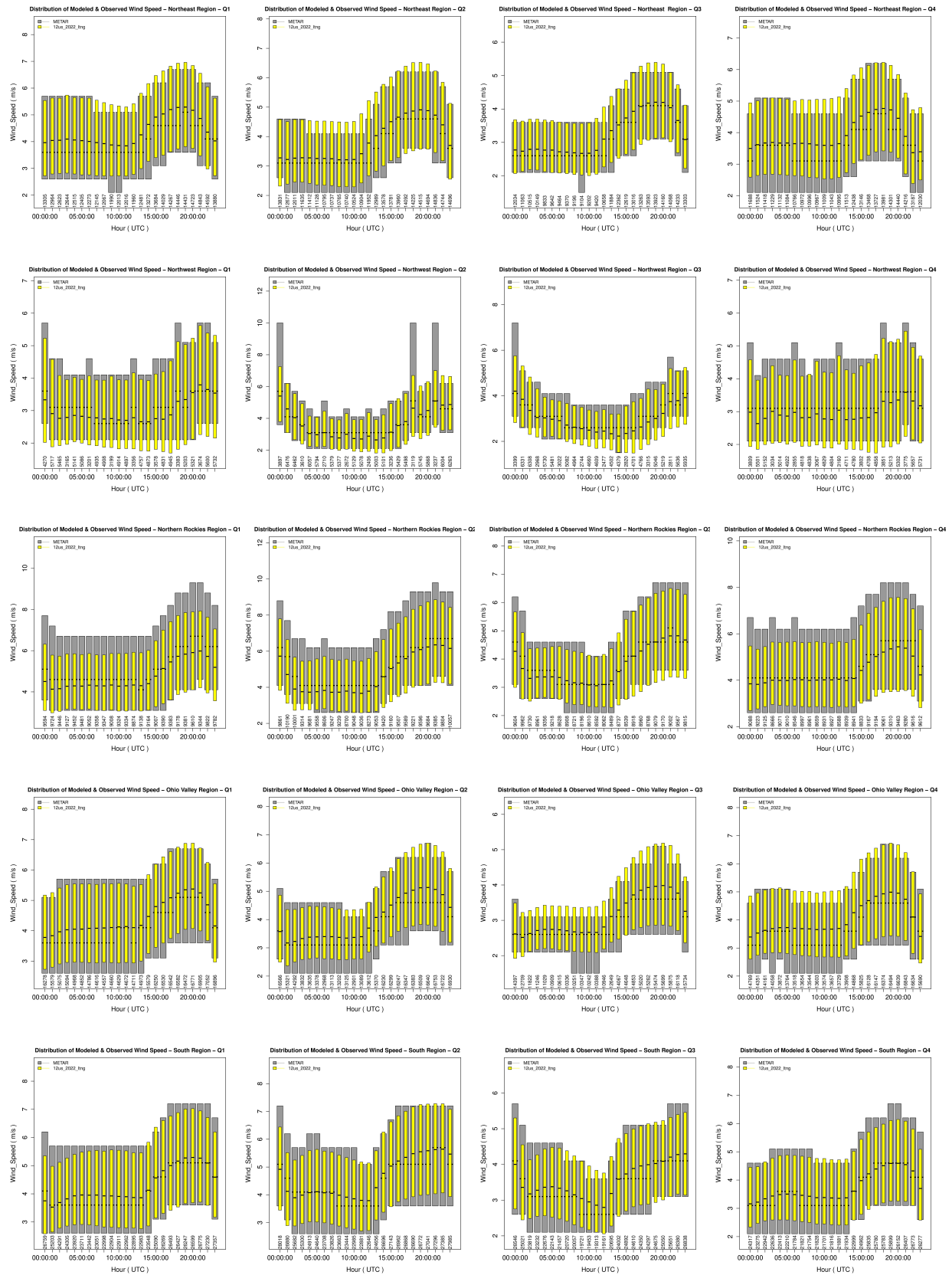
**Figure 3.1.16.** Spatial distribution of wind speed bias (m/s) across daytime hours for the months of April, May, and June (top to bottom) for the 12US domain.



**Figure 3.1.17.** Spatial distribution of wind speed bias (m/s) across daytime hours for the months of July, August, and September (top to bottom) for the 12US domain.



**Figure 3.1.18.** Spatial distribution of wind speed bias (m/s) across daytime hours for the months of October, November, and December (top to bottom) for the 12US domain.



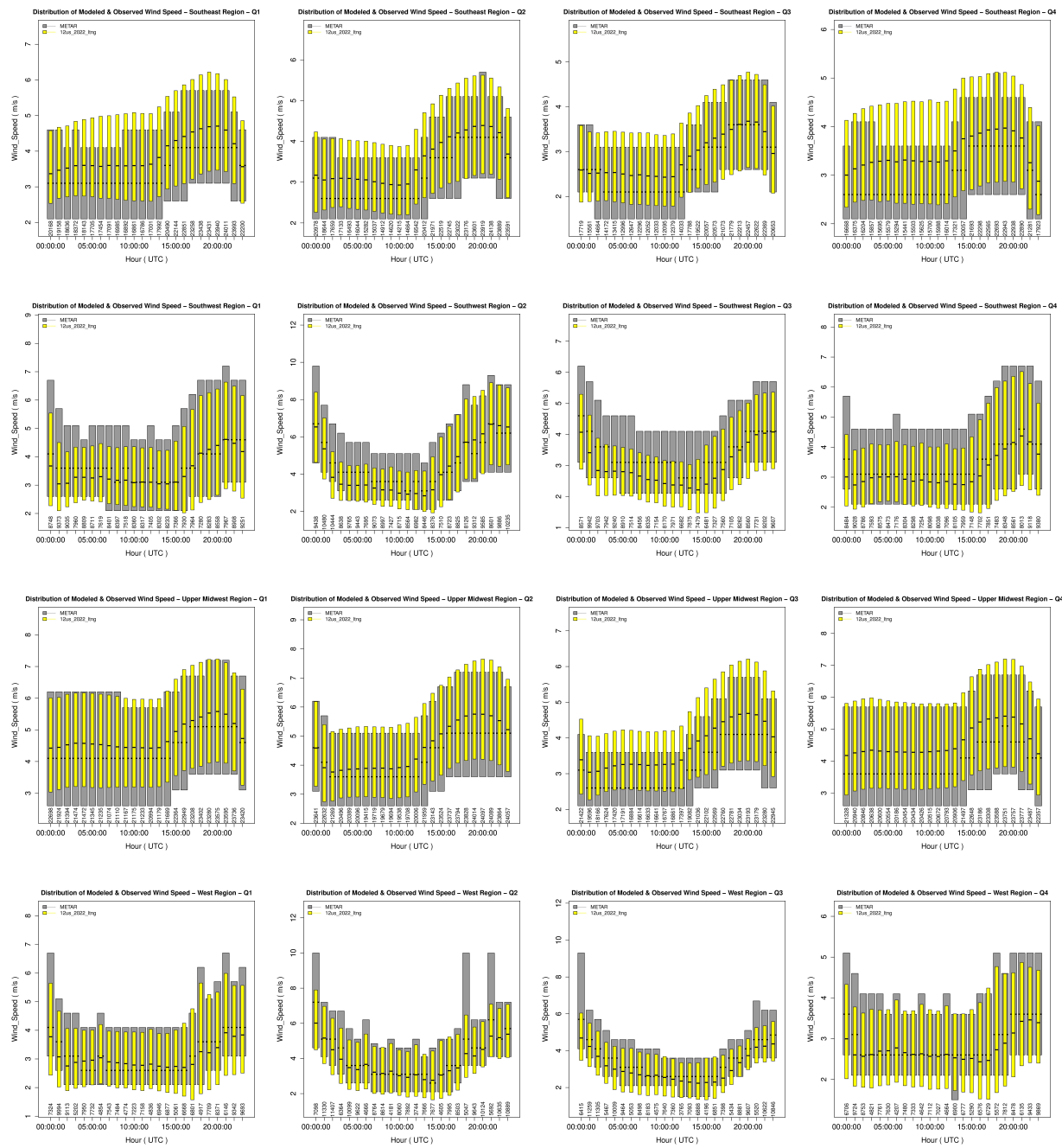


**Figure 3.1.19.** Hourly average distribution of observed and predicted wind speeds (m/s) for the 12US domain in the Northeast, Northwest, Northern Rockies & Plains, Ohio Valley, South, Southeast, Southwest, Upper Midwest, and West Climate Regions (respectively, top to bottom) for each quarter.

Climate Region	Season	Mean Obs	Mean Mod	MAE	MB	NMB	NME	RMSE
Northeast	Q1	4.54	4.25	1.4	0.16	3.53	30.77	2.01
	Q2	4.11	3.78	1.24	0.09	2.09	30.08	1.78
	Q3	3.5	3.13	1.11	0.02	0.54	31.58	1.63
	Q4	4.15	3.83	1.3	0.18	4.4	31.28	1.91
N. Rockies & Plains	Q1	5.66	4.81	1.54	-0.63	-11.19	27.21	2.08
	Q2	5.81	4.92	1.53	-0.61	-10.45	26.38	2.07
	Q3	4.25	3.78	1.25	-0.24	-5.65	29.37	1.72
	Q4	5.31	4.44	1.42	-0.56	-10.62	26.85	1.93
Northwest	Q1	3.8	3.05	1.39	-0.36	-9.6	36.69	1.88
	Q2	4.27	3.58	1.42	-0.25	-5.87	33.29	1.91
	Q3	3.57	2.94	1.21	-0.31	-8.79	33.78	1.63
	Q4	3.82	3.04	1.42	-0.32	-8.4	37.22	1.93
Ohio Valley	Q1	4.59	4.33	1.1	0.07	1.59	24.01	1.45
	Q2	4.19	3.92	1.11	0.1	2.27	26.41	1.46
	Q3	3.21	2.96	0.94	0.13	3.92	29.28	1.24
	Q4	4.28	3.99	1.05	0.14	3.27	24.46	1.38
South	Q1	4.84	4.27	1.21	-0.18	-3.67	24.98	1.63
	Q2	5.01	4.54	1.31	-0.14	-2.75	26.14	1.76
	Q3	3.79	3.38	1.07	-0.06	-1.71	28.22	1.43
	Q4	4.29	3.75	1.14	-0.15	-3.41	26.5	1.54
Southeast	Q1	3.92	3.77	1.2	0.36	9.26	30.48	1.6
	Q2	3.58	3.36	1.12	0.22	6.25	31.35	1.49
	Q3	3.15	2.8	1.05	0.12	3.7	33.34	1.43
	Q4	3.44	3.28	1.09	0.37	10.82	31.83	1.46
Southwest	Q1	4.39	3.54	1.56	-0.54	-12.24	35.41	2.14
	Q2	5.24	4.38	1.75	-0.52	-9.97	33.37	2.37
	Q3	3.83	2.96	1.48	-0.67	-17.58	38.65	2.03
	Q4	4.26	3.32	1.55	-0.61	-14.24	36.51	2.17
Upper Midwest	Q1	4.87	4.68	1.2	0.15	3.05	24.72	1.59
	Q2	4.79	4.63	1.24	0.18	3.7	25.92	1.63
	Q3	3.61	3.6	1.08	0.38	10.47	29.89	1.43
	Q4	4.66	4.59	1.22	0.3	6.49	26.18	1.63
West	Q1	3.86	3.1	1.37	-0.33	-8.55	35.56	1.86
	Q2	4.82	3.9	1.54	-0.45	-9.36	31.89	2.07
	Q3	3.97	3.11	1.33	-0.53	-13.28	33.4	1.82
	Q4	3.55	2.82	1.26	-0.34	-9.46	35.43	1.73

**Table 3.1.1.** Mean observed, mean modeled, mean absolute error (MAE), mean bias (MB), normalized mean bias (NMB), normalized mean error (NME), and root mean square error (RMSE) for wind speed (m/s).

Wind vector displacement (km) is presented below for the 36NOAM (Figure 3.1.20) and 12US (Figure 3.1.21) domains utilizing the ds472 observation network described earlier. These plots show the entire distribution of hourly wind displacement by month and by hour of the day. The average wind displacement for the WRF simulation is around 5-km for all months and hours of the day. The interquartile ranges are roughly 2-10km. As the displacement is generally less than the resolution of the model for either simulation, minimal impacts due to displacement of wind vectors are expected.

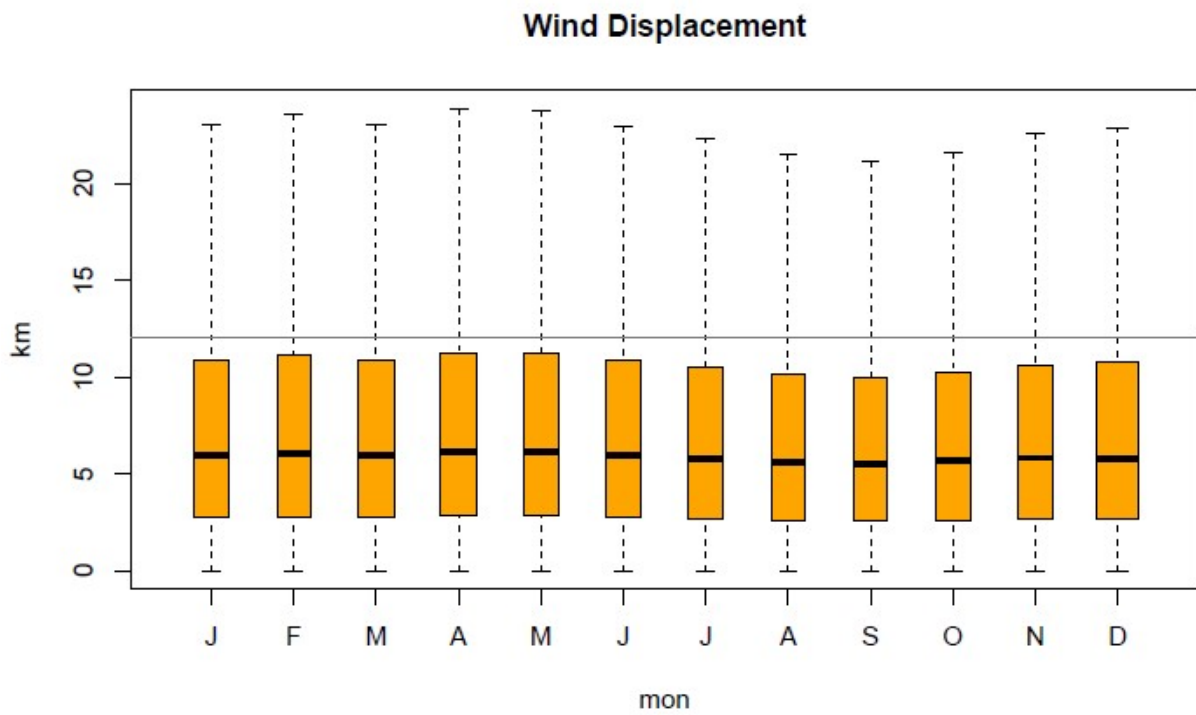
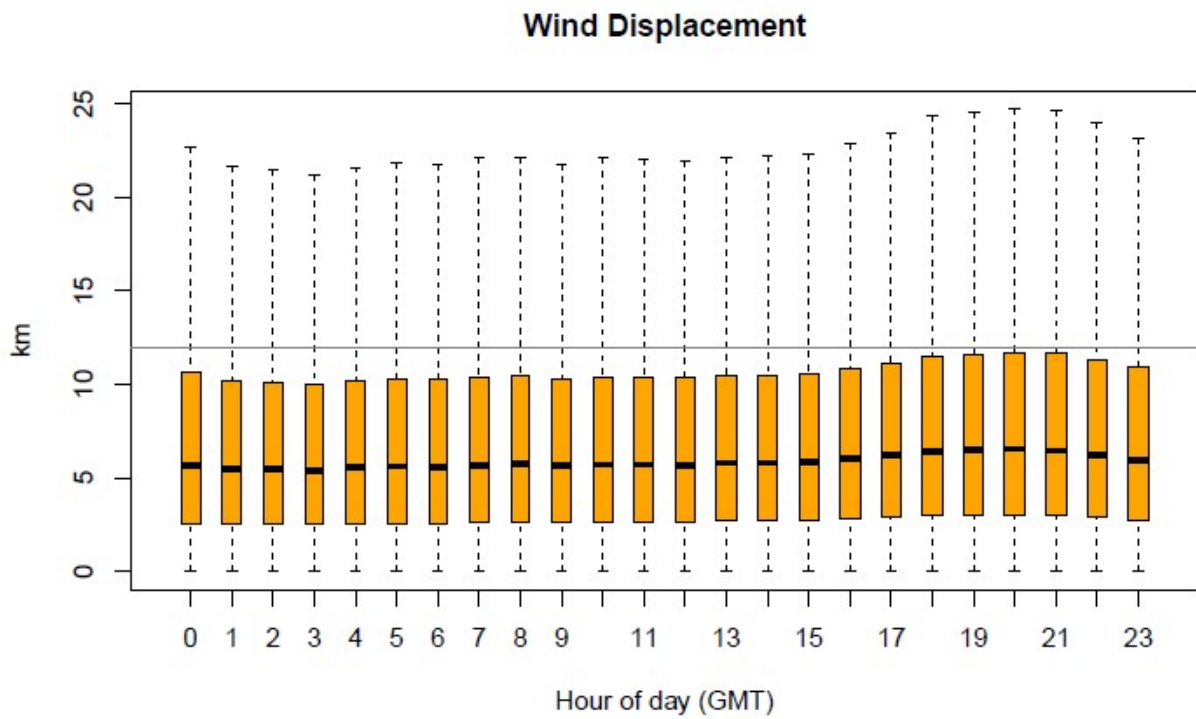


**Figure 3.1.20.** Distribution of hourly wind displacement by hour and month for the 36NOAM domain.

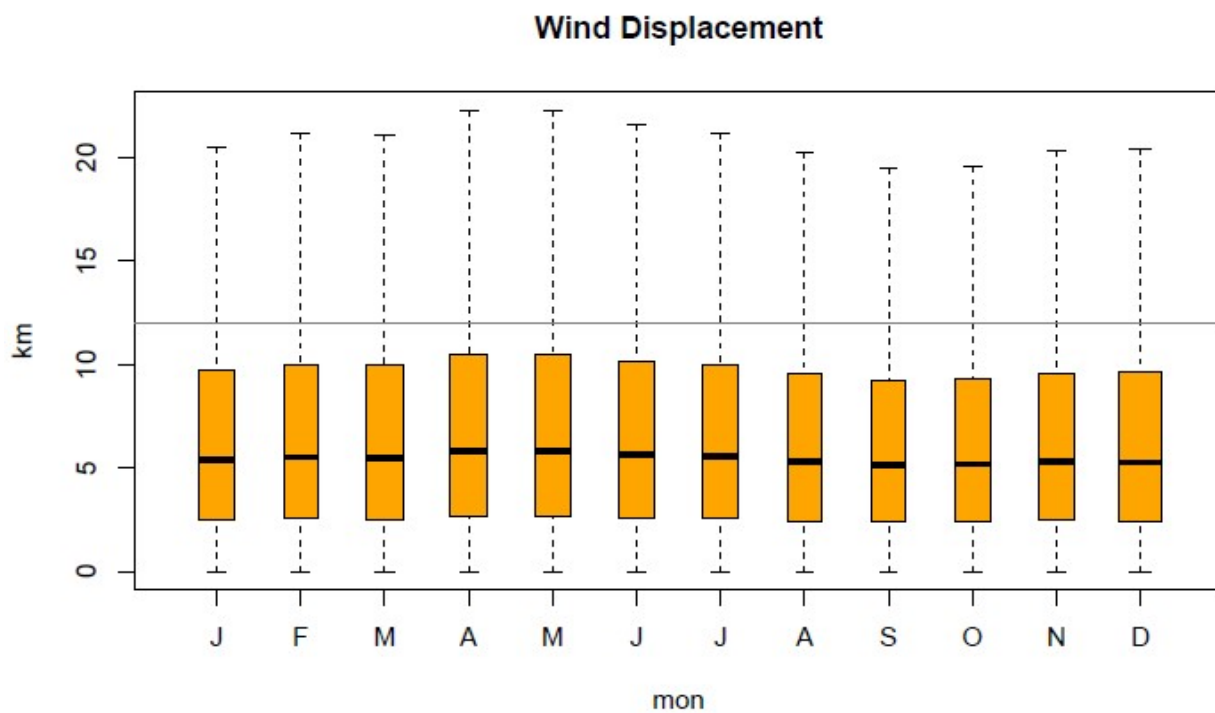
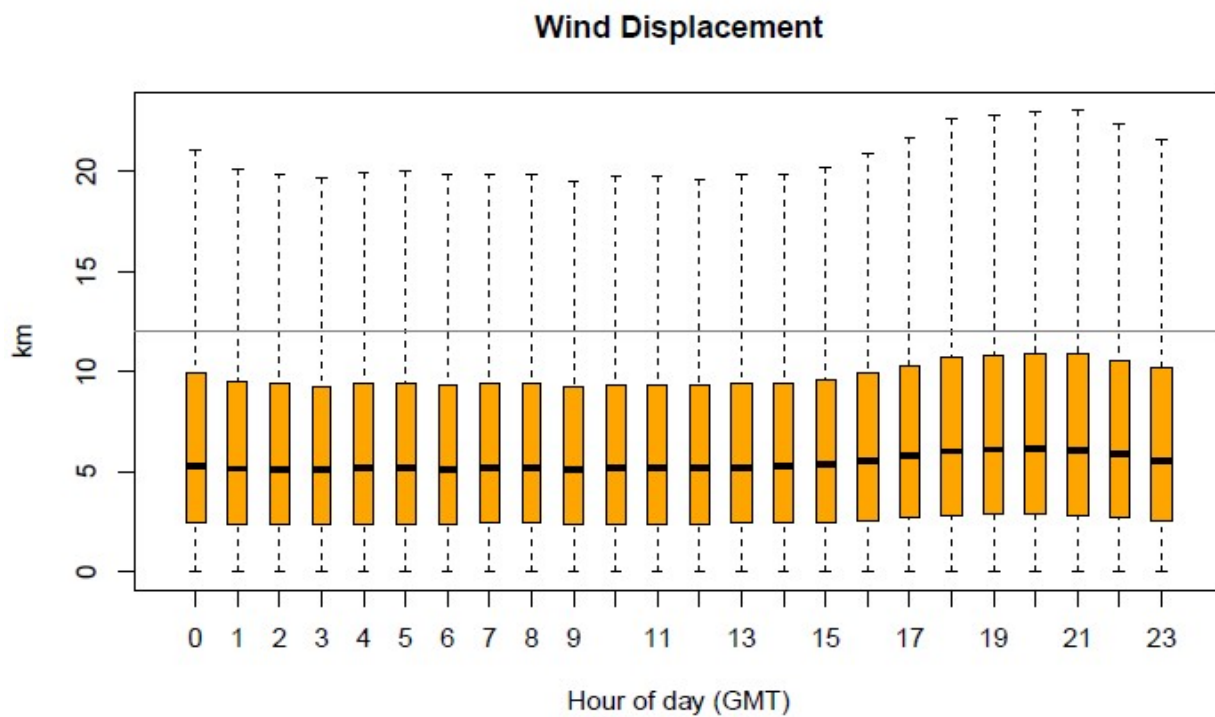


**Figure 3.1.21.** Distribution of hourly wind displacement by hour and month for the 12US domain.

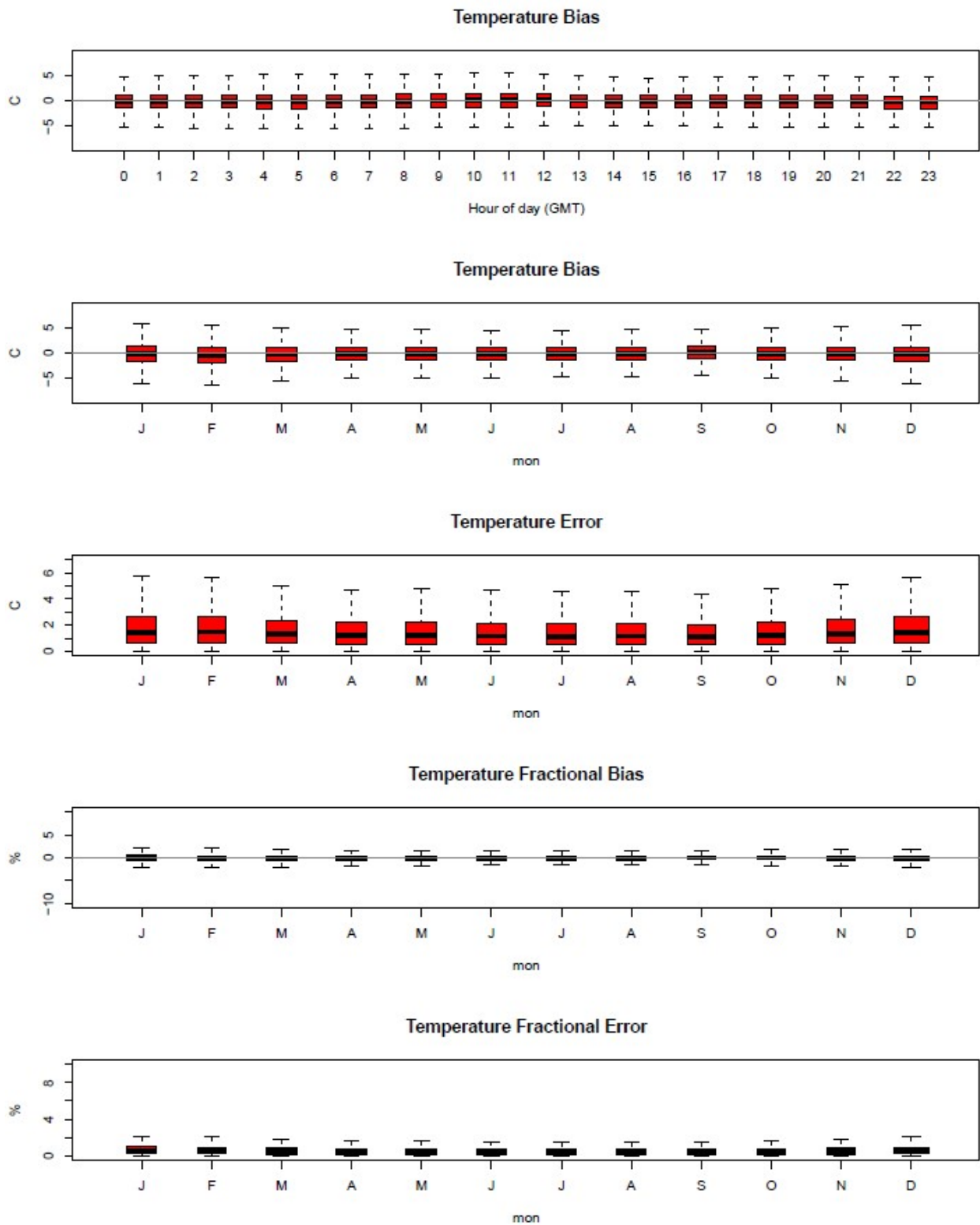
### 3.2 Model Performance for Temperature

Temperature estimates are compared to the ds472 observation network described earlier and are presented below for the 36NOAM (Figure 3.2.1) and 12US (Figure 3.2.1) domains. Regional analysis of statistical metrics for temperature performance by quarter is shown in Table 3.2.1 for the 12US domain only.

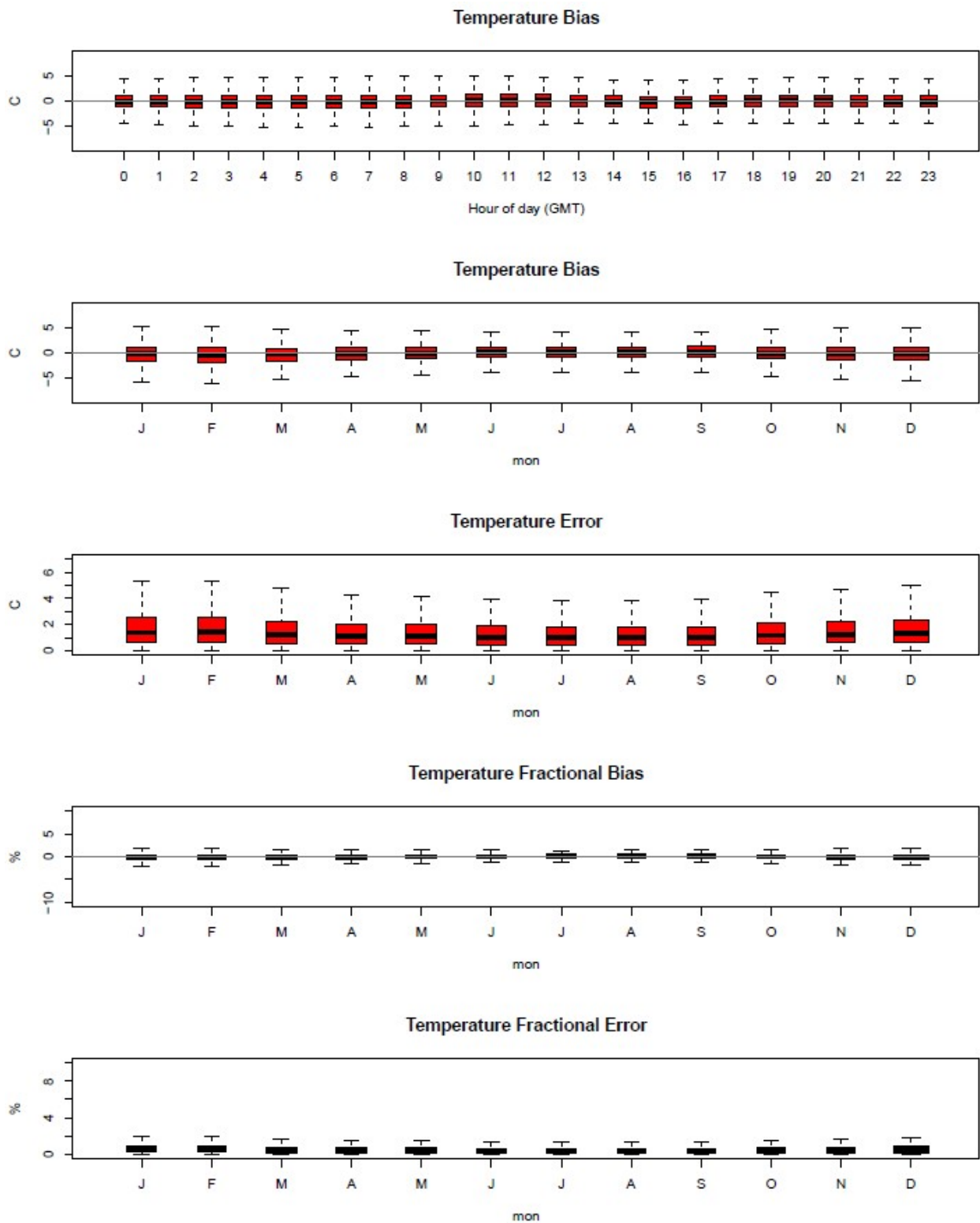
WRF performs very well in terms of predicting temperature, showing a bias that oscillates around 0 degrees for most hours of the day and months of the year. Model error decreases slightly during the Spring and Summer months. In general, the interquartile range of the bias of +/- 1 degree is persistent across all hours of the day and all months of the year.

Spatial distribution of monthly biases is presented across all hours for the 36NOAM (Figures 3.2.3-3.2.6) and 12US (Figures 3.2.7-3.2.10) domains. The spatial distribution of monthly biases across daytime hours only is presented for the 36NOAM (Figures 3.2.11-3.2.14) and 12US (Figures 3.2.15-3.2.18) domains. The hourly distribution of observed and predicted temperatures by Climate Region and quarter are shown in Figure 3.2.19. WRF generally underpredicts temperatures slightly across the eastern US during the Winter into the early Spring with the underprediction persisting longest in the northeast. A more noticeable overprediction is noted across the eastern US during the summer and fall months with an average overprediction of 0.25 to 0.5 degrees.

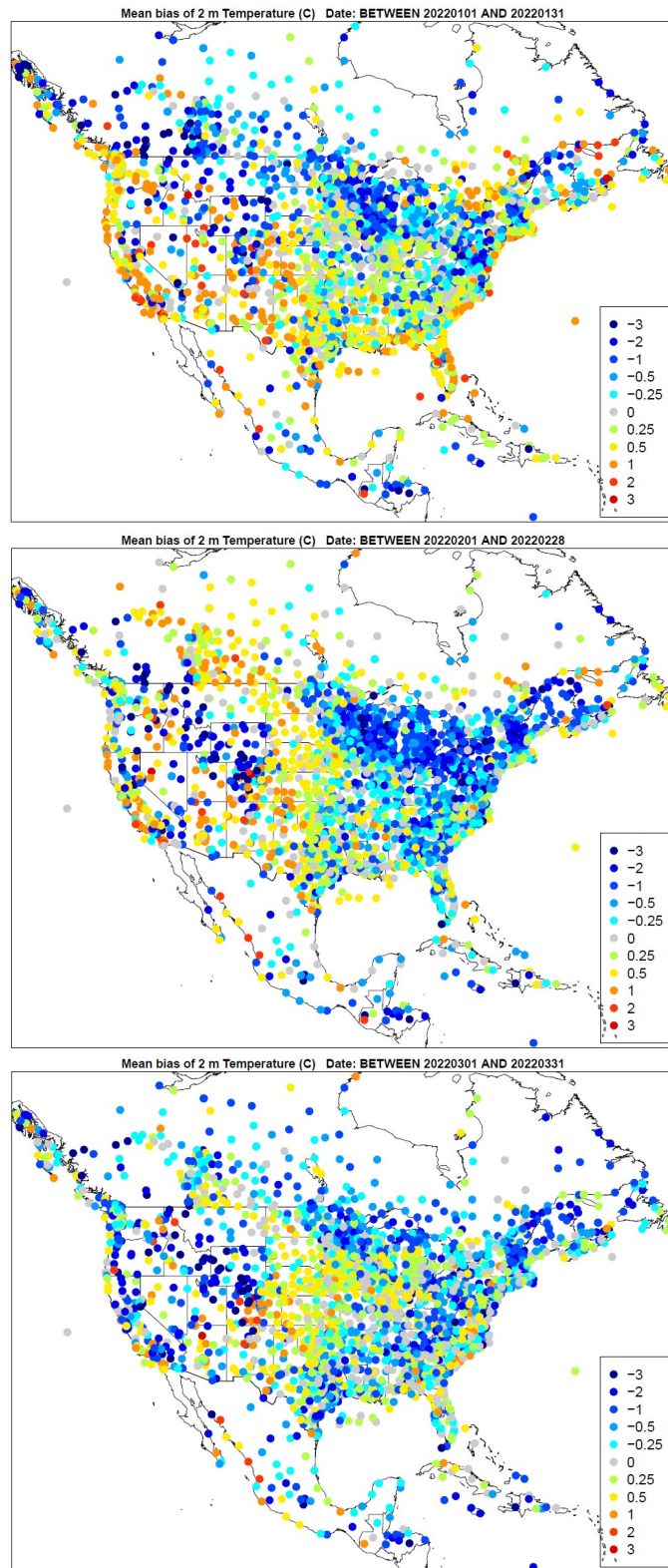
In areas of the western US, performance for temperature is mixed, with persistent significant overpredictions and underpredictions observed in varying locations. Across daytime hours, there is a more noticeable underprediction in the 36NOAM simulation compared the 12US simulation. However, the range of the biases in both simulations tends to be mainly between +/- 0.5 degrees.



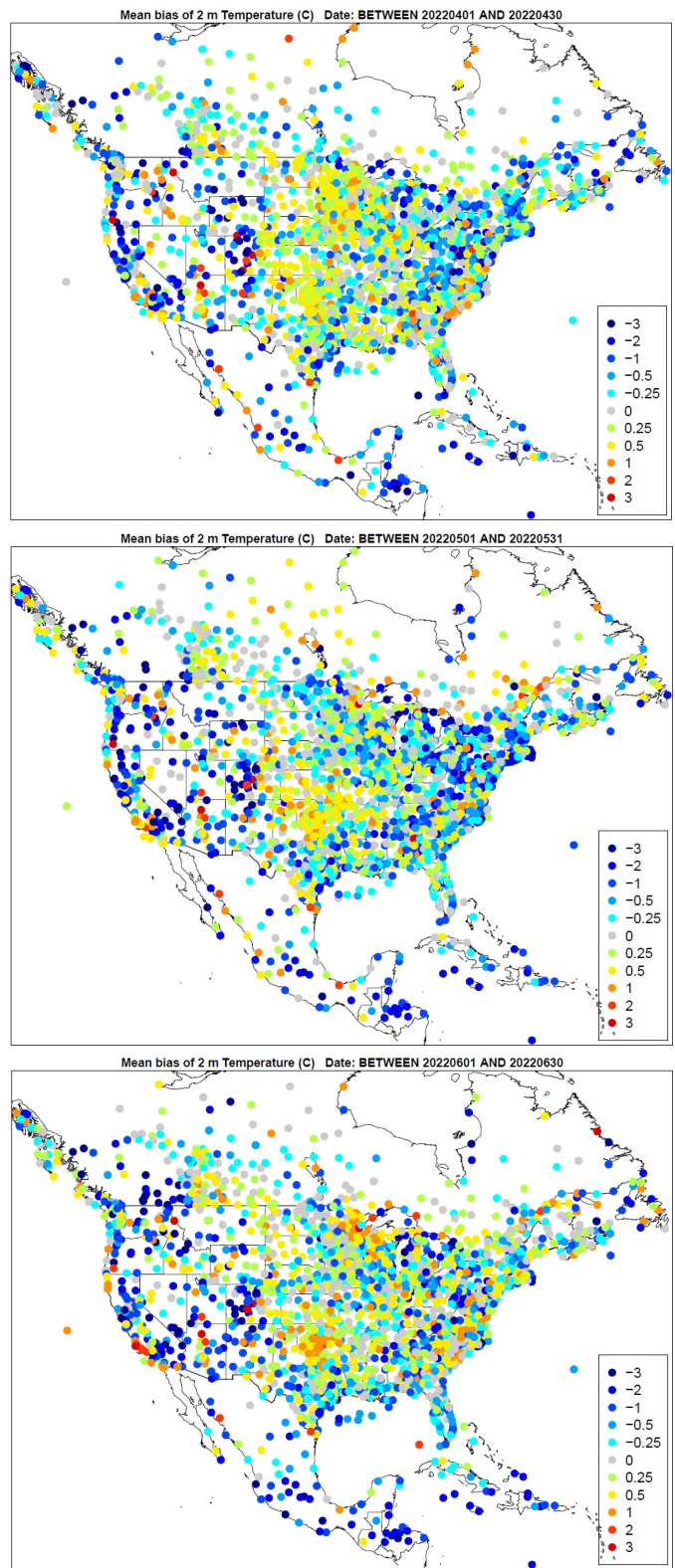
**Figure 3.2.1.** Distribution of hourly bias by hour and hourly bias, error, fractional bias, and fractional error for temperature by month for the 36NOAM domain.



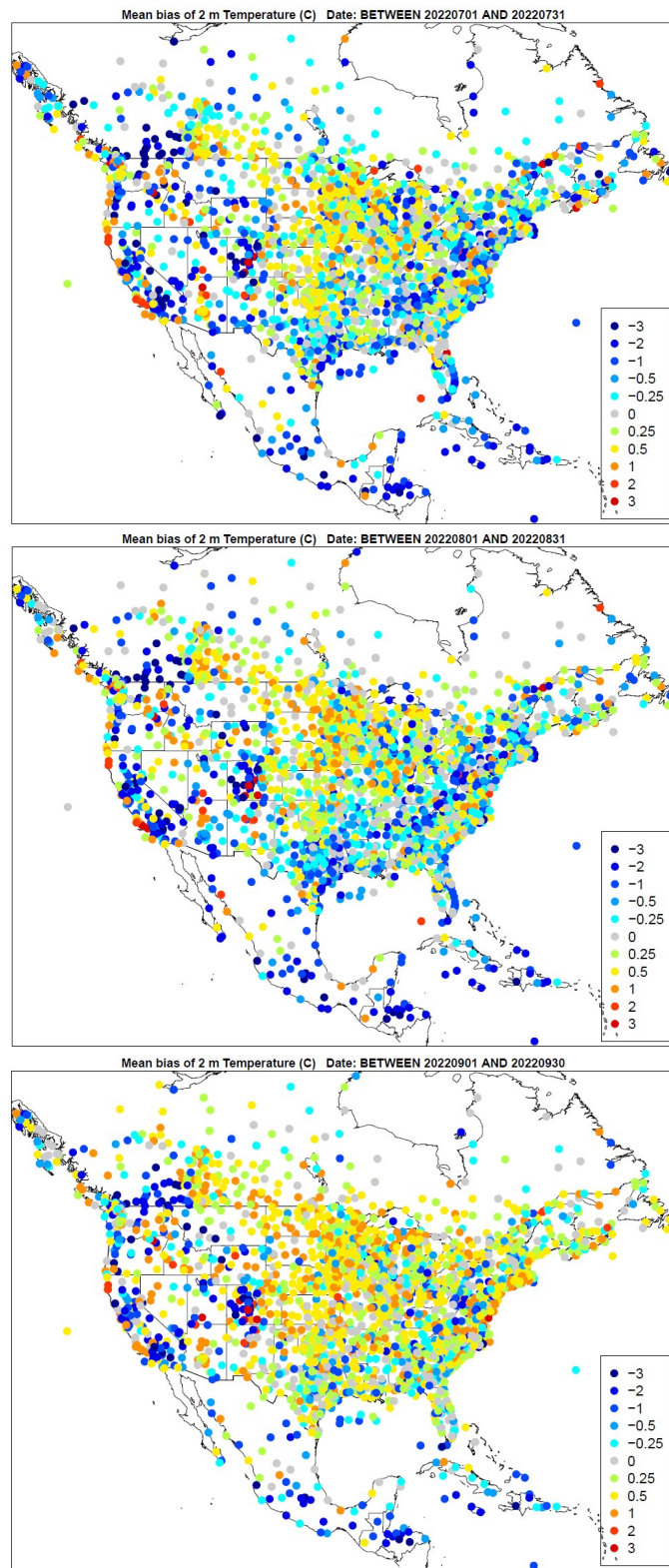
**Figure 3.2.2.** Distribution of hourly bias by hour and hourly bias, error, fractional bias, and fractional error for temperature by month for the 12US domain.



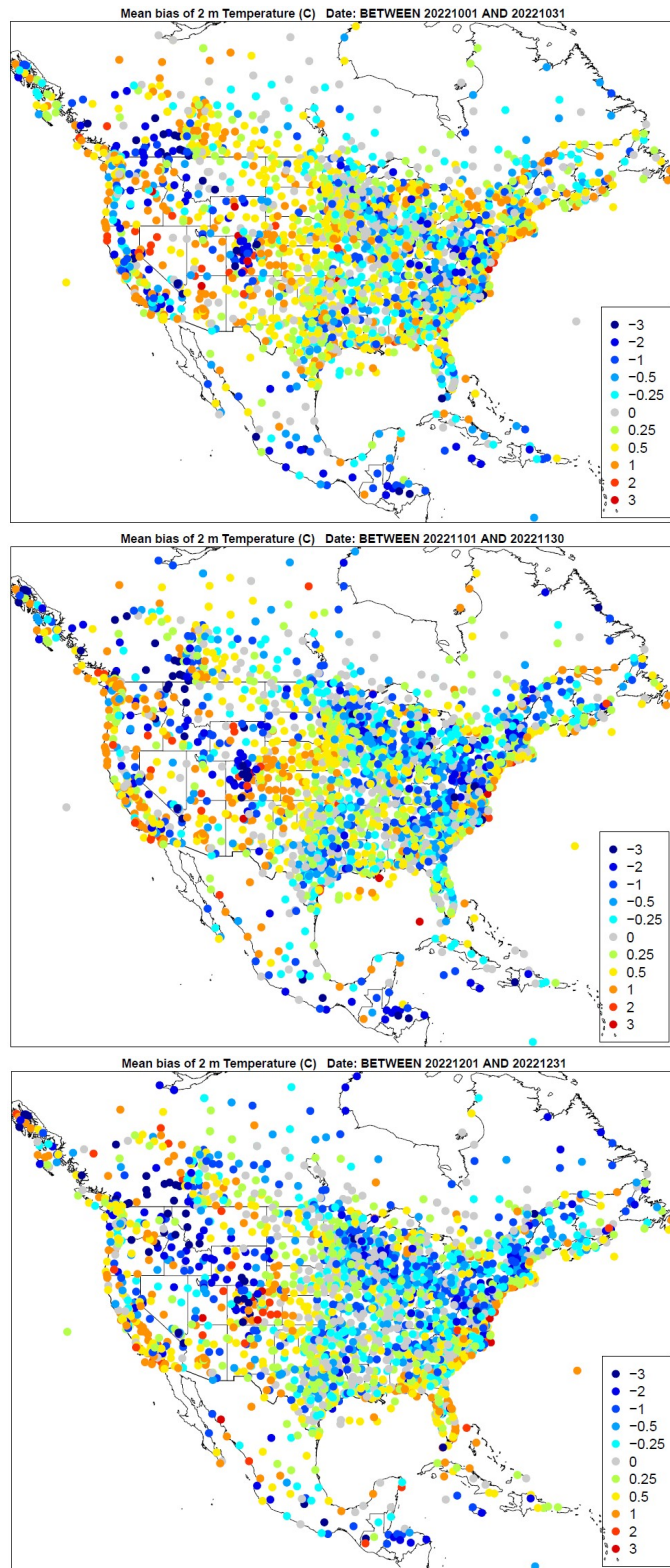
**Figure 3.2.3.** Spatial distribution of temperature bias (C) across all hours for the months of January, February, and March (top to bottom) for the 36NOAM domain.



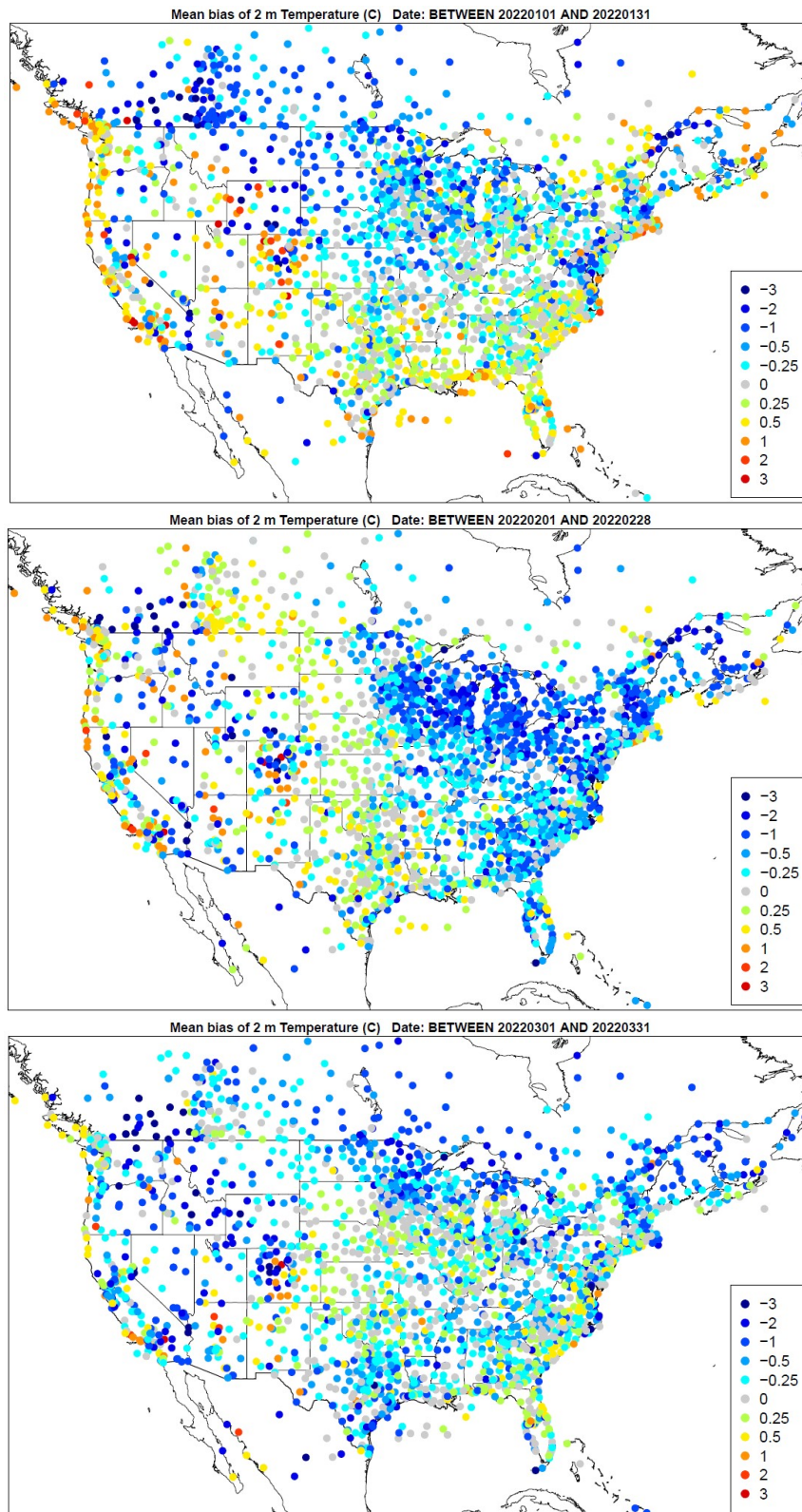
**Figure 3.2.4.** Spatial distribution of temperature bias (C) across all hours for the months of April, May, and June (top to bottom) for the 36NOAM domain.



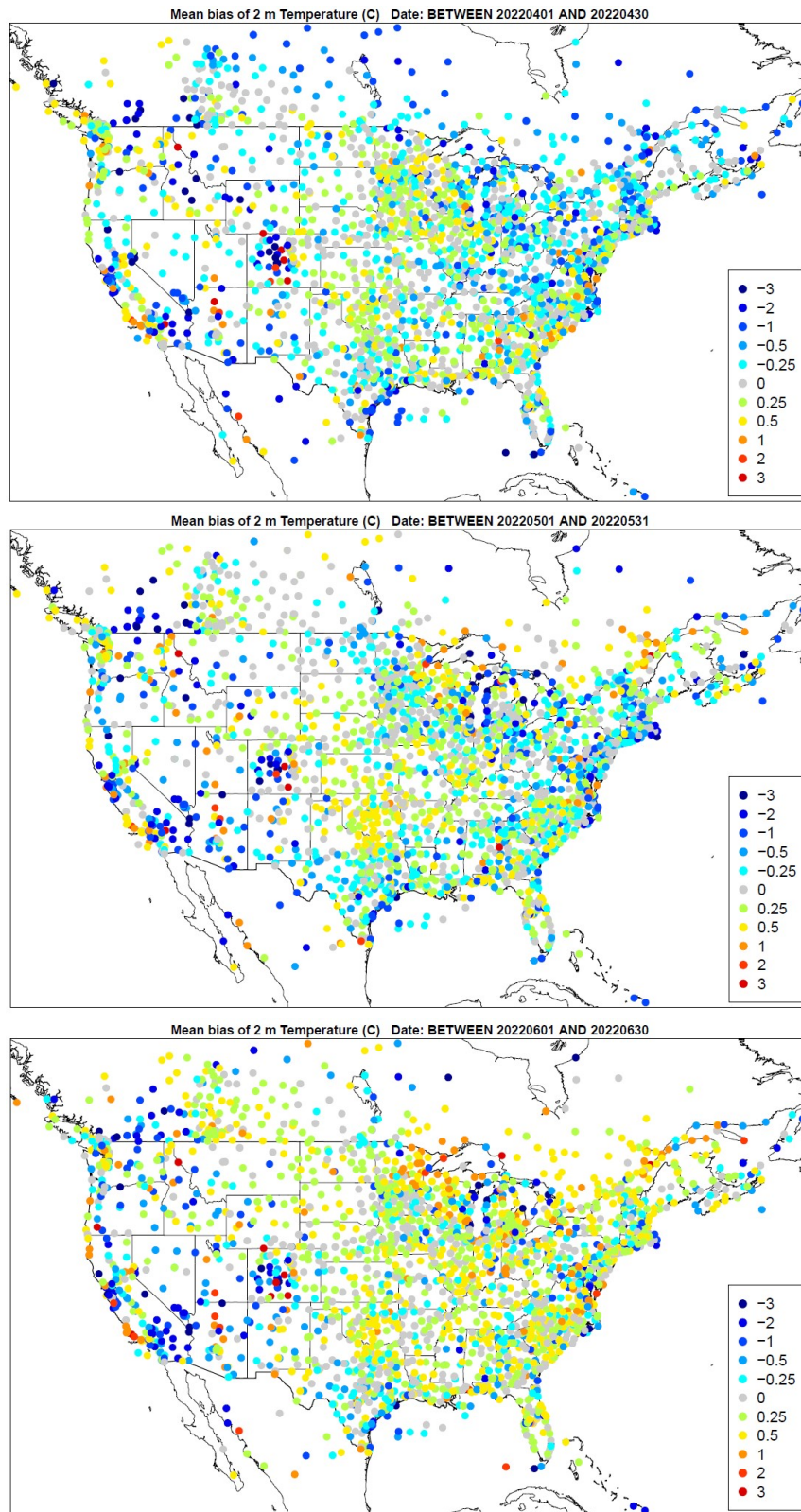
**Figure 3.2.5.** Spatial distribution of temperature bias (C) across all hours for the months of July, August, and September (top to bottom) for the 36NOAM domain.



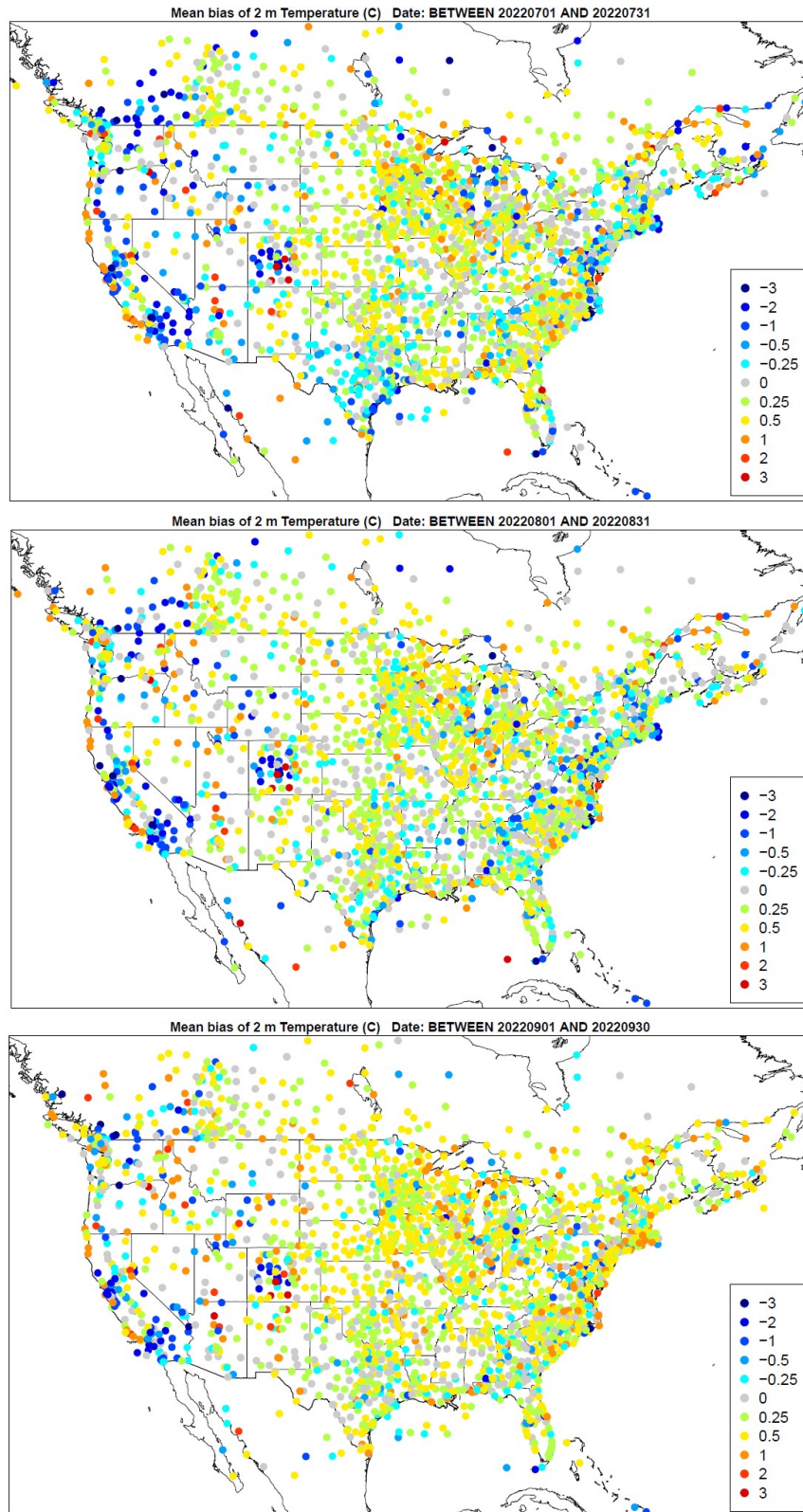
**Figure 3.2.6.** Spatial distribution of temperature bias (C) across all hours for the months of October, November, and December (top to bottom) for the 36NOAM domain.



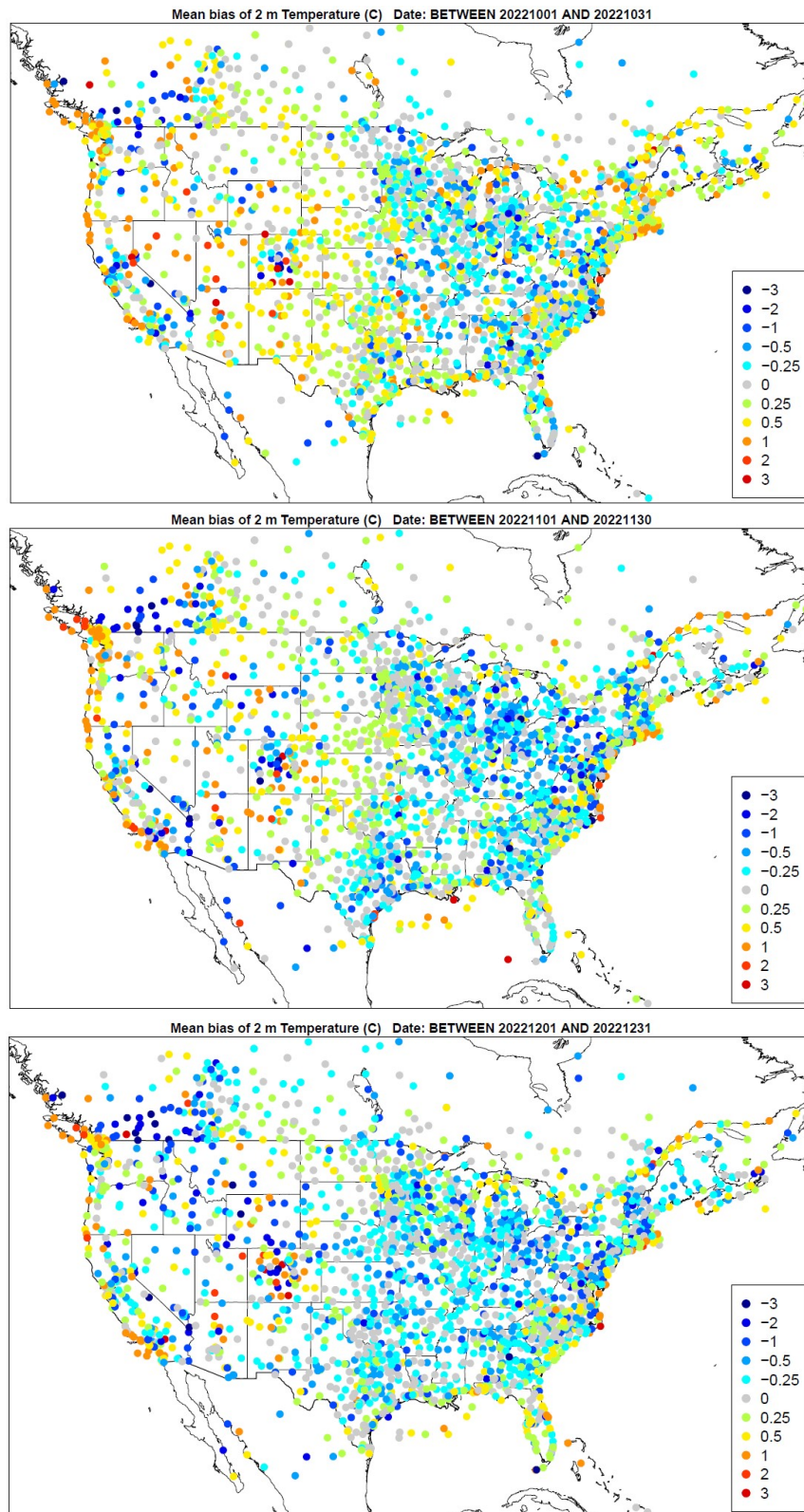
**Figure 3.2.7.** Spatial distribution of temperature bias (C) across all hours for the months of January, February, and March (top to bottom) for the 12US domain.



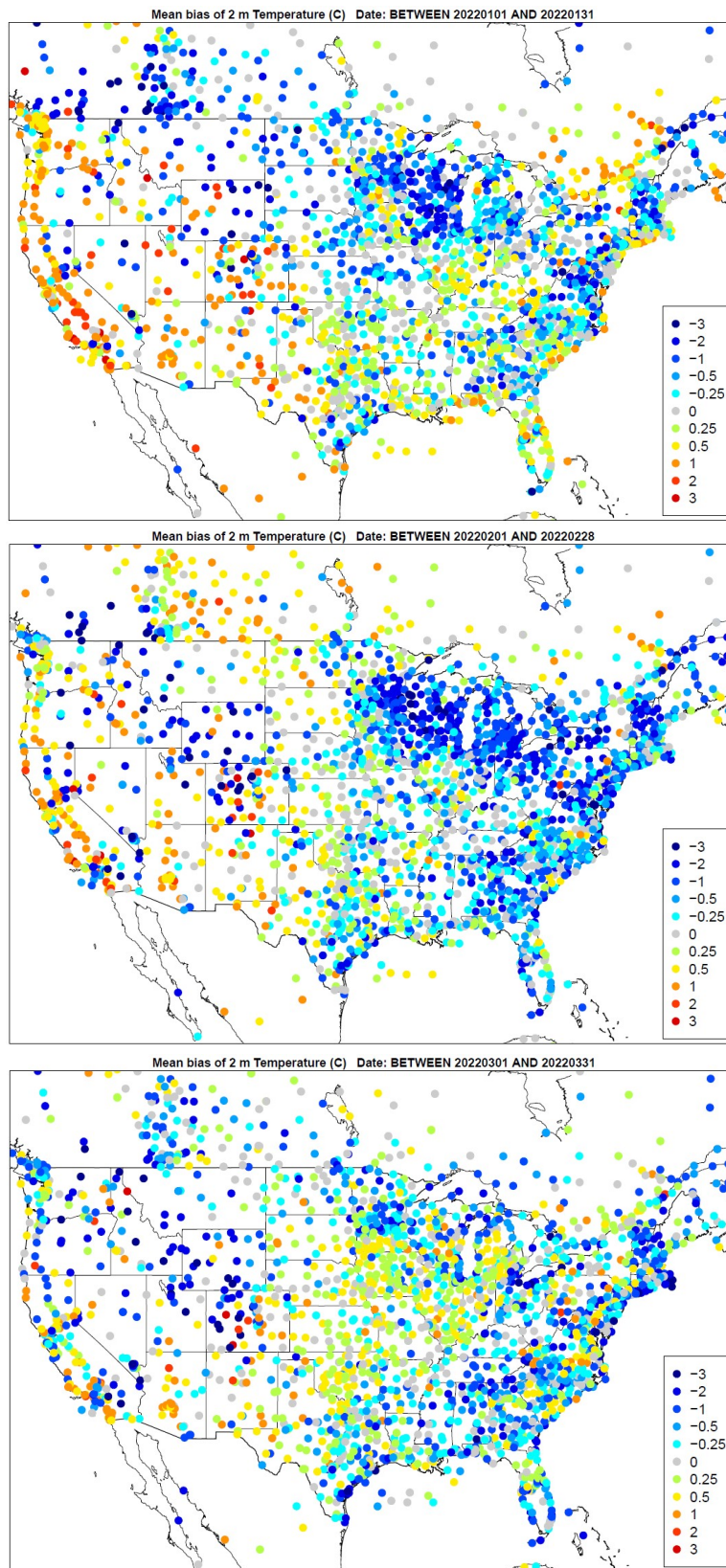
**Figure 3.2.8.** Spatial distribution of temperature bias (C) across all hours for the months of April, May, and June (top to bottom) for the 12US domain.



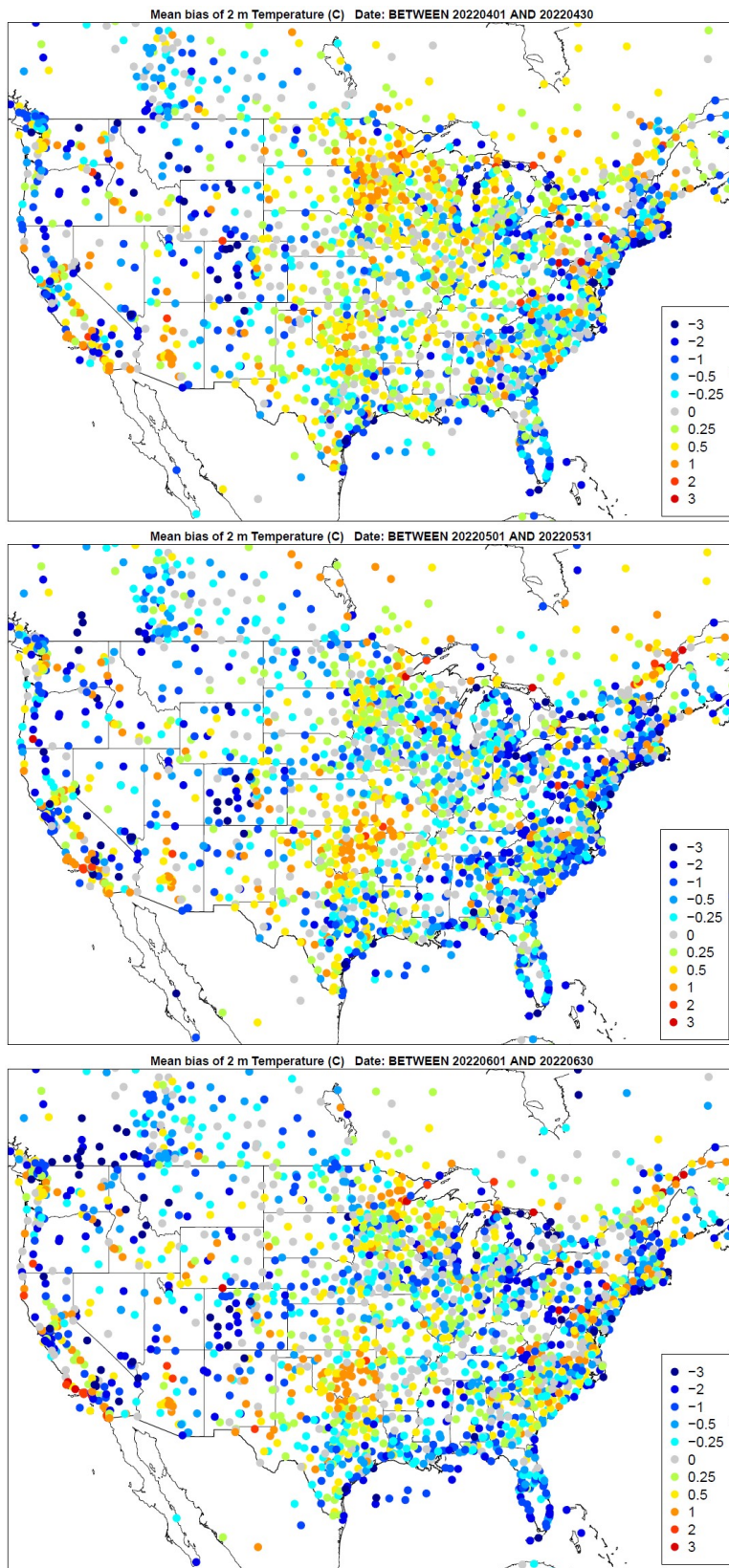
**Figure 3.2.9.** Spatial distribution of temperature bias (C) across all hours for the months of July, August, and September (top to bottom) for the 12US domain.



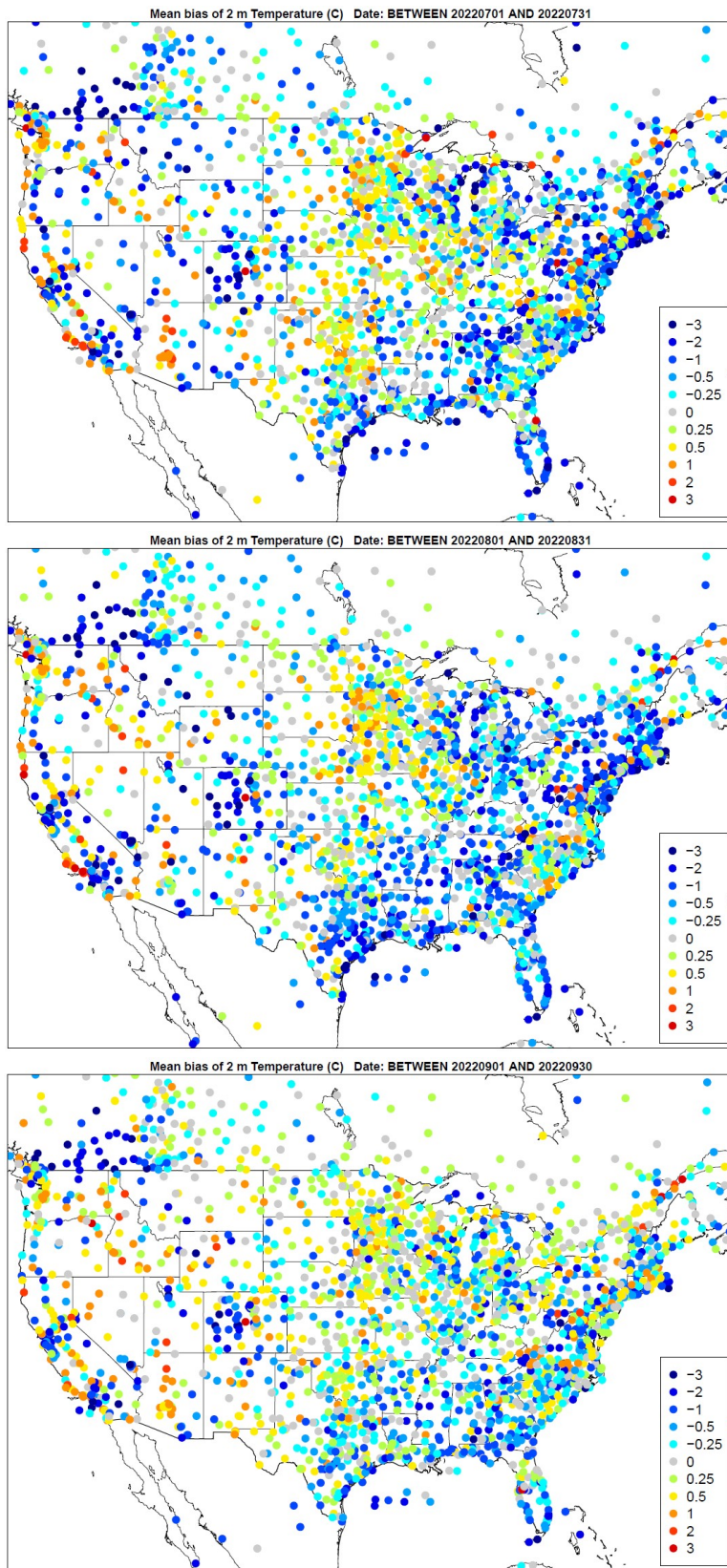
**Figure 3.2.10.** Spatial distribution of temperature bias (C) across all hours for the months of October, November, and December (top to bottom) for the 12US domain.



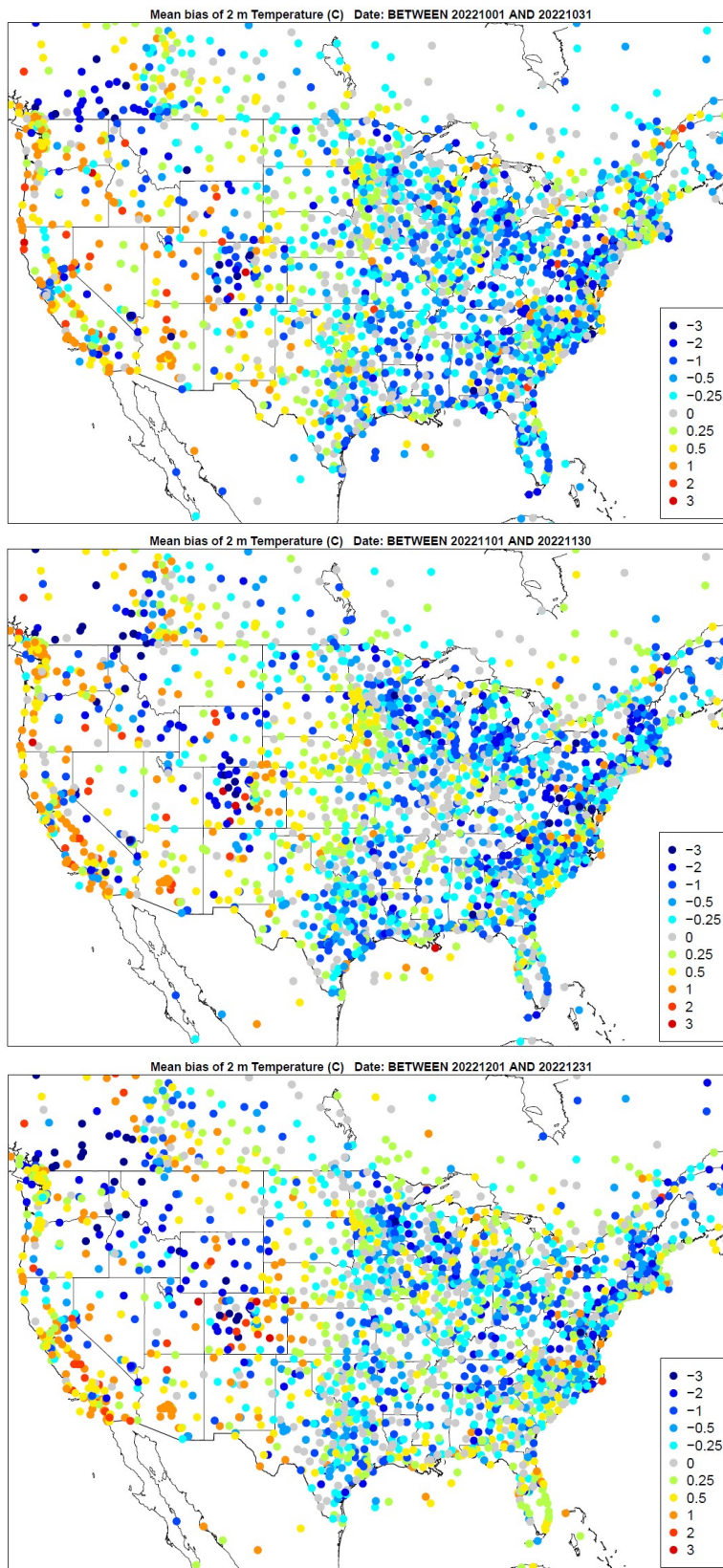
**Figure 3.2.11.** Spatial distribution of temperature bias (C) across daytime hours for the months of January, February, and March (top to bottom) for the 36NOAM domain.



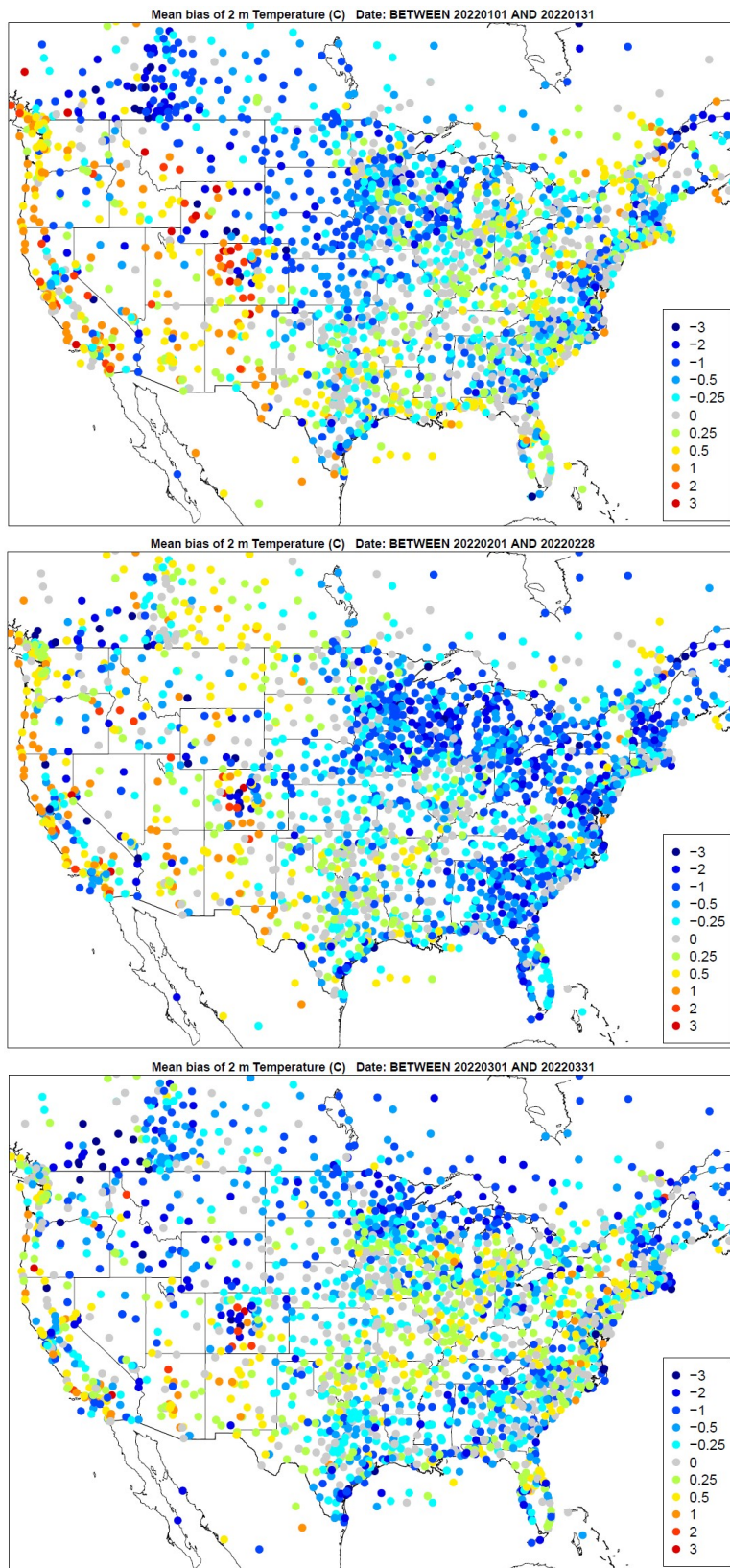
**Figure 3.2.12.** Spatial distribution of temperature bias (C) across daytime hours for the months of April, May, and June (top to bottom) for the 36NOAM domain.



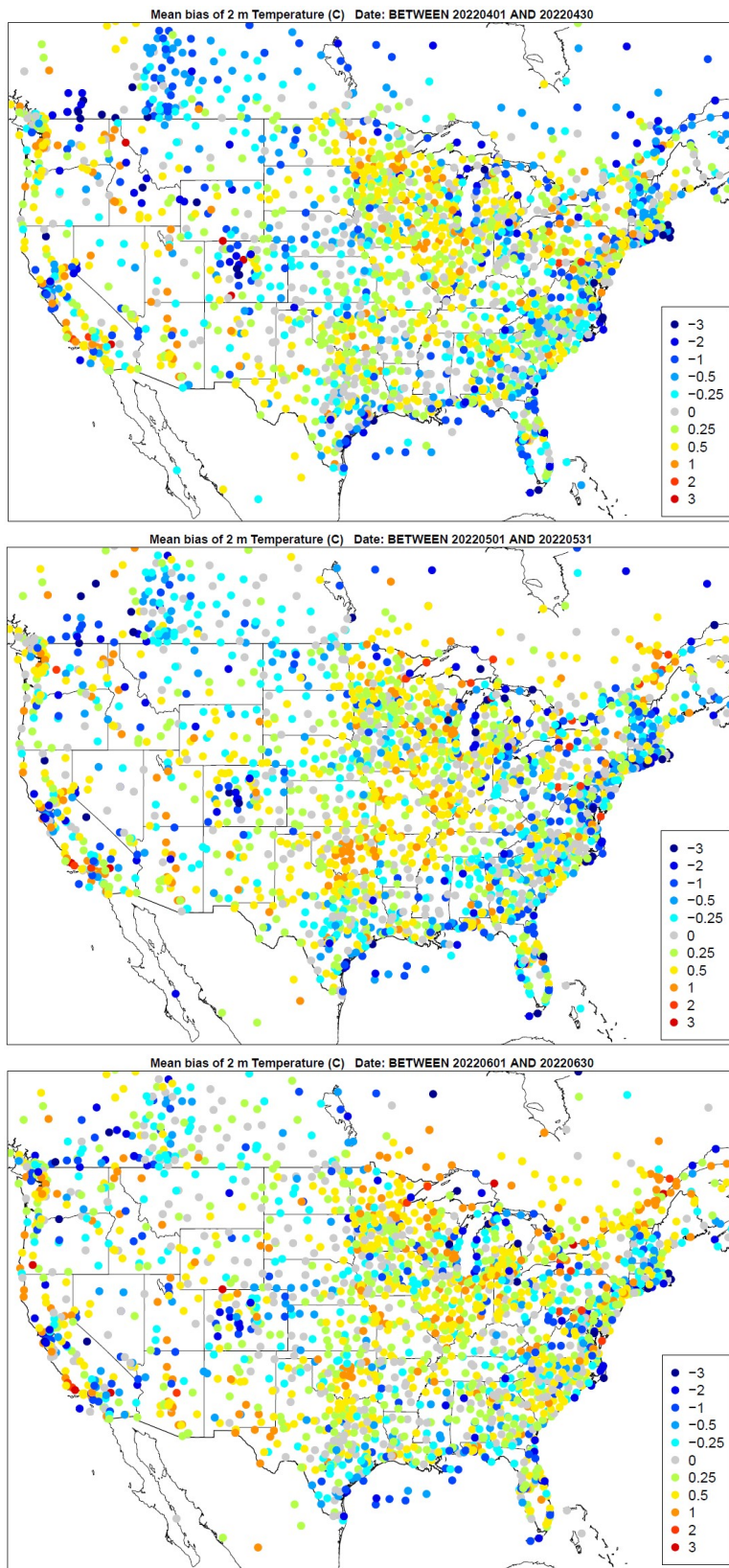
**Figure 3.2.13.** Spatial distribution of temperature bias (C) across daytime hours for the months of July, August, and September (top to bottom) for the 36NOAM domain.



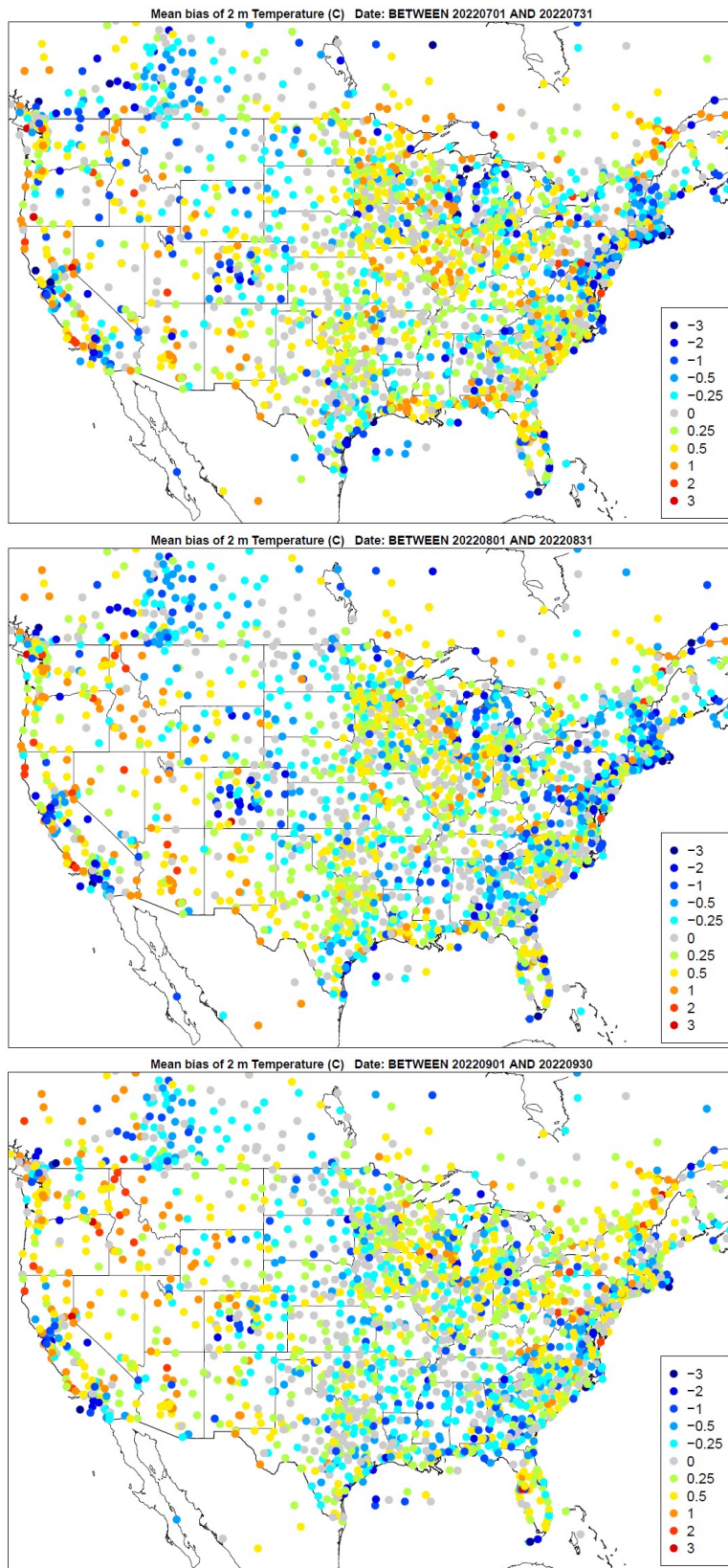
**Figure 3.2.14.** Spatial distribution of temperature bias (C) across daytime hours for the months of October, November, and December (top to bottom) for the 36NOAM domain.



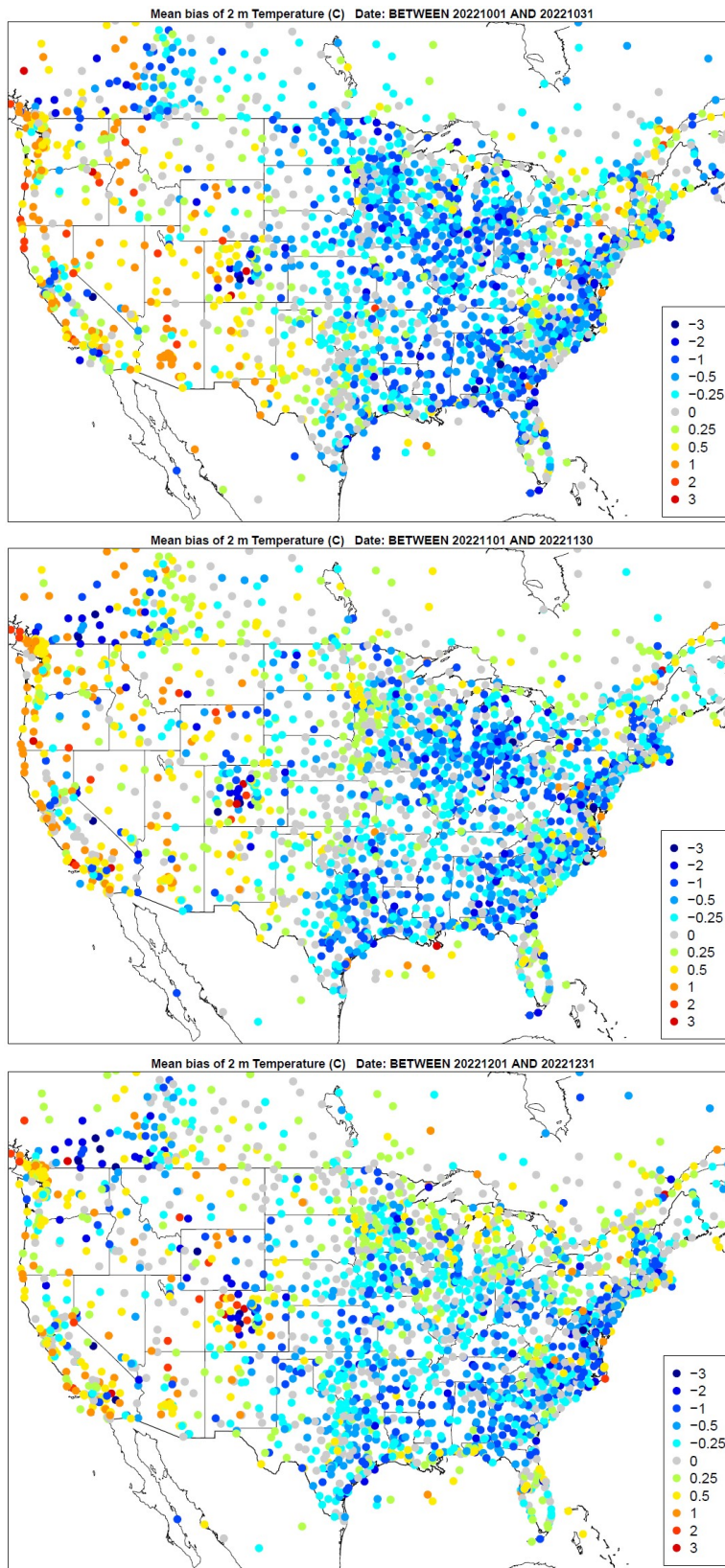
**Figure 3.2.15.** Spatial distribution of temperature bias (C) across daytime hours for the months of January, February, and March (top to bottom) for the 12US domain.



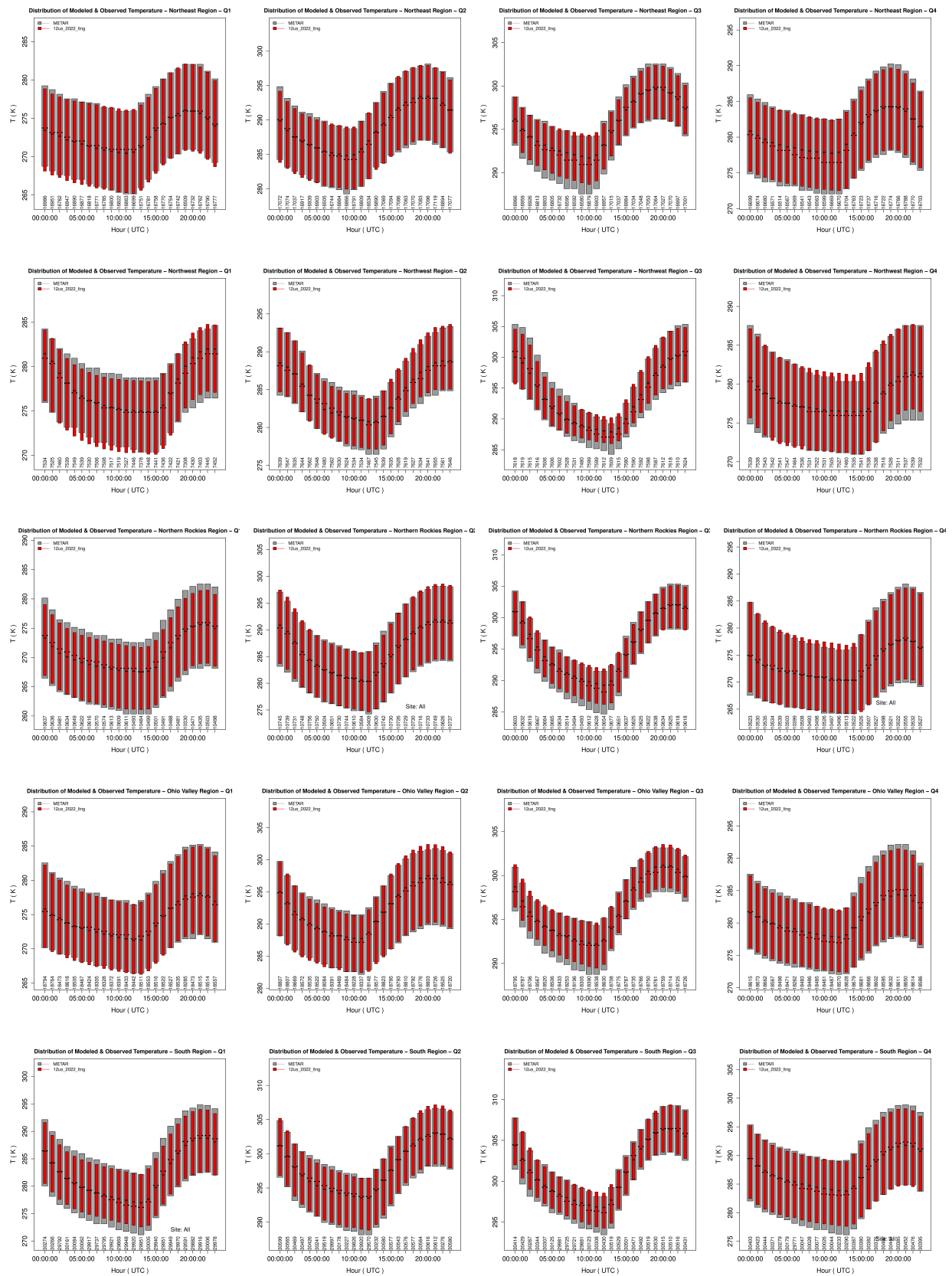
**Figure 3.2.16.** Spatial distribution of temperature bias (C) across daytime hours for the months of April, May, and June (top to bottom) for the 12US domain.



**Figure 3.2.17.** Spatial distribution of temperature bias (C) across daytime hours for the months of July, August, and September (top to bottom) for the 12US domain.



**Figure 3.2.18.** Spatial distribution of temperature bias (C) across daytime hours for the months of October, November, and December (top to bottom) for the 12US domain.



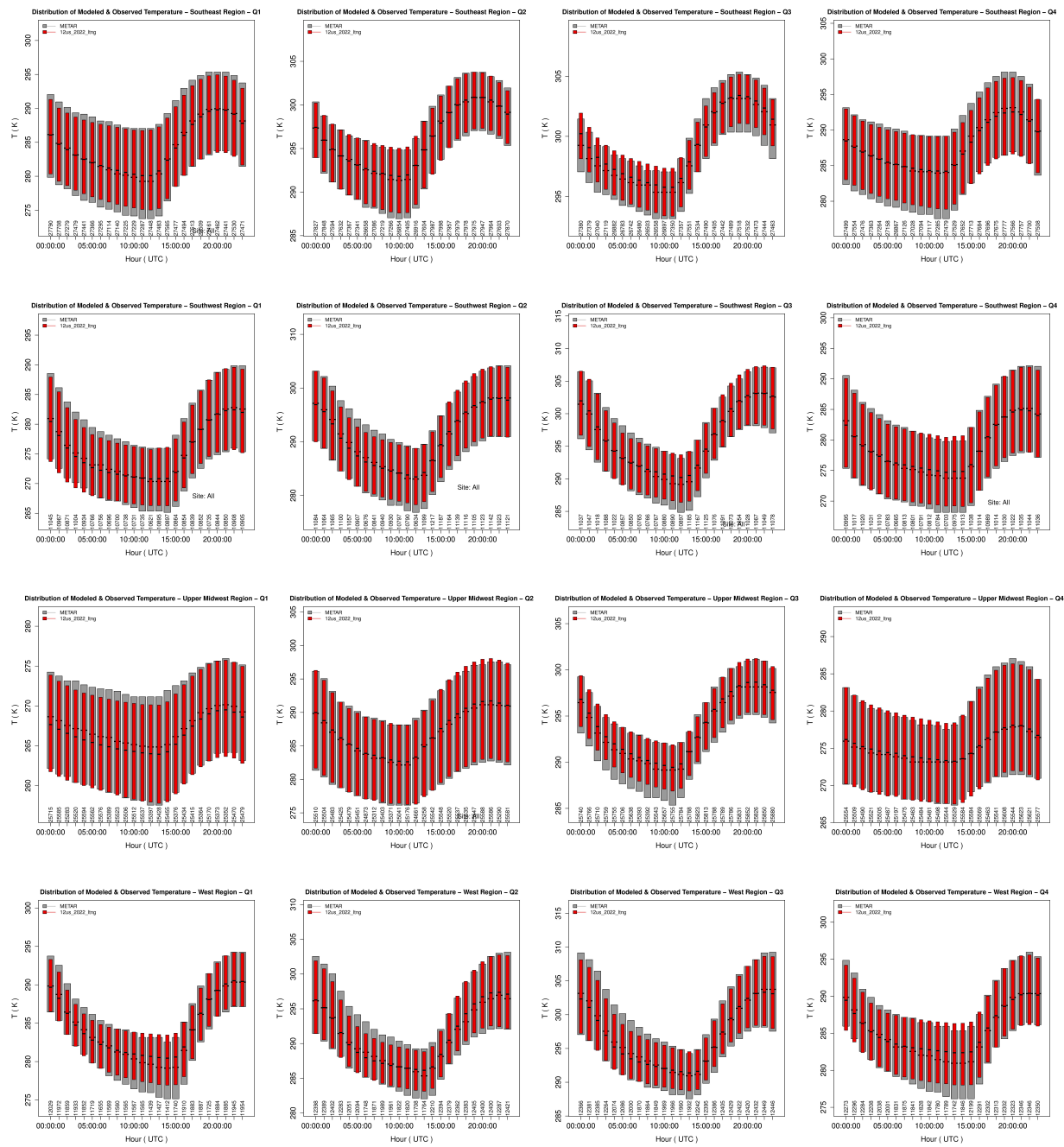


**Figure 3.2.19.** Hourly average distribution of observed and predicted temperatures (K) for the 12US domain in the Northeast, Northwest, Northern Rockies & Plains, Ohio Valley, South, Southeast, Southwest, Upper Midwest, and West Climate Regions (respectively, top to bottom) for each quarter.

Climate Region	Season	Mean Obs	Mean Mod	MAE	MB	NMB	NME	RMSE
Northeast	Q1	273.15	272.96	1.71	-0.19	-0.07	0.63	2.27
	Q2	288.21	288.25	1.39	0.04	0.01	0.48	1.88
	Q3	294.68	294.96	1.3	0.28	0.1	0.44	1.8
	Q4	279.9	280.02	1.6	0.11	0.04	0.57	2.12
N. Rockies & Plains	Q1	269.78	269.55	2.08	-0.24	-0.09	0.77	2.69
	Q2	285.6	285.73	1.48	0.14	0.05	0.52	1.98
	Q3	294.53	294.87	1.48	0.34	0.12	0.5	2.01
	Q4	273.17	273.33	1.99	0.16	0.06	0.73	2.63
Northwest	Q1	276.42	276.44	1.85	0.02	0.01	0.67	2.48
	Q2	284.58	284.64	1.43	0.06	0.02	0.5	1.91
	Q3	293.59	293.86	1.69	0.27	0.09	0.58	2.26
	Q4	277.92	278.27	1.86	0.35	0.13	0.67	2.49
Ohio Valley	Q1	274.91	274.75	1.49	-0.16	-0.06	0.54	1.94
	Q2	290.97	291.12	1.36	0.14	0.05	0.47	1.77
	Q3	295.7	296.1	1.18	0.39	0.13	0.4	1.59
	Q4	280.14	280.06	1.47	-0.08	-0.03	0.53	1.9
South	Q1	281.95	282.01	1.74	0.06	0.02	0.62	2.22
	Q2	296.65	296.79	1.27	0.14	0.05	0.43	1.72
	Q3	300.69	300.95	1.12	0.25	0.08	0.37	1.57
	Q4	286.23	286.35	1.58	0.12	0.04	0.55	2.08
Southeast	Q1	284.29	284.28	1.59	-0.01	0	0.56	2.06
	Q2	295.05	295.2	1.28	0.15	0.05	0.43	1.71
	Q3	298.35	298.67	1.19	0.32	0.11	0.4	1.62
	Q4	286.86	286.95	1.53	0.09	0.03	0.53	2
Southwest	Q1	275.72	275.75	2.17	0.04	0.01	0.79	2.89
	Q2	290.26	290.27	1.94	0.02	0.01	0.67	2.61
	Q3	295.8	296.17	1.81	0.37	0.13	0.61	2.45
	Q4	278.61	278.94	2.02	0.33	0.12	0.73	2.67
Upper Midwest	Q1	266.51	266.18	1.72	-0.33	-0.12	0.64	2.29
	Q2	286.17	286.28	1.43	0.11	0.04	0.5	1.91
	Q3	292.9	293.33	1.28	0.43	0.15	0.44	1.71
	Q4	274.91	274.93	1.55	0.02	0.01	0.56	2.01
West	Q1	283.82	283.85	1.86	0.03	0.01	0.65	2.49
	Q2	291.58	291.42	1.71	-0.17	-0.06	0.59	2.31
	Q3	297.2	297.07	1.7	-0.13	-0.04	0.57	2.31
	Q4	285.12	285.37	1.76	0.25	0.09	0.62	2.38

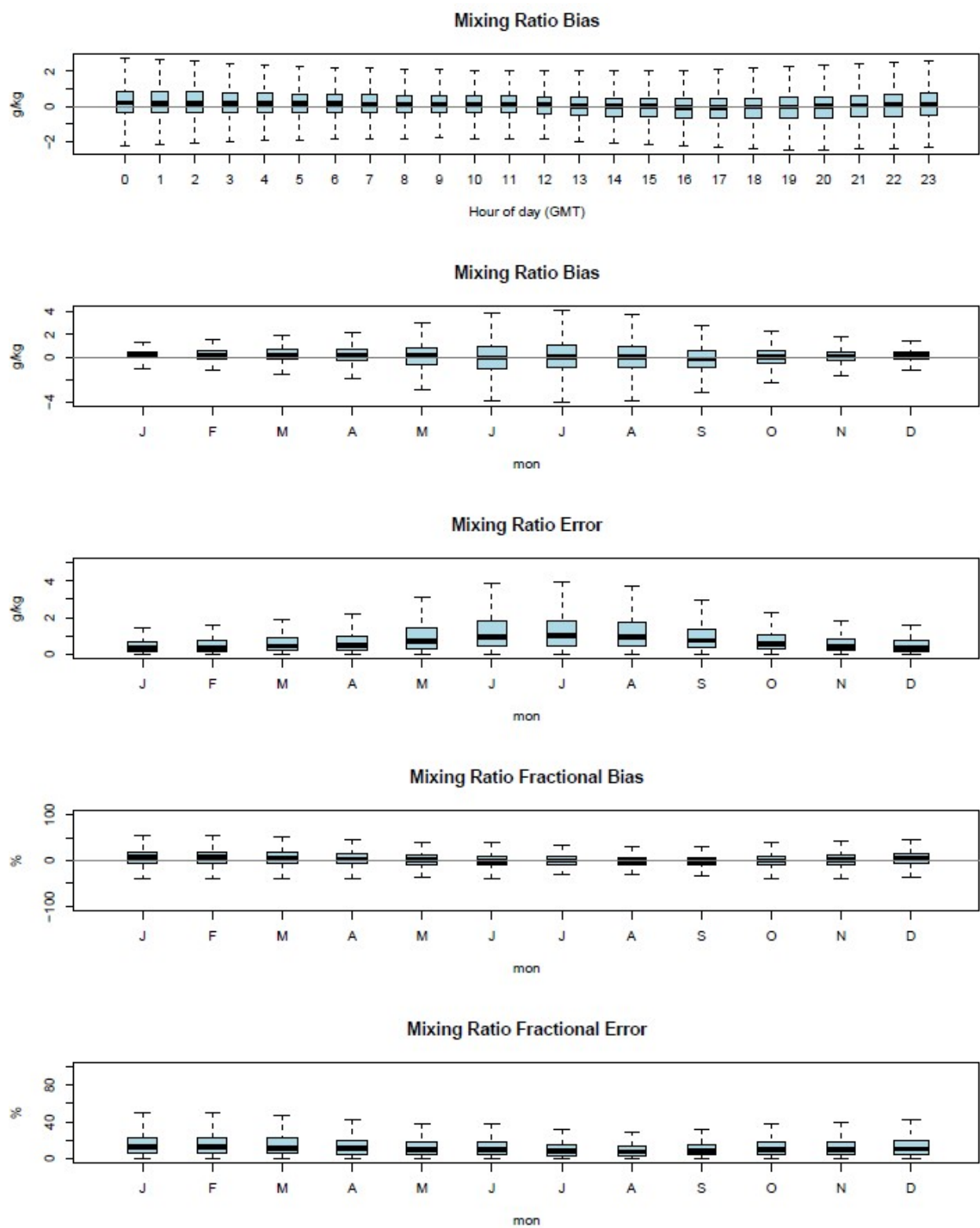
**Table 3.2.1.** Mean observed, mean modeled, mean absolute error (MAE), mean bias (MB), normalized mean bias (NMB), normalized mean error (NME), and root mean square error (RMSE) for temperature (K) for the 12US domain.

### 3.3 Model Performance for Mixing Ratio

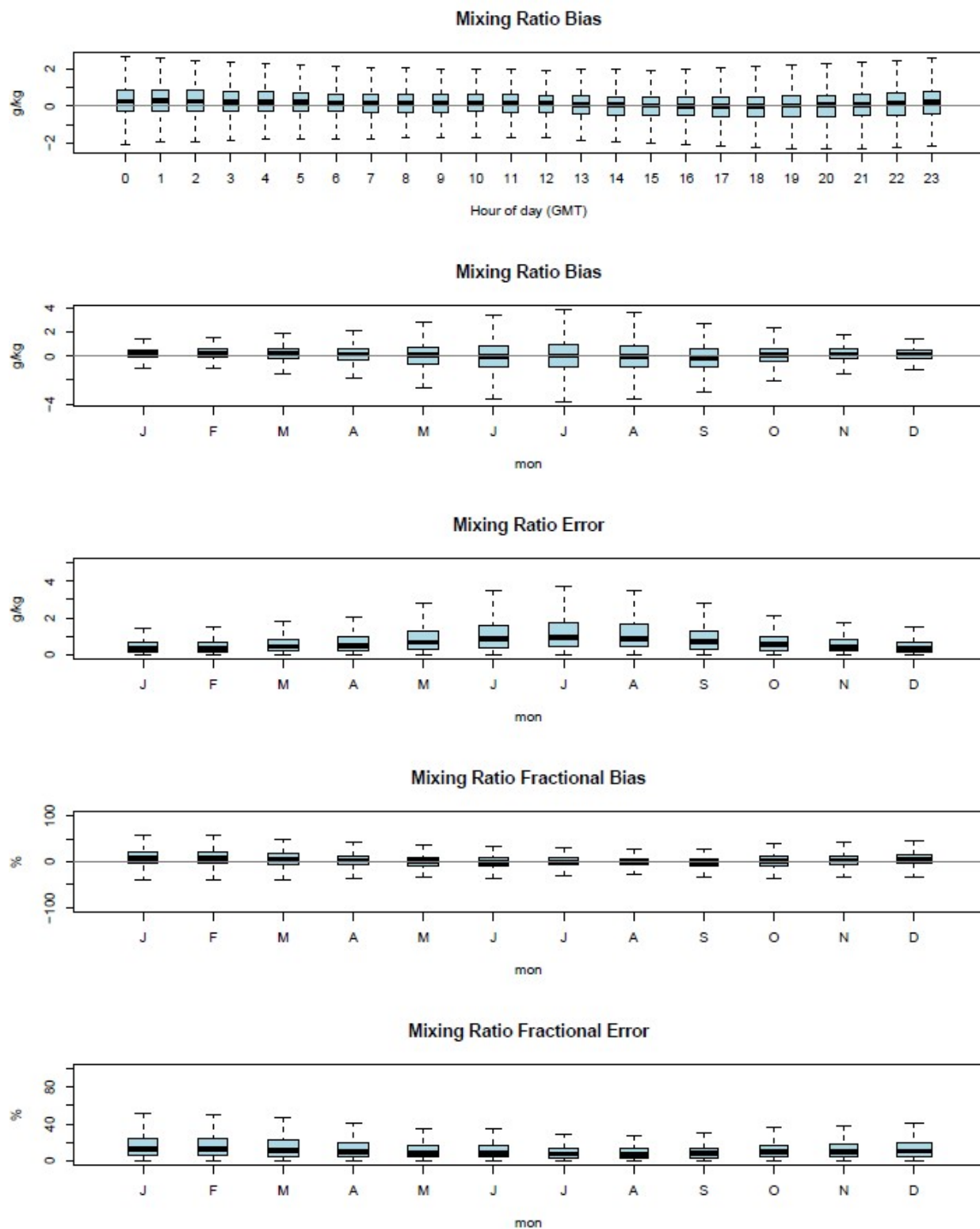
Water mixing ratio estimates are compared to the ds472 observation network described earlier and are presented below for the 36NOAM (Figure 3.3.1) and 12US (Figure 3.3.2) domains. Regional analysis of statistical metrics for water vapor mixing ratio performance by quarter is shown in Table 3.3.1 for the 12US domain only.

Mixing ratio is generally overpredicted across most hours of the day with a greater spread in the bias in the early morning and evening hours. Increased spread in the bias also occurs during the late Spring to early Fall when increased moisture levels across the country are noted. In general, the model error is less than a g/kg across the year and all hours of the day.

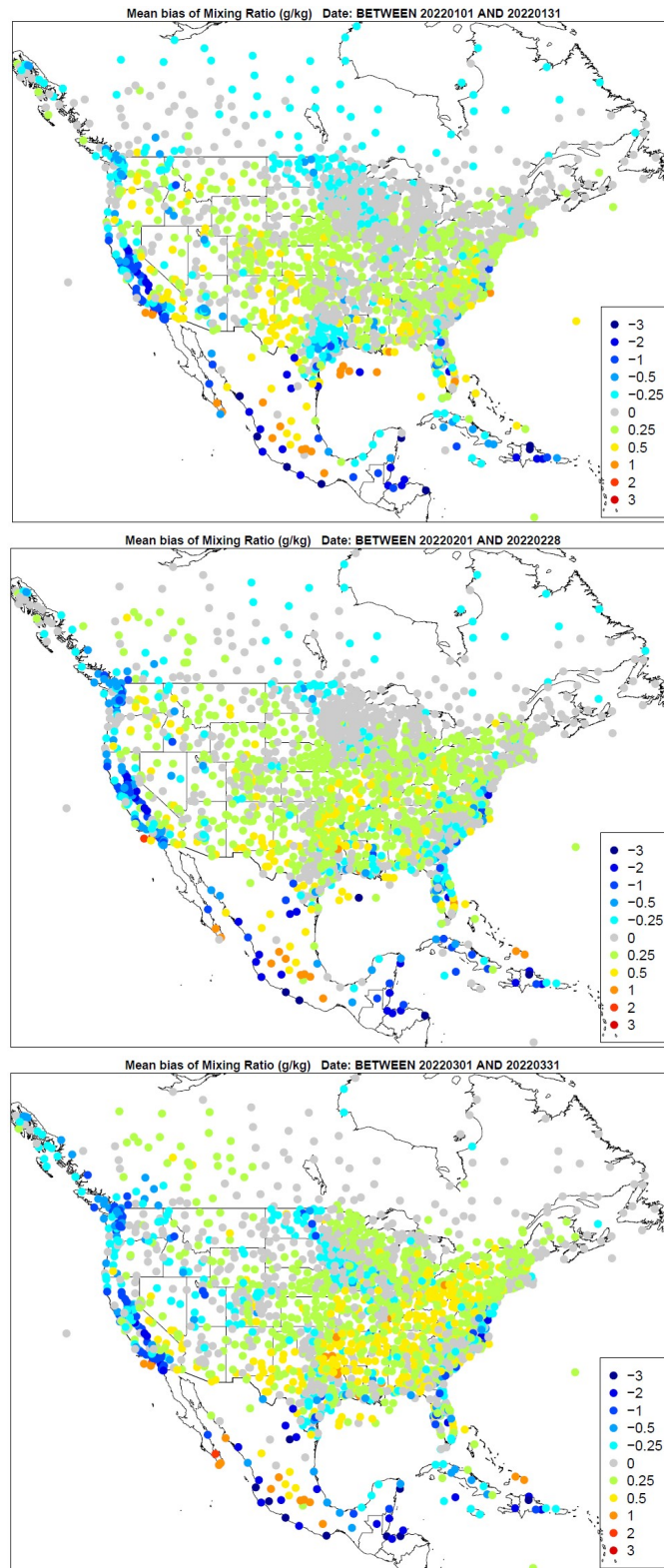
The monthly spatial distributions of the mixing ratio bias across all hours are shown for the 36NOAM (Figures 3.3.3-3.3.6) and 12US (Figures 3.3.7-3.3.10) domains. Monthly spatial distributions of the mixing ratio bias across daytime hours only are shown for the 36NOAM (Figures 3.3.11-3.3.14) and 12US (Figures 3.3.15-3.3.18) domains. Hourly distributions of the observed and predicted mixing ratios are shown for each Climate Region and quarter in Figure 3.3.19. As noted in the earlier figures, a general overprediction of moisture is observed across much of the year, particularly in the Winter and Spring in the eastern US for both the 36NOAM and 12US domains. An underprediction during the months of September and October is noted in both domains. In the 12US simulation, there is a noticeable overprediction in the southeast during July. Some slight variations appear across regions, with a noticeable underprediction of moisture that persists across the Southeast for much of the year. During daytime hours only, there is an underprediction during the late Spring months through the Summer period in both the 36NOAM and 12US simulations. The slight overprediction during the Winter and late Fall periods persists during the daytime hours, as well.



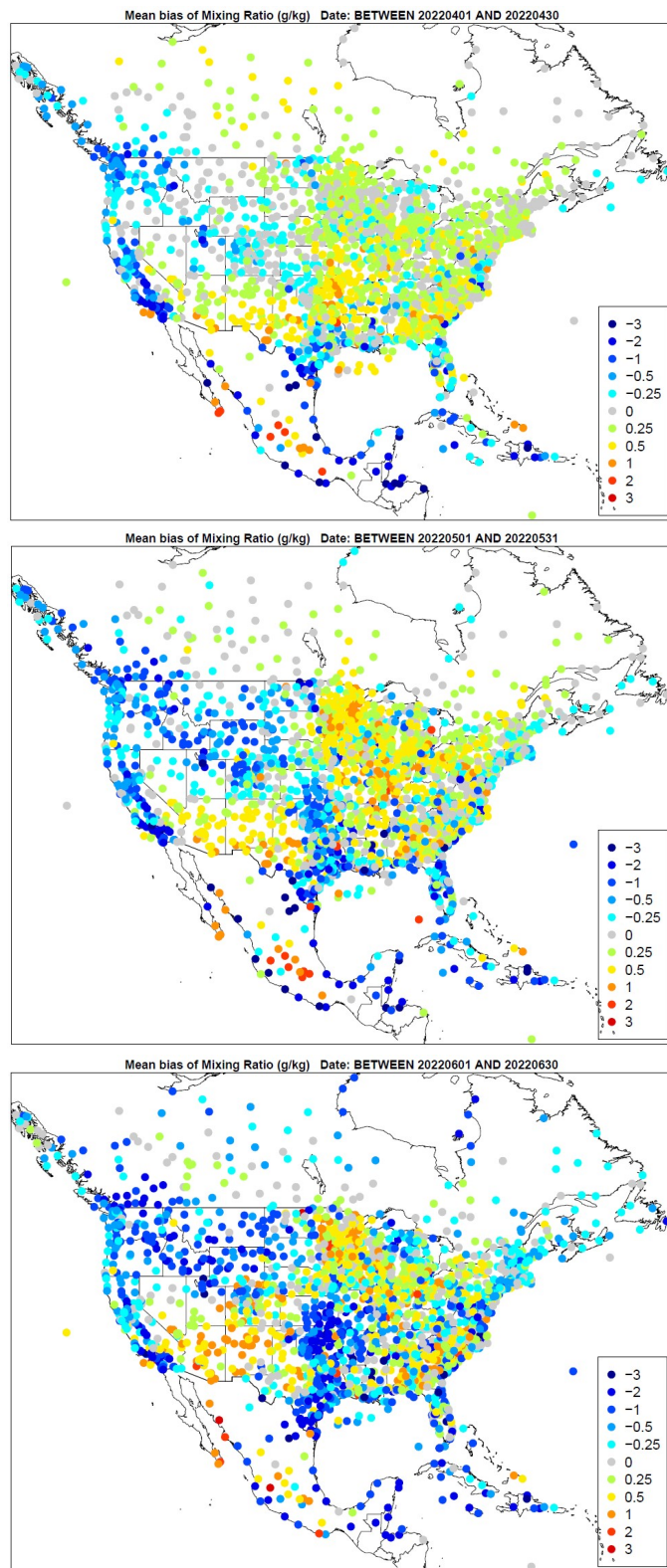
**Figure 3.3.1.** Distribution of hourly bias by hour and hourly bias, error, fractional bias, and fractional error for water vapor mixing ratio by month for the 36NOAM domain.



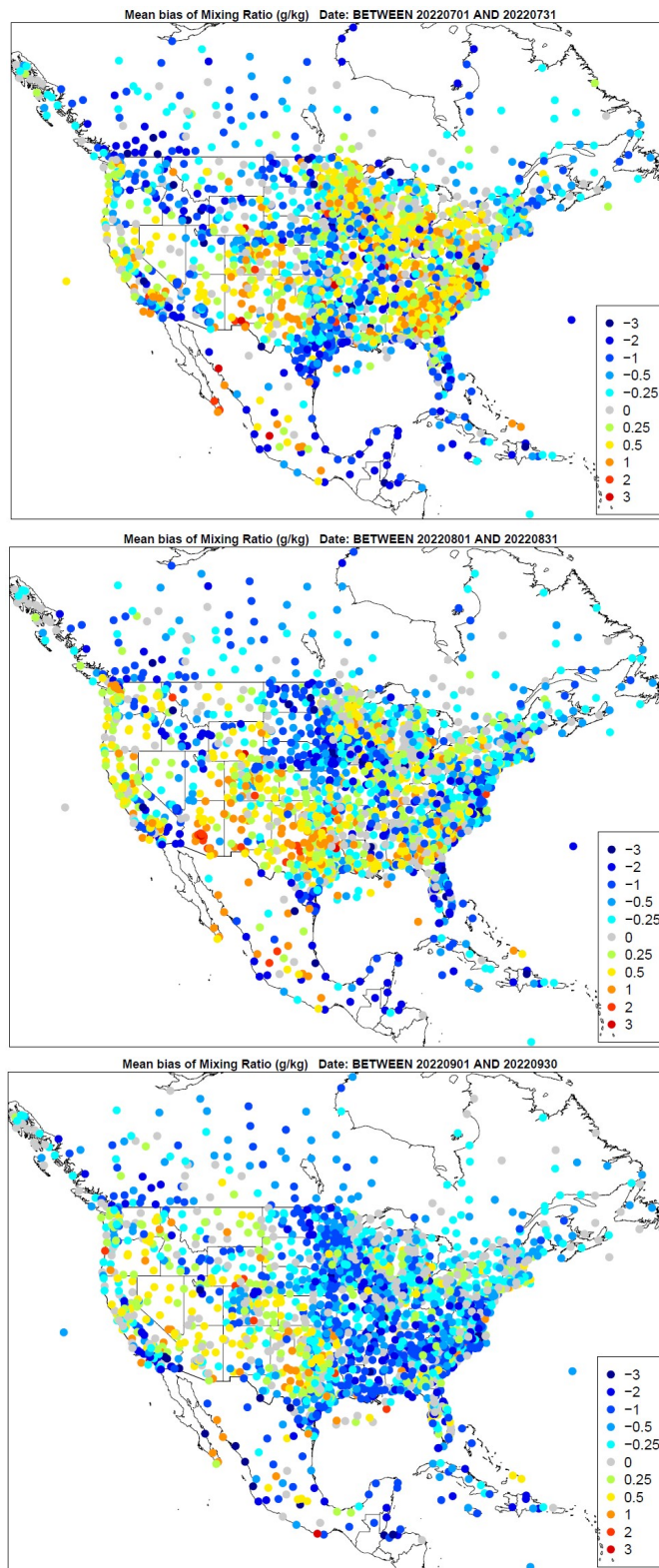
**Figure 3.3.2.** Distribution of hourly bias by hour and hourly bias, error, fractional bias, and fractional error for water vapor mixing ratio by month for the 12US domain.



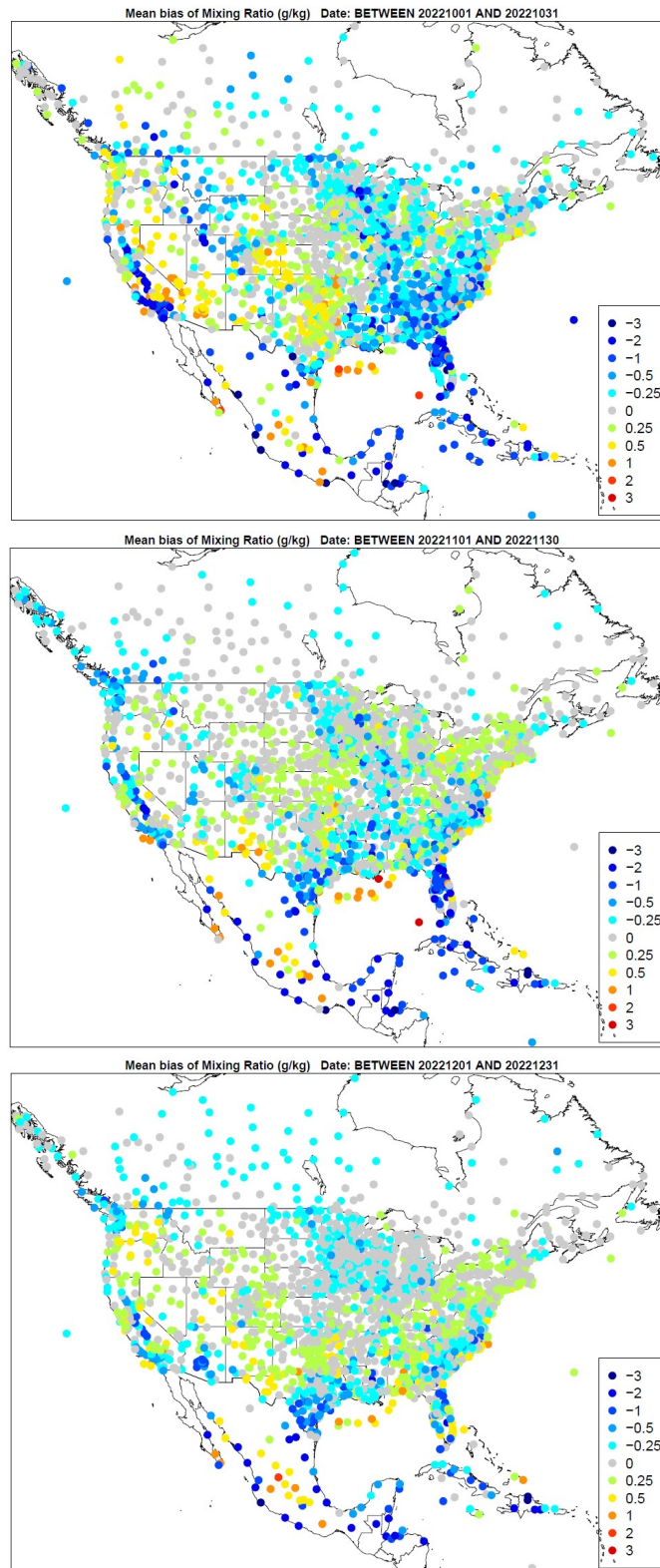
**Figure 3.3.3.** Spatial distribution of water vapor mixing ratio bias (g/kg) across all hours for the months of January, February, and March (top to bottom) for the 36NOAM domain.



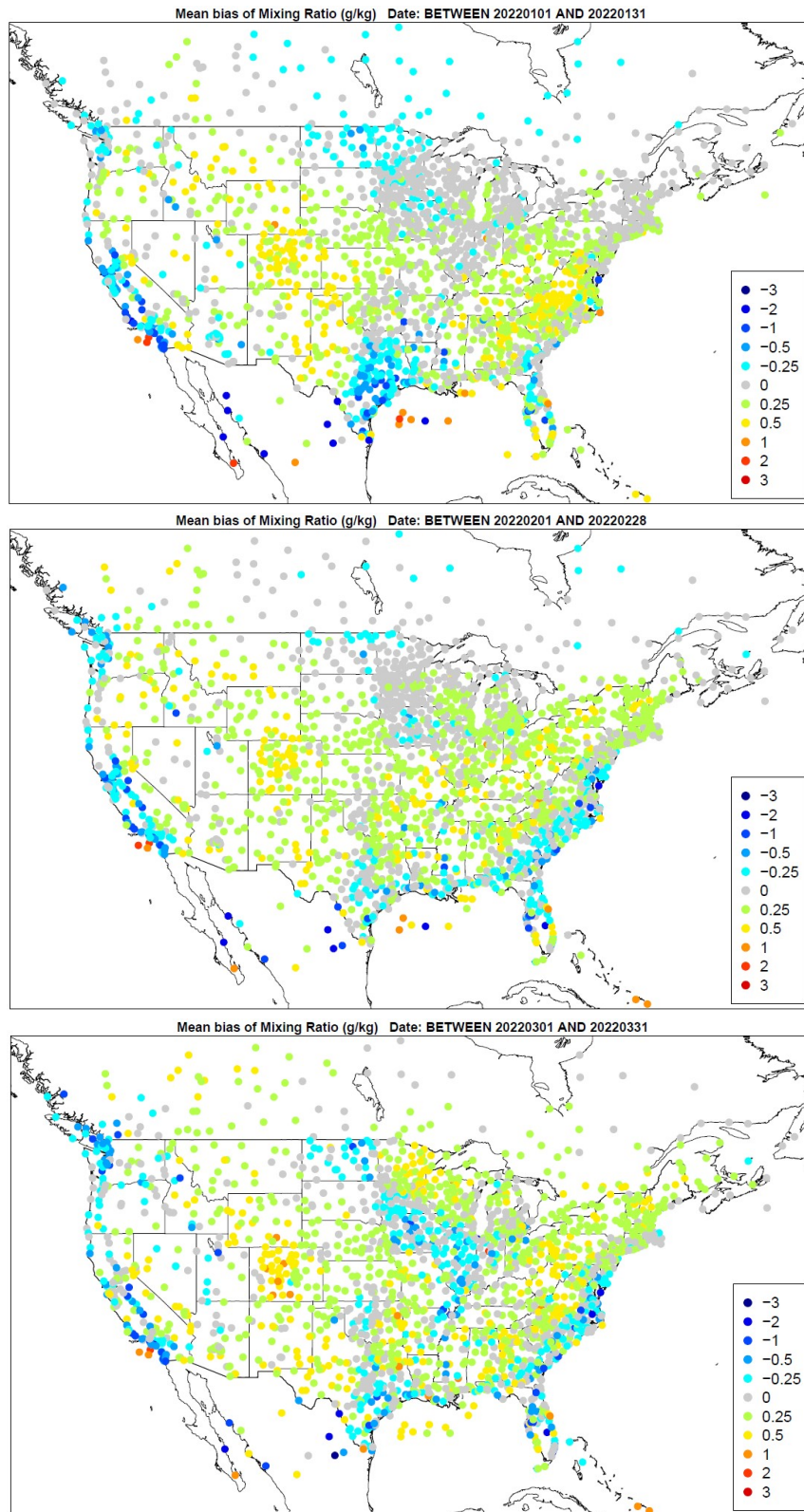
**Figure 3.3.4.** Spatial distribution of water vapor mixing ratio bias (g/kg) across all hours for the months of April, May, and June (top to bottom) for the 36NOAM domain.



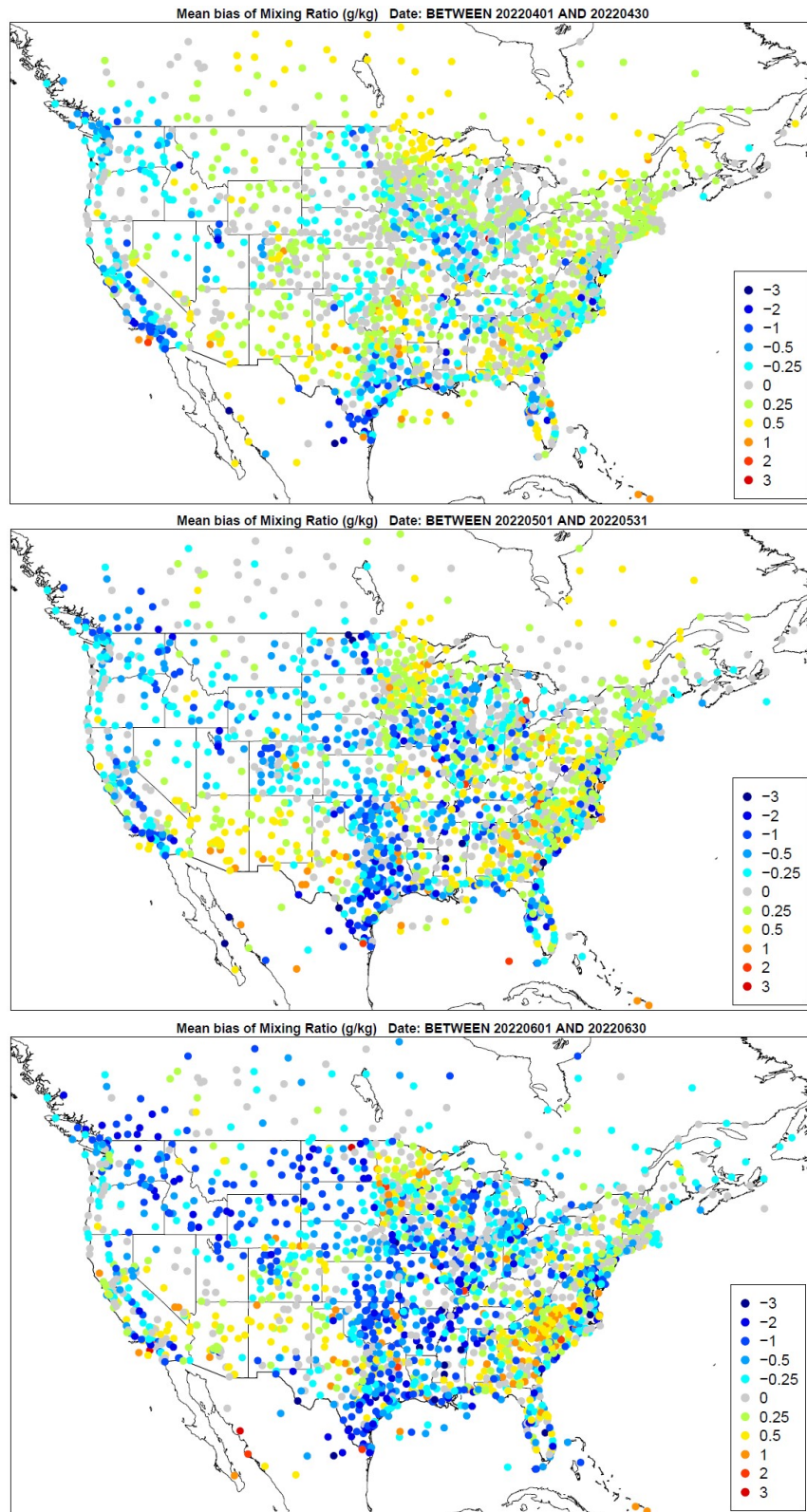
**Figure 3.3.5.** Spatial distribution of water vapor mixing ratio bias (g/kg) across all hours for the months of July, August, and September (top to bottom) for the 36NOAM domain.



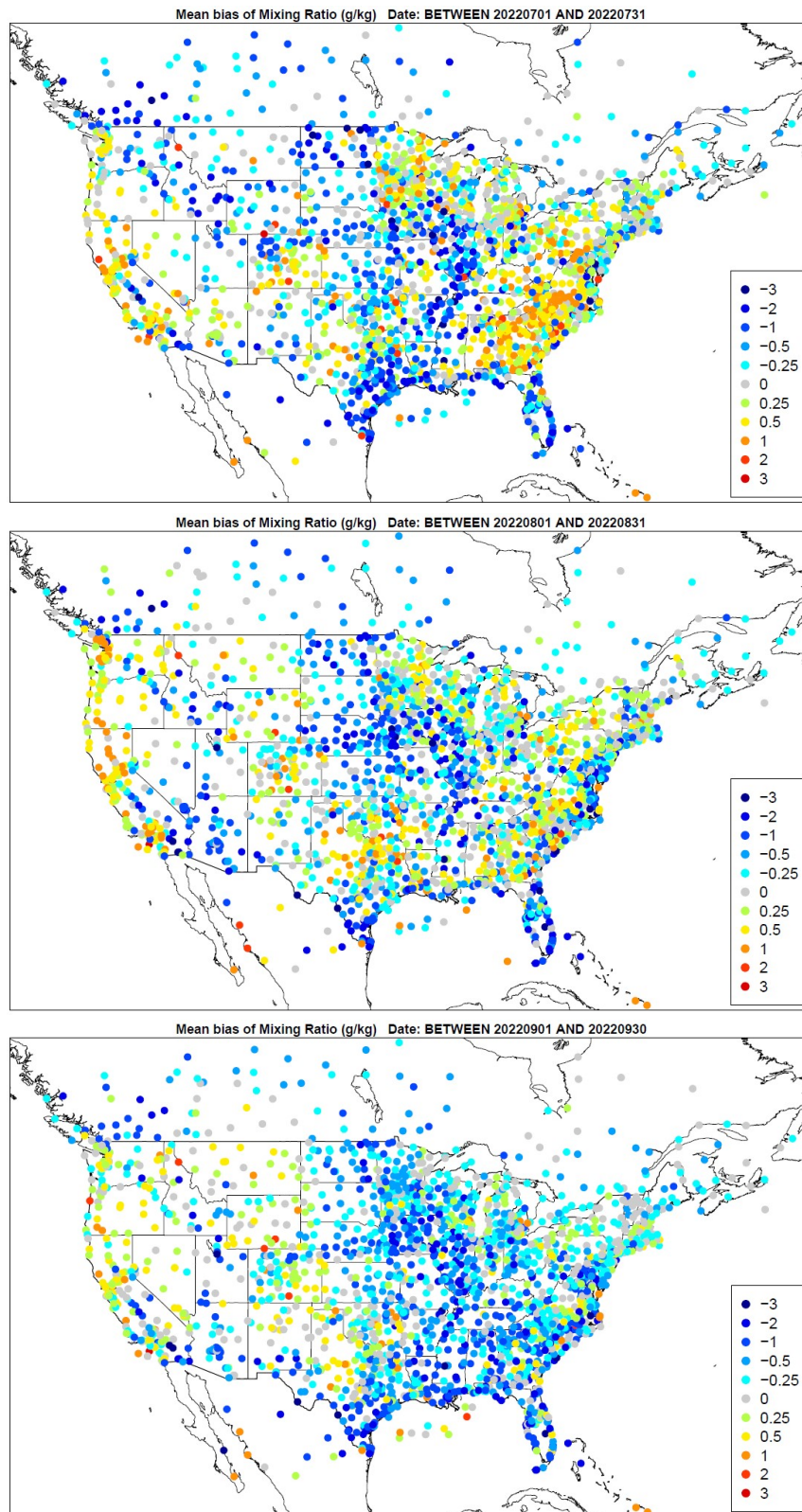
**Figure 3.3.6.** Spatial distribution of water vapor mixing ratio bias (g/kg) across all hours for the months of October, November, and December (top to bottom) for the 36NOAM domain.



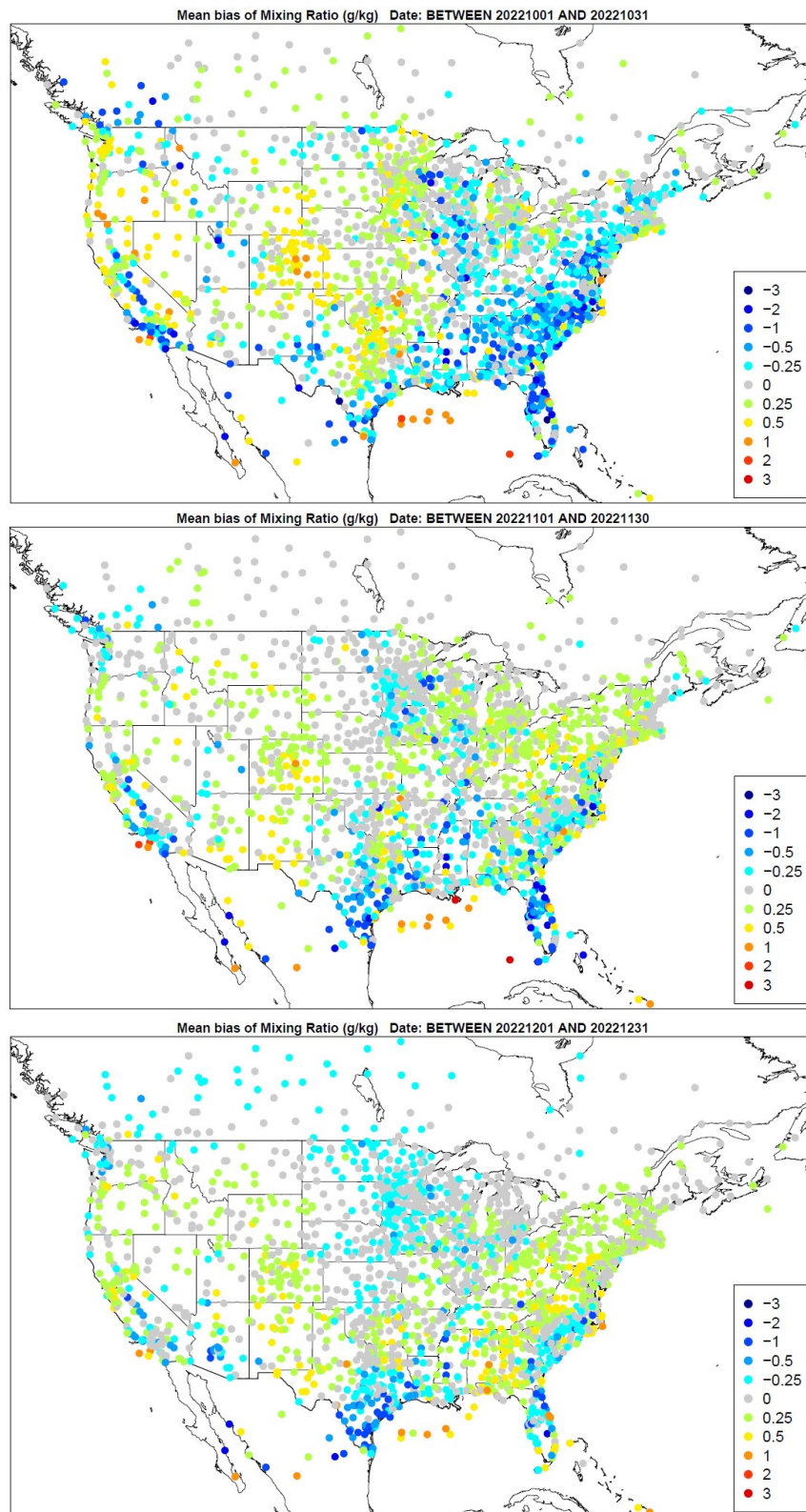
**Figure 3.3.7.** Spatial distribution of water vapor mixing ratio bias (g/kg) across all hours for the months of January, February, and March (top to bottom) for the 12US domain.



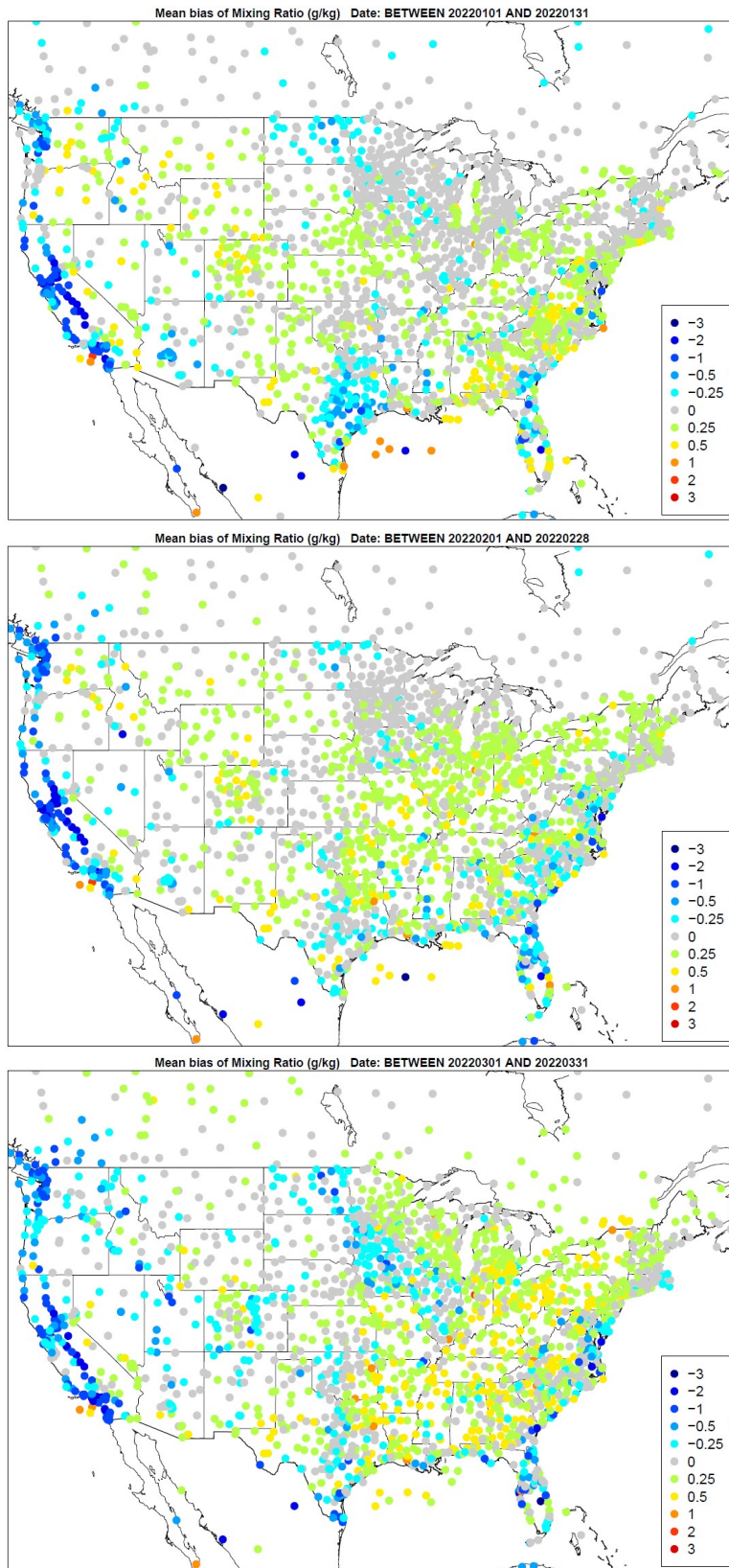
**Figure 3.3.8.** Spatial distribution of water vapor mixing ratio bias (g/kg) across all hours for the months of April, May, and June (top to bottom) for the 12US domain.



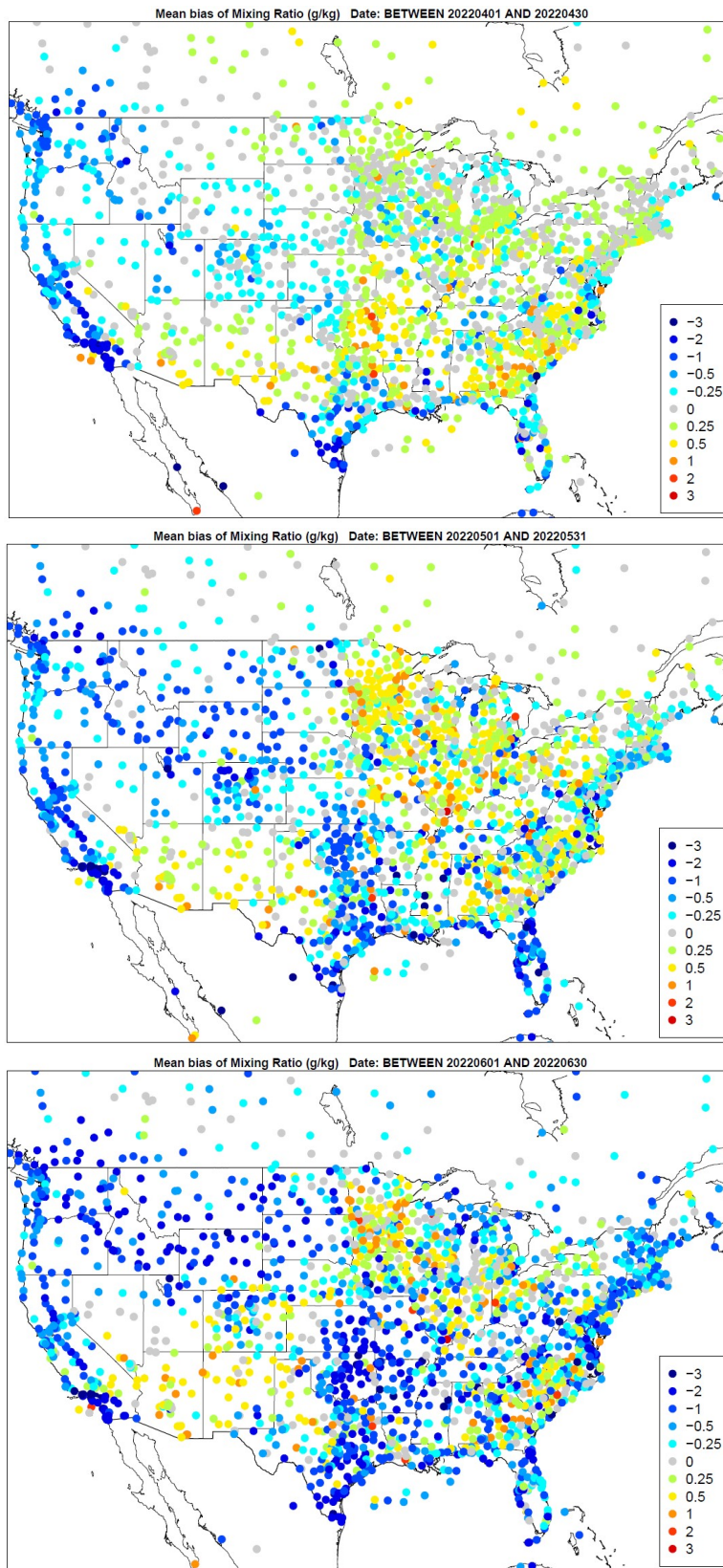
**Figure 3.3.9.** Spatial distribution of water vapor mixing ratio bias (g/kg) across all hours for the months of July, August, and September (top to bottom) for the 12US domain.



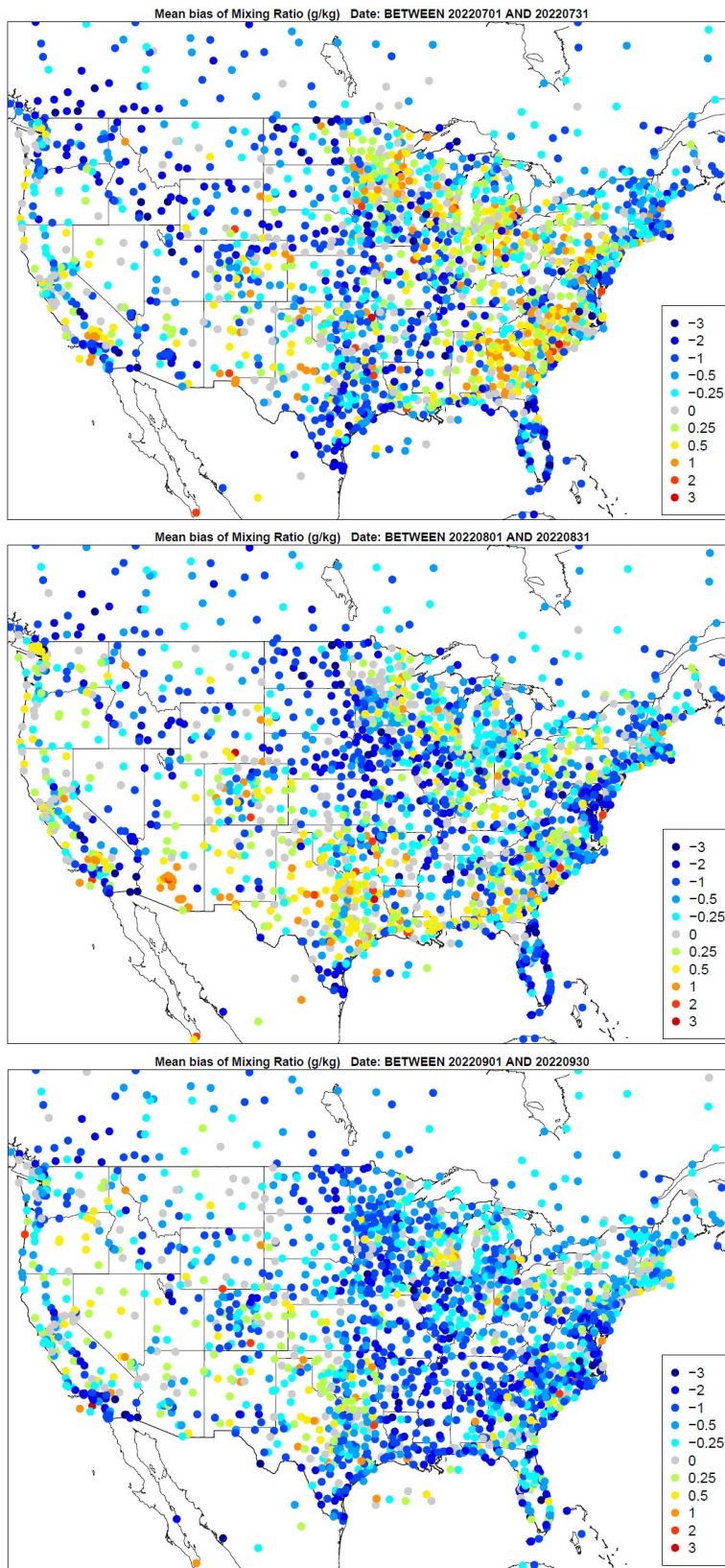
**Figure 3.3.10.** Spatial distribution of water vapor mixing ratio bias (g/kg) across all hours for the months of October, November, and December (top to bottom) for the 12US domain.



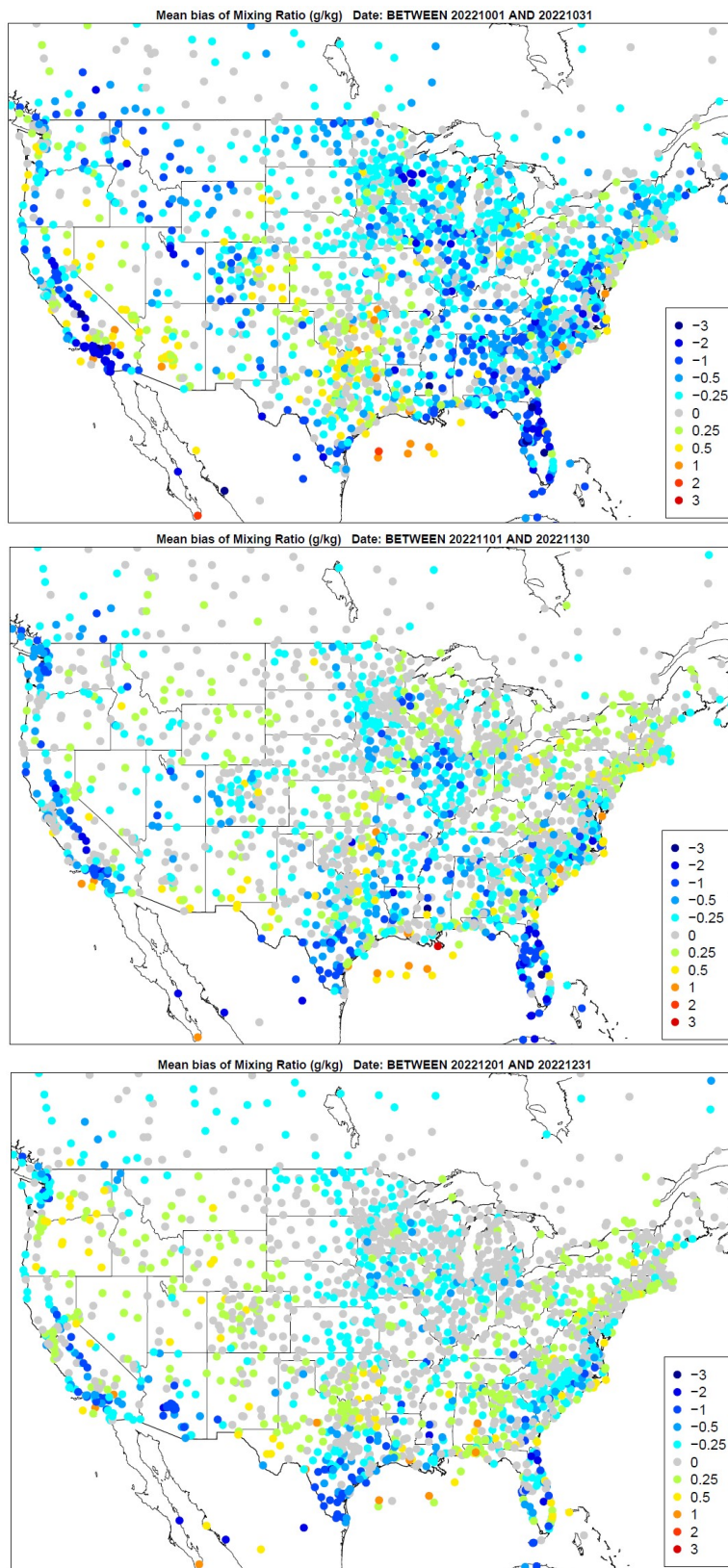
**Figure 3.3.11.** Spatial distribution of water vapor mixing ratio bias (g/kg) across daytime hours for the months of January, February, and March (top to bottom) for the 36NOAM domain.



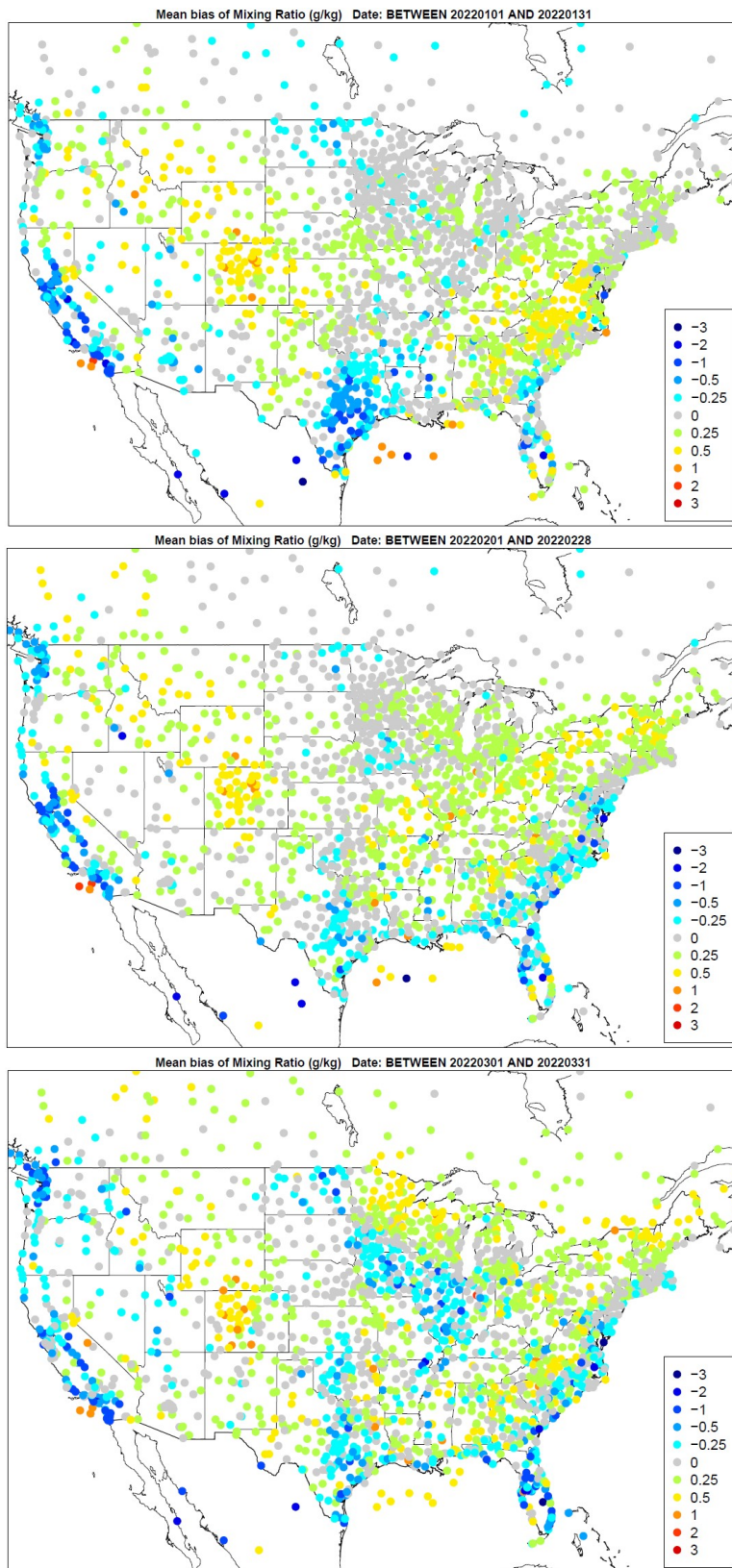
**Figure 3.3.12.** Spatial distribution of water vapor mixing ratio bias (g/kg) across daytime hours for the months of April, May, and June (top to bottom) for the 36NOAM domain.



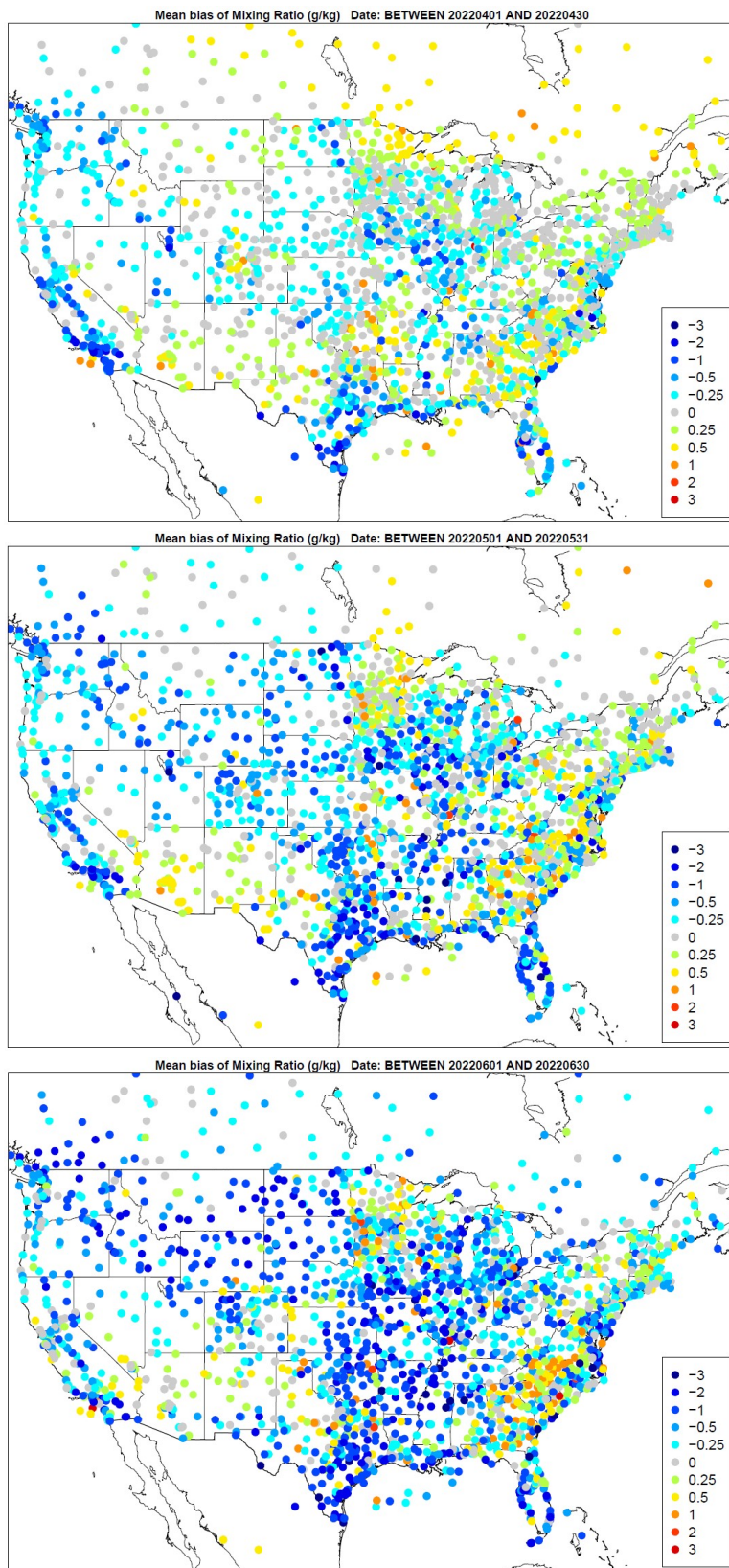
**Figure 3.3.13.** Spatial distribution of water vapor mixing ratio bias (g/kg) across daytime hours for the months of July, August, and September (top to bottom) for the 36NOAM domain.



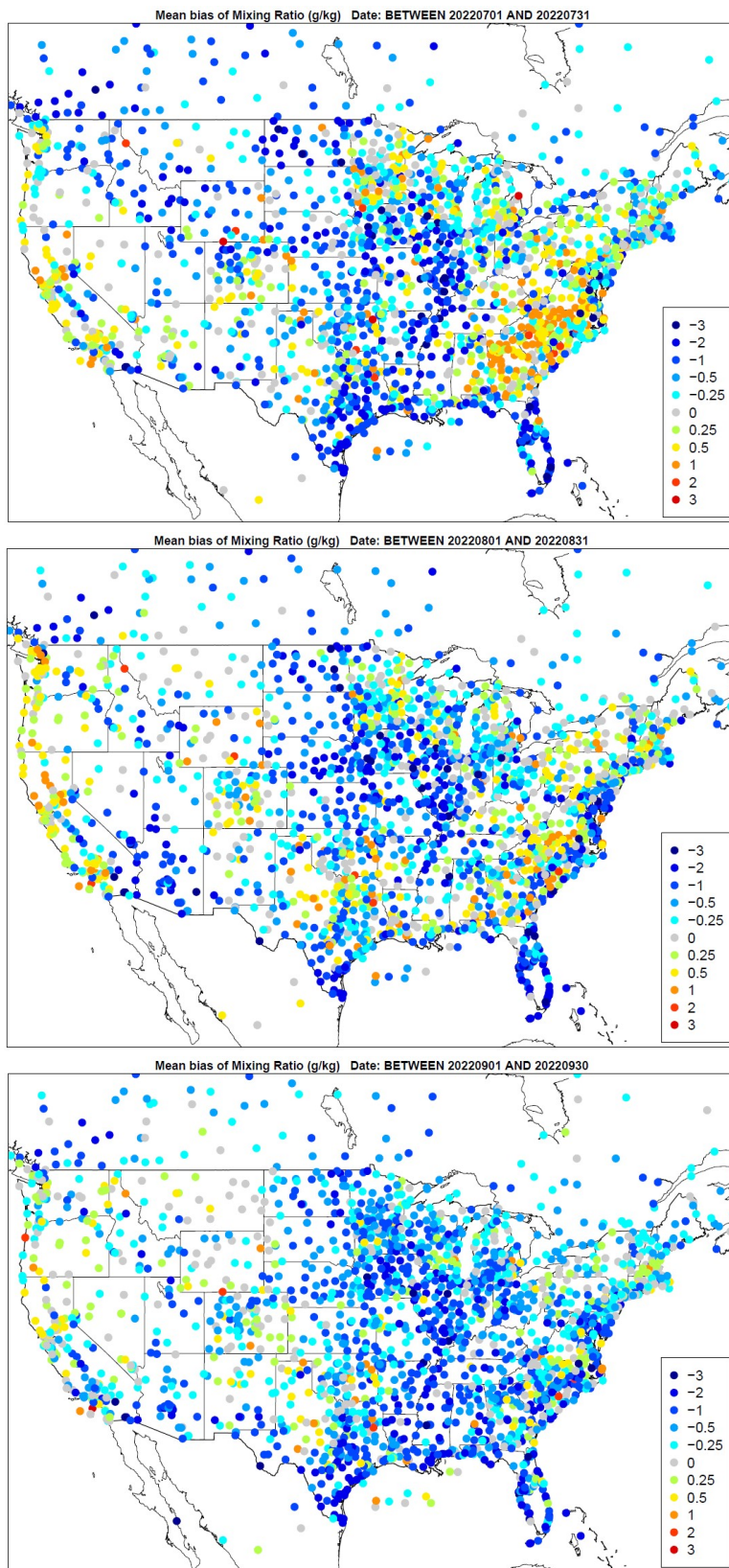
**Figure 3.3.14.** Spatial distribution of water vapor mixing ratio bias (g/kg) across daytime hours for the months of October, November, and December (top to bottom) for 36NOAM domain.



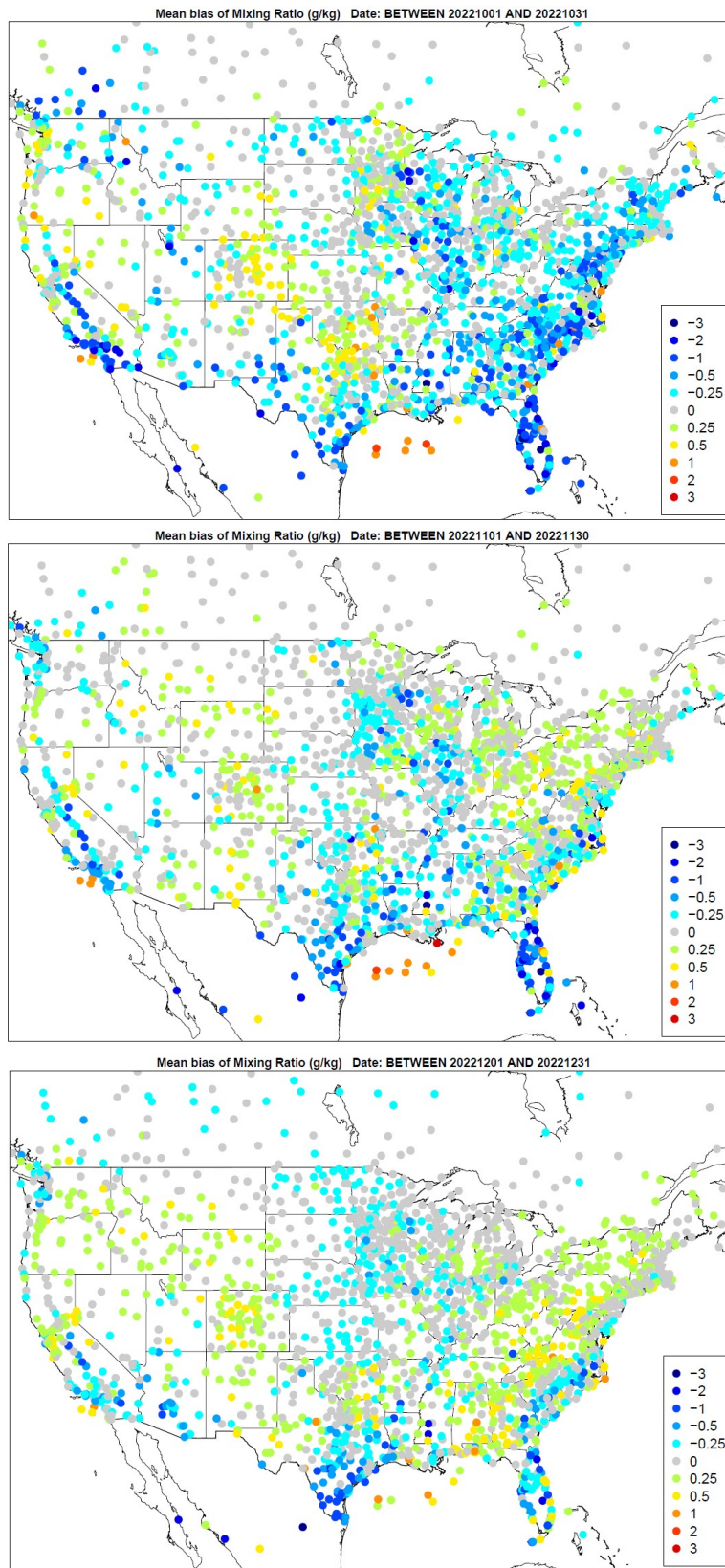
**Figure 3.3.15.** Spatial distribution of water vapor mixing ratio bias (g/kg) across daytime hours for the months of January, February, and March (top to bottom) for the 12US domain.



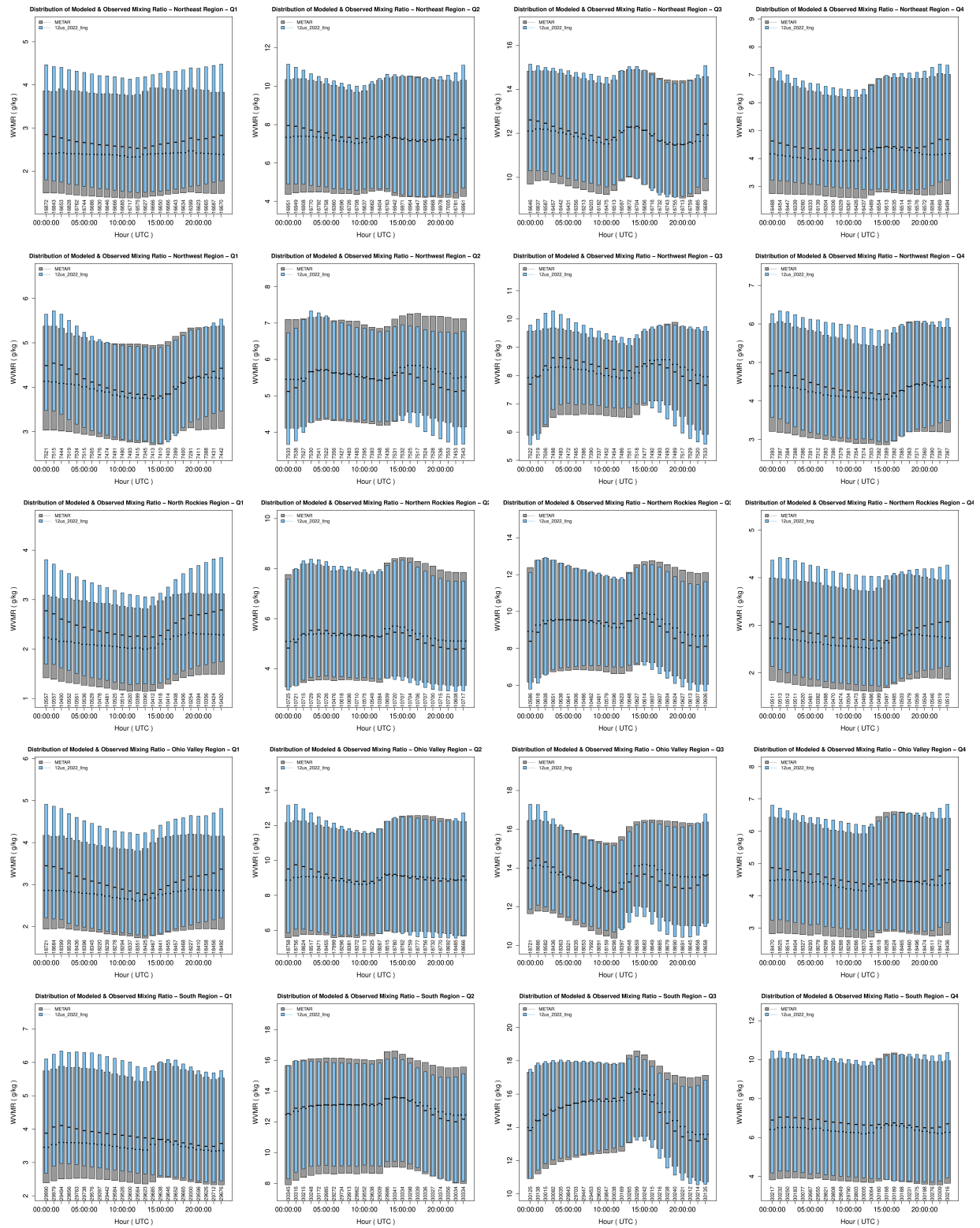
**Figure 3.3.16.** Spatial distribution of water vapor mixing ratio bias (g/kg) across daytime hours for the months of April, May, and June (top to bottom) for the 12US domain.



**Figure 3.3.17.** Spatial distribution of water vapor mixing ratio bias (g/kg) across daytime hours for the months of July, August, and September (top to bottom) for the 12US domain.



**Figure 3.3.18.** Spatial distribution of water vapor mixing ratio bias (g/kg) across daytime hours for the months of October, November, and December (top to bottom) for the 12US domain.



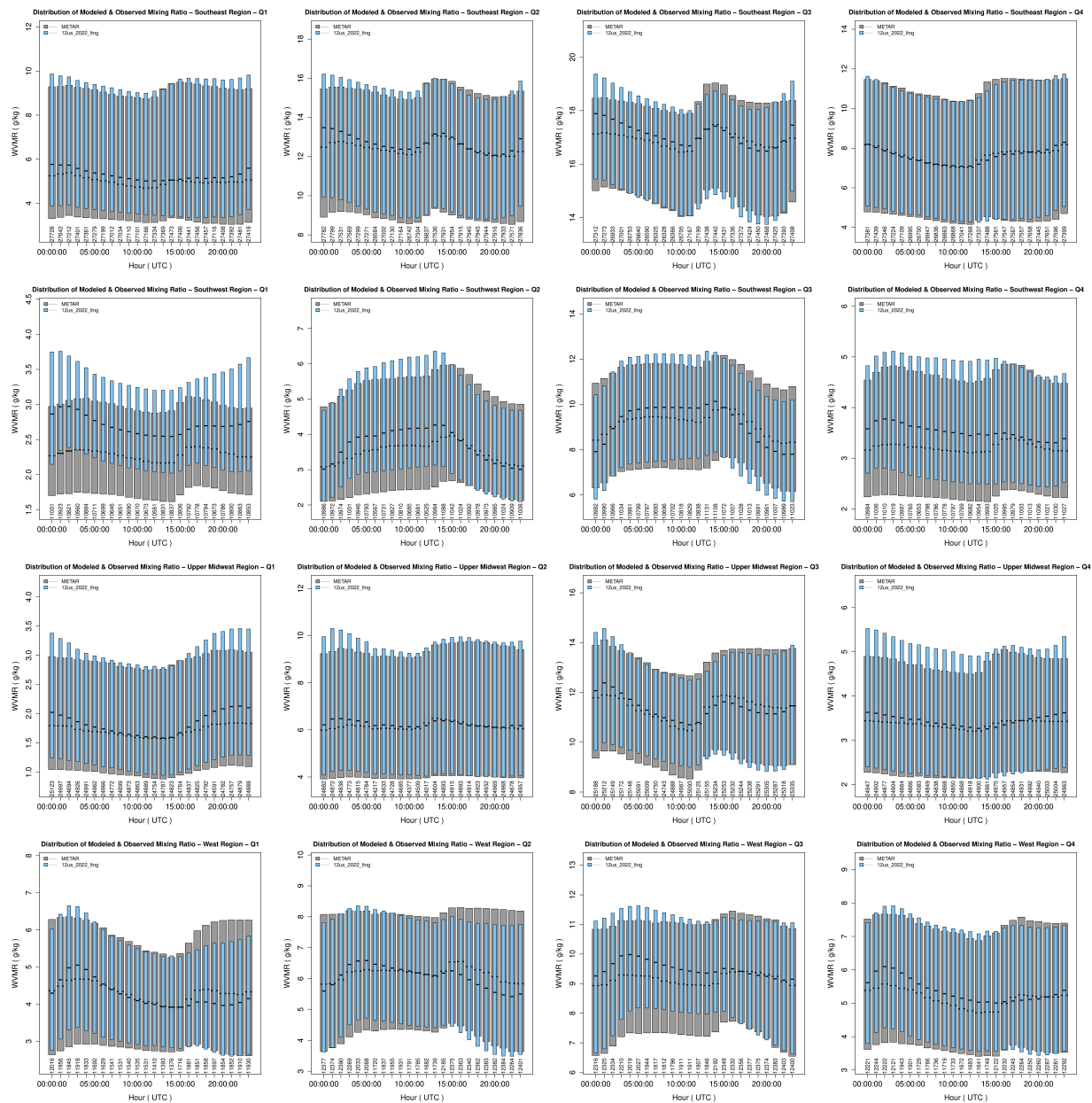


**Figure 3.3.19.** Hourly average distribution of observed and water vapor mixing ratios (g/kg) for the 12US domain in the Northeast, Northwest, Northern Rockies & Plains, Ohio Valley, South, Southeast, Southwest, Upper Midwest, and West Climate Regions (respectively, top to bottom) for each quarter.

Climate Region	Season	Mean Obs	Mean Mod	MAE	MB	NMB	NME	RMSE
Northeast	Q1	2.98	3.26	0.46	0.28	9.49	15.44	0.65
	Q2	7.61	7.82	0.74	0.21	2.8	9.74	1.02
	Q3	12	12.1	0.95	0.1	0.82	7.9	1.27
	Q4	4.97	5.18	0.56	0.2	4.11	11.33	0.76
N. Rockies & Plains	Q1	2.21	2.53	0.46	0.32	14.6	20.81	0.66
	Q2	6.15	6.11	0.83	-0.04	-0.62	13.44	1.21
	Q3	9.66	9.56	1.13	-0.1	-1.06	11.68	1.55
	Q4	3.08	3.29	0.45	0.21	6.71	14.76	0.66
Northwest	Q1	4.04	4.17	0.52	0.13	3.11	12.9	0.72
	Q2	5.79	5.61	0.65	-0.18	-3.17	11.22	0.91
	Q3	8.04	8.18	0.97	0.14	1.76	12.03	1.31
	Q4	4.5	4.73	0.57	0.23	5.15	12.65	0.77
Ohio Valley	Q1	3.31	3.59	0.51	0.28	8.6	15.39	0.7
	Q2	9.23	9.3	0.97	0.07	0.75	10.48	1.32
	Q3	13.49	13.35	1.1	-0.14	-1.02	8.17	1.47
	Q4	4.78	4.94	0.57	0.16	3.38	11.84	0.78
South	Q1	4.7	4.9	0.63	0.21	4.37	13.35	0.9
	Q2	12.13	12.05	1.25	-0.08	-0.64	10.33	1.7
	Q3	14.66	14.55	1.24	-0.11	-0.78	8.47	1.64
	Q4	7.21	7.35	0.81	0.14	1.93	11.17	1.15
Southeast	Q1	6.33	6.55	0.72	0.22	3.44	11.39	0.97
	Q2	11.97	12.16	1.08	0.19	1.57	9.03	1.44
	Q3	16.08	16.08	1.24	-0.01	-0.05	7.69	1.63
	Q4	8.03	8.02	0.82	-0.01	-0.09	10.16	1.11
Southwest	Q1	2.47	2.87	0.6	0.41	16.44	24.2	0.81
	Q2	4.3	4.52	0.89	0.22	5.2	20.79	1.28
	Q3	9.36	9.36	1.25	0	0.04	13.34	1.66
	Q4	3.79	4.08	0.63	0.29	7.58	16.63	0.84
Upper Midwest	Q1	2.06	2.22	0.35	0.17	8.11	16.9	0.51
	Q2	7.02	7.15	0.8	0.13	1.85	11.39	1.18
	Q3	11.35	11.31	0.98	-0.04	-0.36	8.66	1.33
	Q4	3.77	3.9	0.44	0.13	3.57	11.75	0.64
West	Q1	4.45	4.45	0.7	0.01	0.17	15.73	0.98
	Q2	6.25	6.18	0.84	-0.07	-1.09	13.41	1.17
	Q3	9.16	9.44	1.12	0.28	3.02	12.17	1.55
	Q4	5.6	5.71	0.72	0.11	1.94	12.83	1

**Table 3.3.1.** Mean observed, mean modeled, mean absolute error (MAE), mean bias (MB), normalized mean bias (NMB), normalized mean error (NME), and root mean square error (RMSE) for water vapor mixing ratio (g/kg) for the 12US domain.

### 3.4 Model Performance for Precipitation

Monthly total rainfall is plotted for each grid cell to assess how well the model captures the spatial variability and magnitude of convective and non-convective rainfall. As described earlier, the PRISM estimations for rainfall are only within the continental United States. With lightning assimilation in the 12US simulation mentioned earlier, the model will either trigger (suppress) convection when lightning is observed (not observed). This assimilation is particularly useful in constraining the model's convection scheme that at times has been observed to be inaccurately active. WRF rainfall estimates by month are shown for all grid cells in the domain. Monthly total estimates are shown in Figures 3.4.1 through 3.4.12 for the 36NOAM domain and Figures 3.4.13 through 3.4.24 for the 12US domain. Domain-wide biases for the 36NOAM and 12US domains are shown in Table 3.4.1.

Overall, the model captures the general spatial patterns and magnitude of the precipitation across the US throughout the year. Precipitation is generally underpredicted across the southern and eastern portions of the US during the spring and winter months. There is a general overprediction that is noted across the western US and portions of the Plains states, particularly in areas of complex terrain (e.g., northern CA, the Rockies, etc.), especially during the Summer months. The overprediction is particularly noticeable in the 36NOAM simulation, where lightning assimilation data were not used and thus, convective precipitation was unconstrained (notable domain-wide biases in summer months are up to 0.6" greater in the 36NOAM simulation versus the 12US simulation).

Precipitation, January 2022

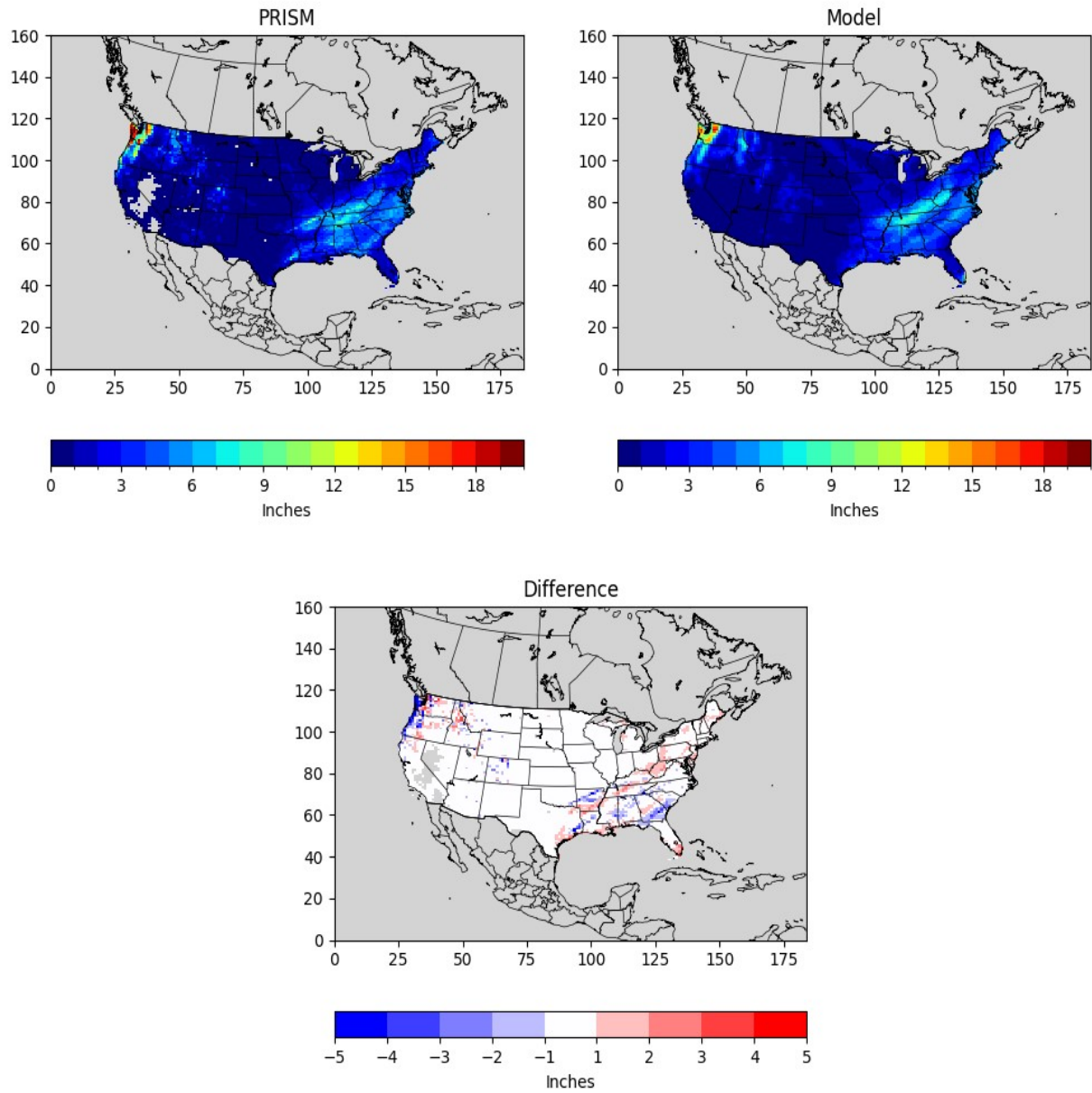
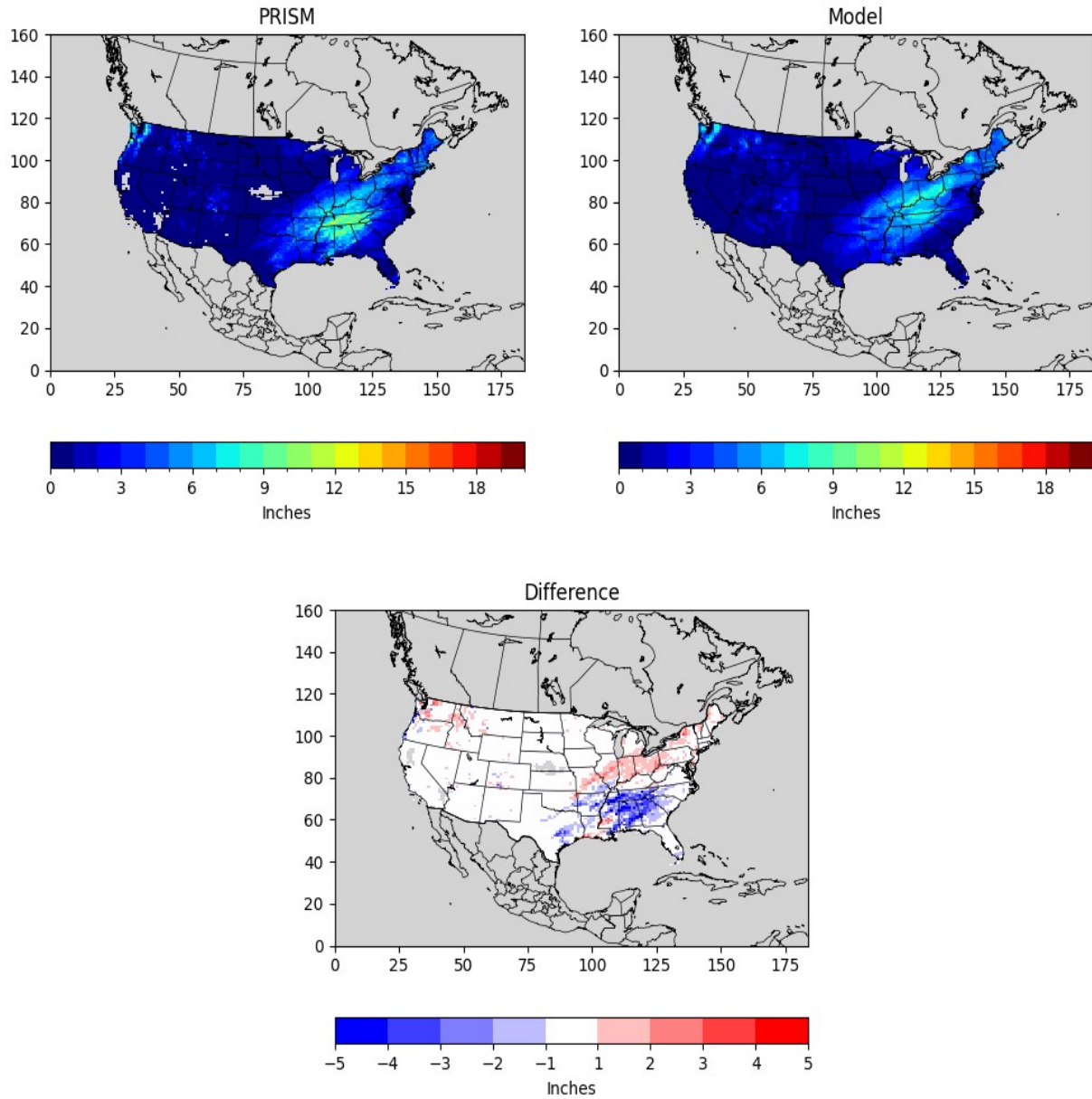


**Figure 3.4.1.** PRISM analysis (top left) and WRF (top right) estimated monthly total rainfall (in) and the difference (bottom) for January for the 36NOAM domain.

Precipitation, February 2022



**3.4.2.** PRISM analysis (top left) and WRF (top right) estimated monthly total rainfall (in) and the difference (bottom) for February for the 36NOAM domain.

Precipitation, March 2022

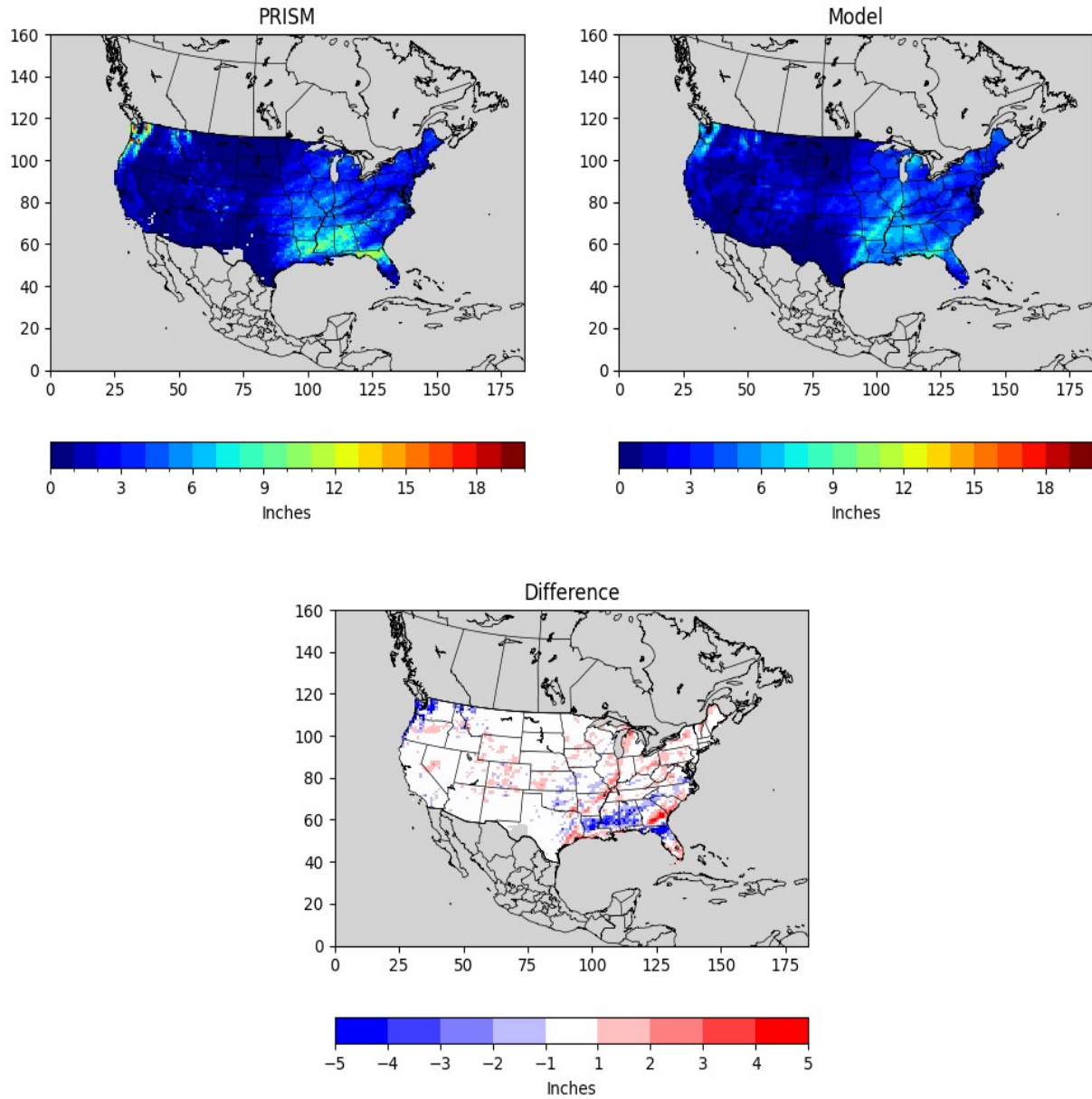


**Figure 3.4.3.** PRISM analysis (top left) and WRF (top right) estimated monthly total rainfall (in) and the difference (bottom) for March for the 36NOAM domain.

Precipitation, April 2022

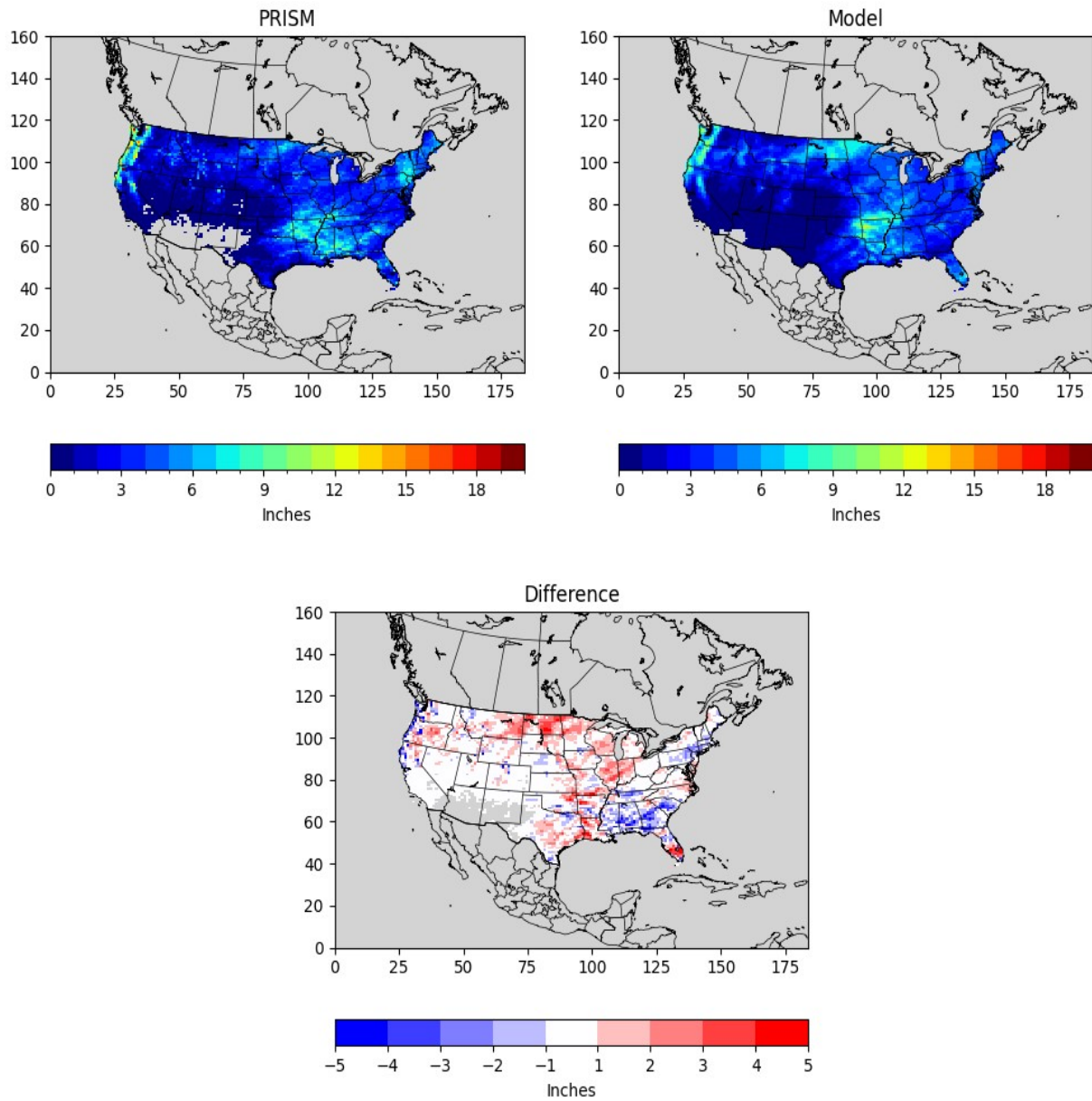


**Figure 3.4.4.** PRISM analysis (top left) and WRF (top right) estimated monthly total rainfall (in) and the difference (bottom) for April for the 36NOAM domain.

Precipitation, May 2022

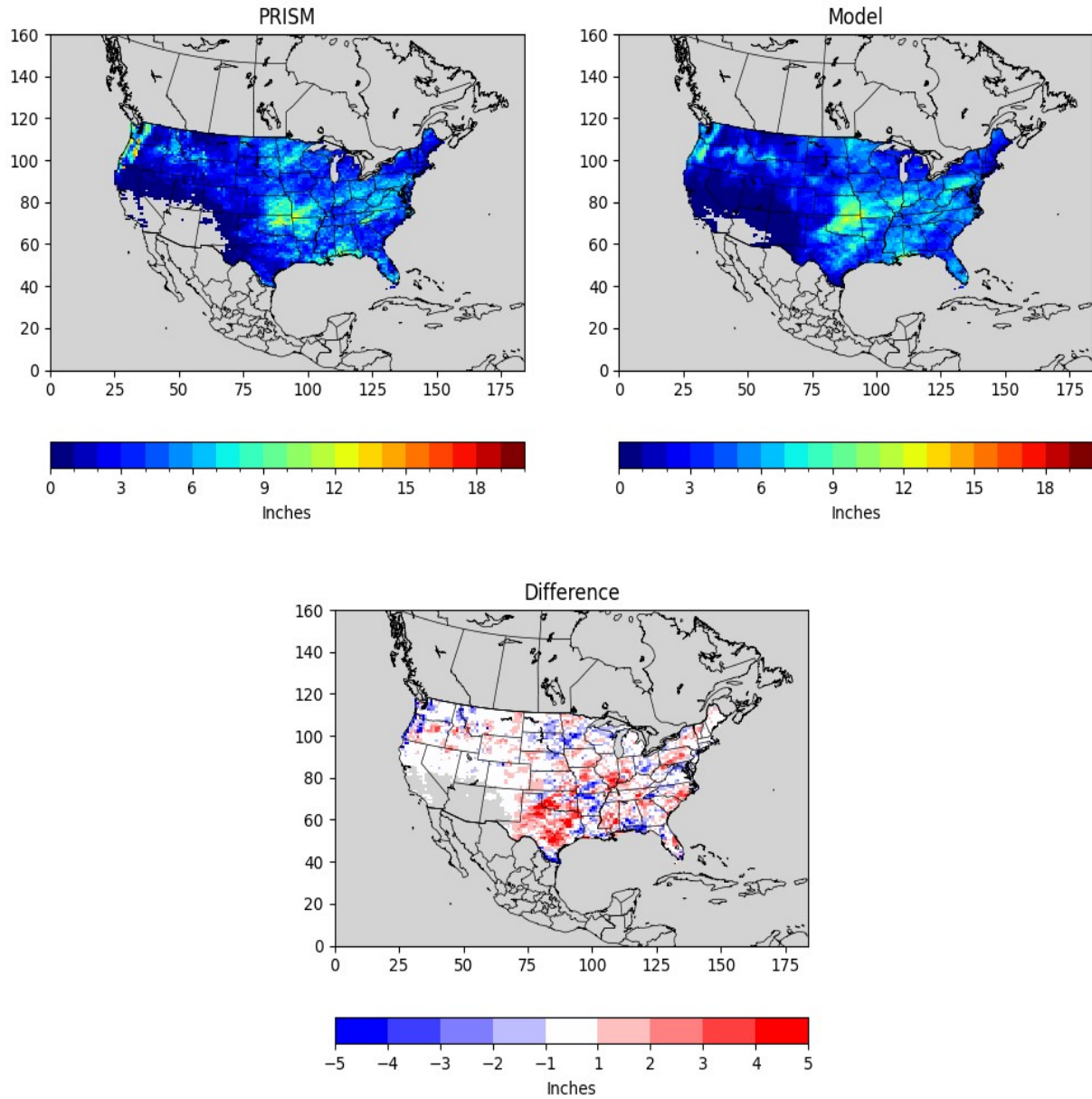


**Figure 3.4.5.** PRISM analysis (top left) and WRF (top right) estimated monthly total rainfall (in) and the difference (bottom) for May for the 36NOAM domain.

Precipitation, June 2022

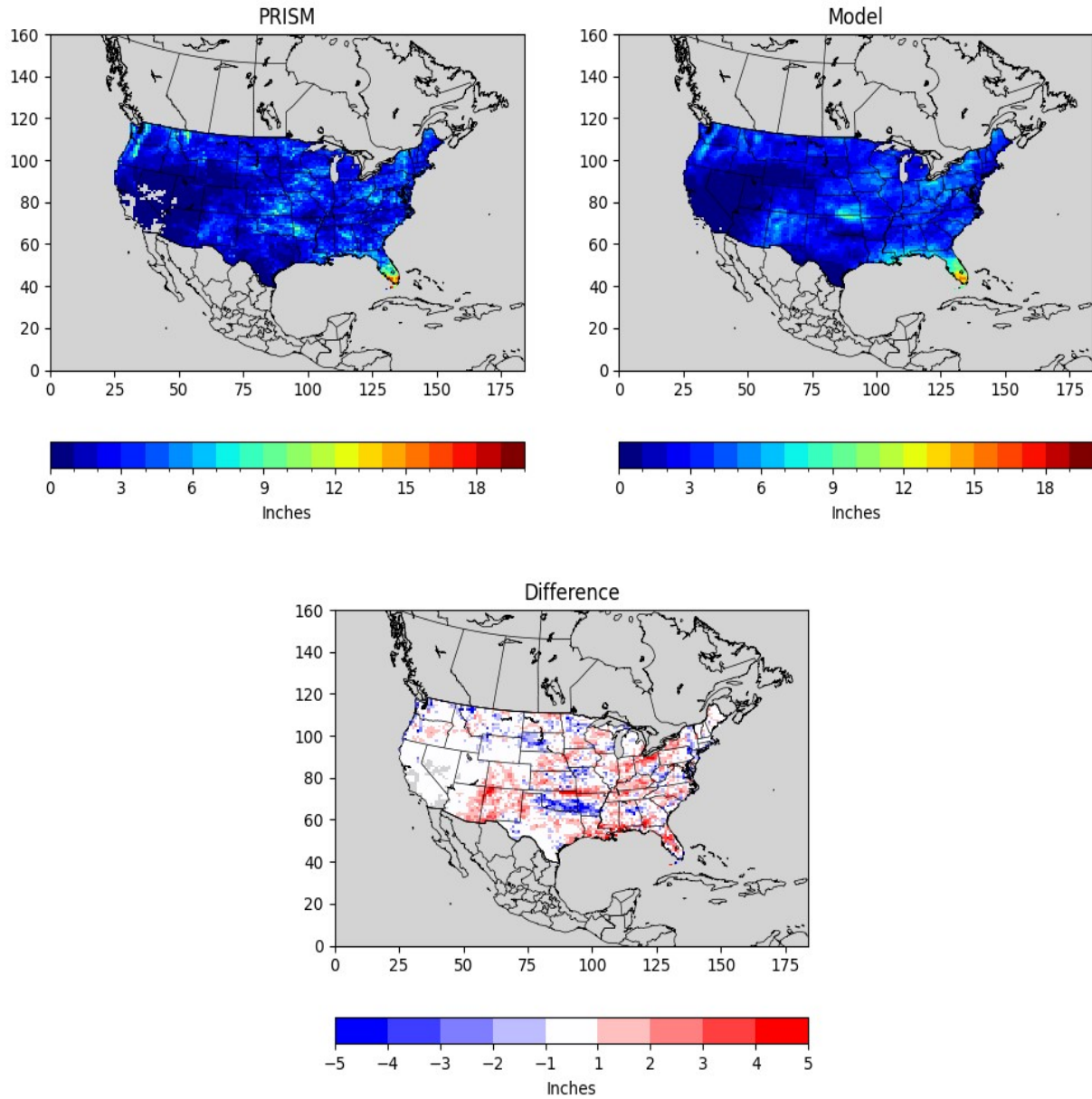


**Figure 3.4.6.** PRISM analysis (top left) and WRF (top right) estimated monthly total rainfall (in) and the difference (bottom) for June for the 36NOAM domain.

Precipitation, July 2022

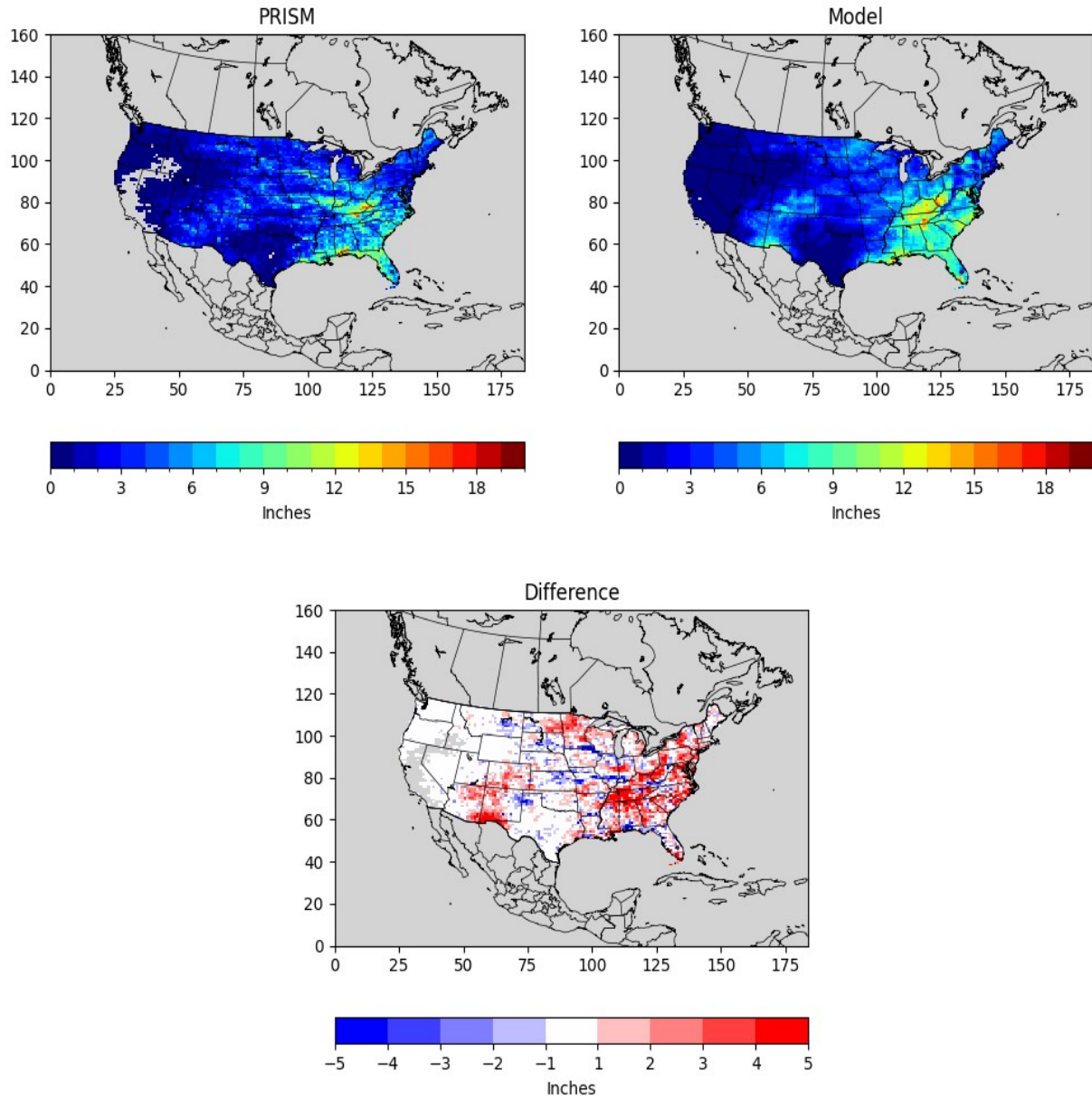


**Figure 3.4.7.** PRISM analysis (top left) and WRF (top right) estimated monthly total rainfall (in) and the difference (bottom) for July for the 36NOAM domain.

Precipitation, August 2022

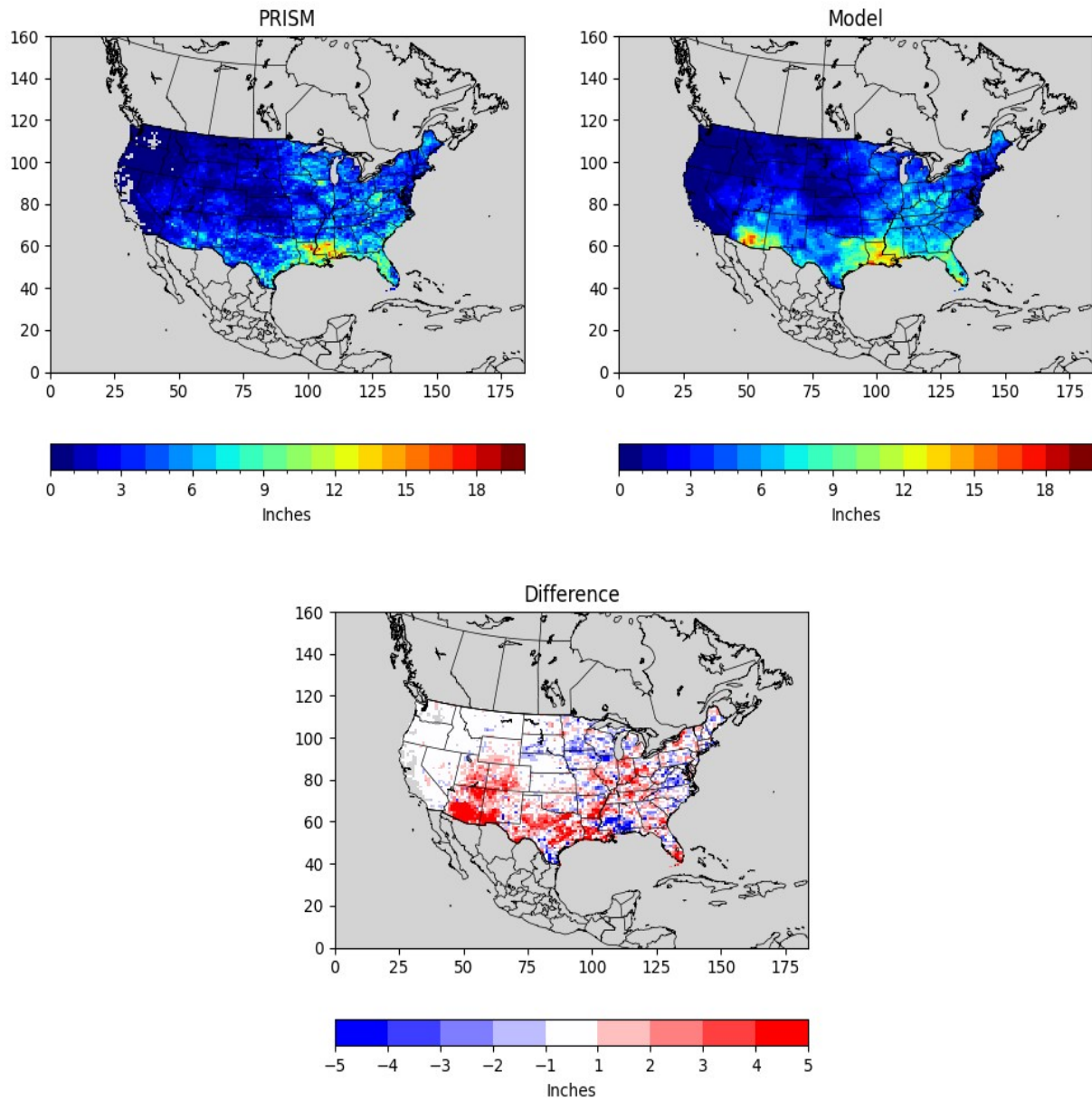


**Figure 3.4.8.** PRISM analysis (top left) and WRF (top right) estimated monthly total rainfall (in) and the difference (bottom) for August for the 36NOAM domain.

Precipitation, September 2022

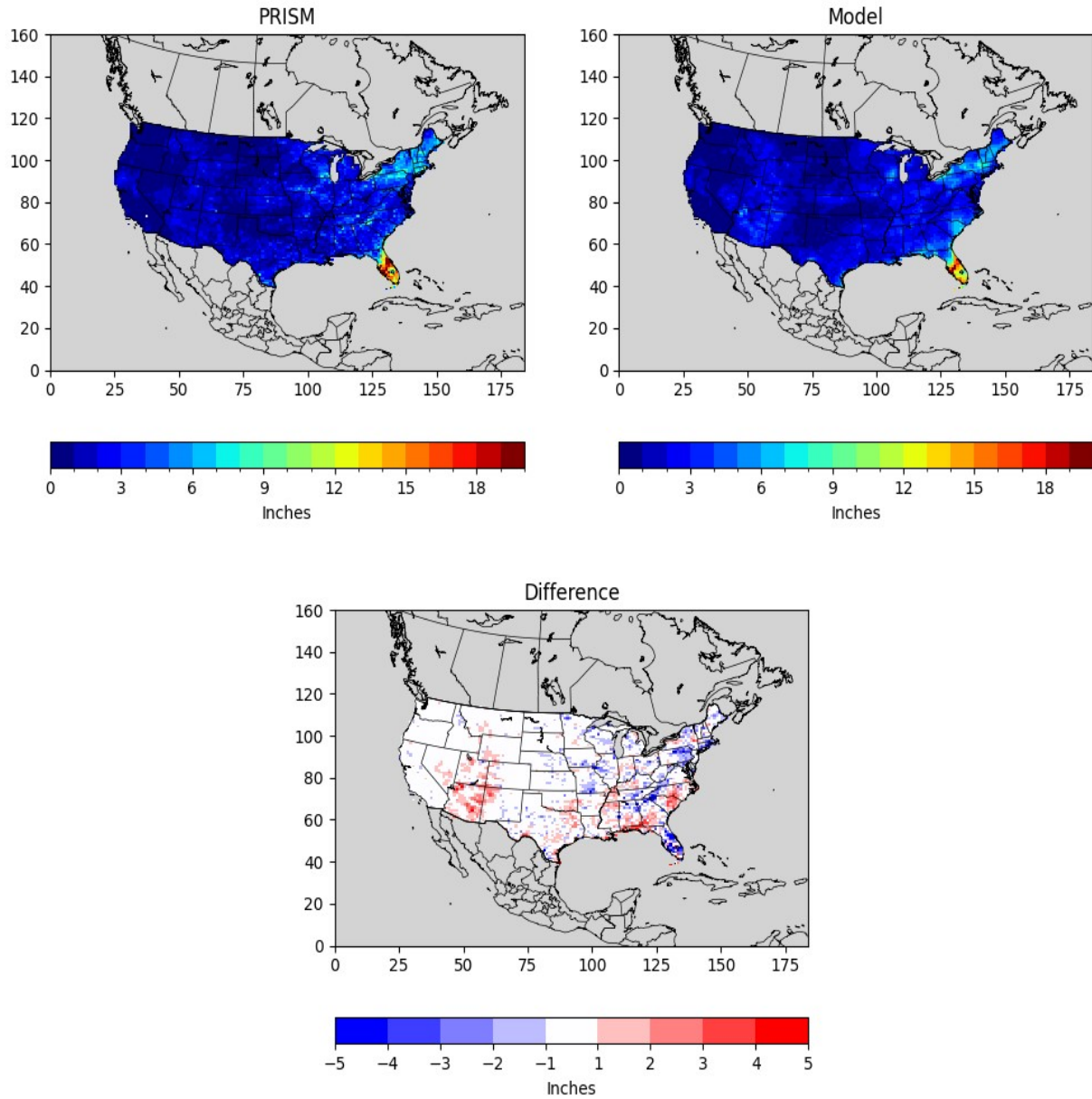


**Figure 3.4.9.** PRISM analysis (top left) and WRF (top right) estimated monthly total rainfall (in) and the difference (bottom) for September for the 36NOAM domain.

Precipitation, October 2022

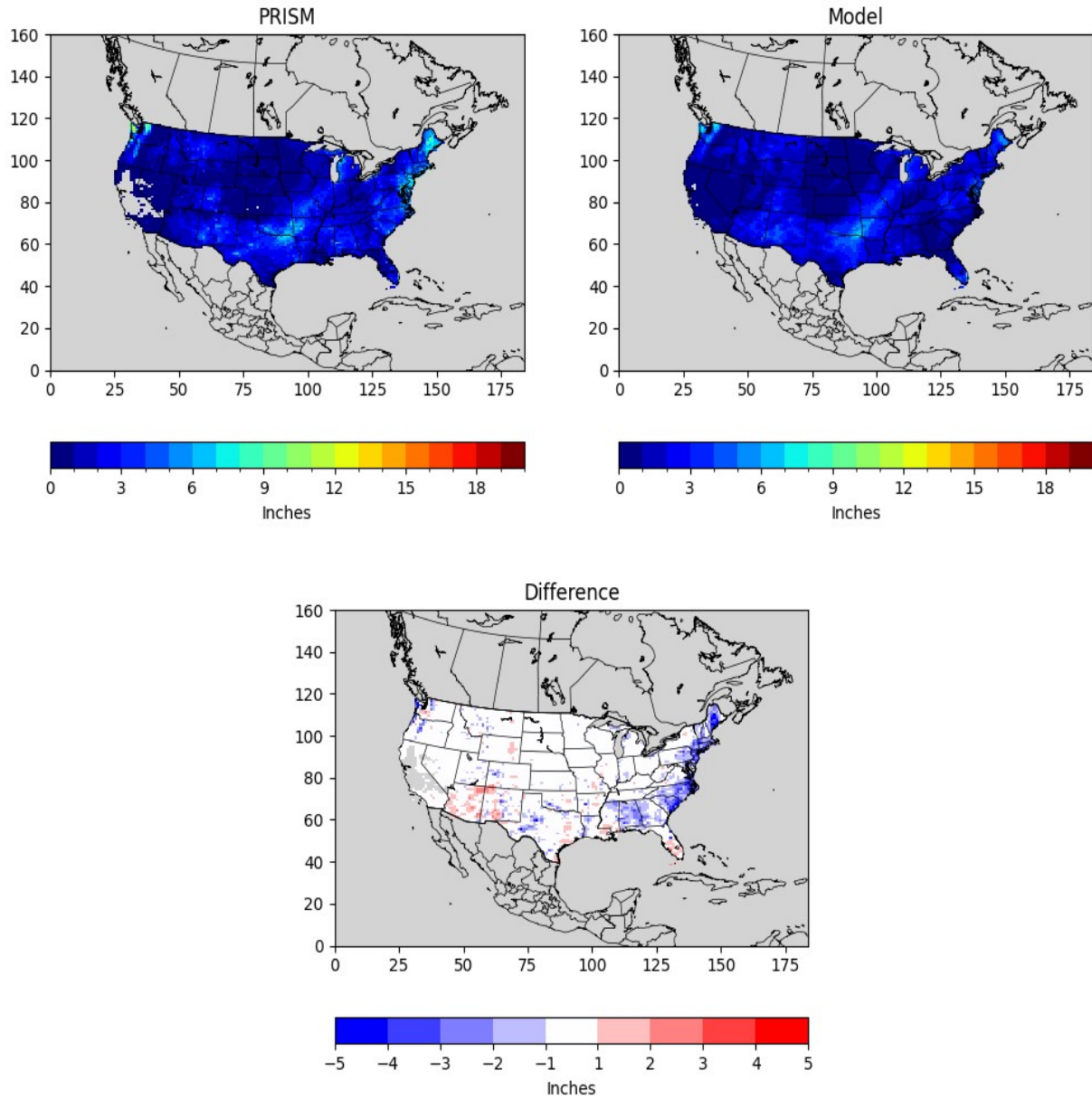


**Figure 3.4.10.** PRISM analysis (top left) and WRF (top right) estimated monthly total rainfall (in) and the difference (bottom) for October for the 36NOAM domain.

Precipitation, November 2022

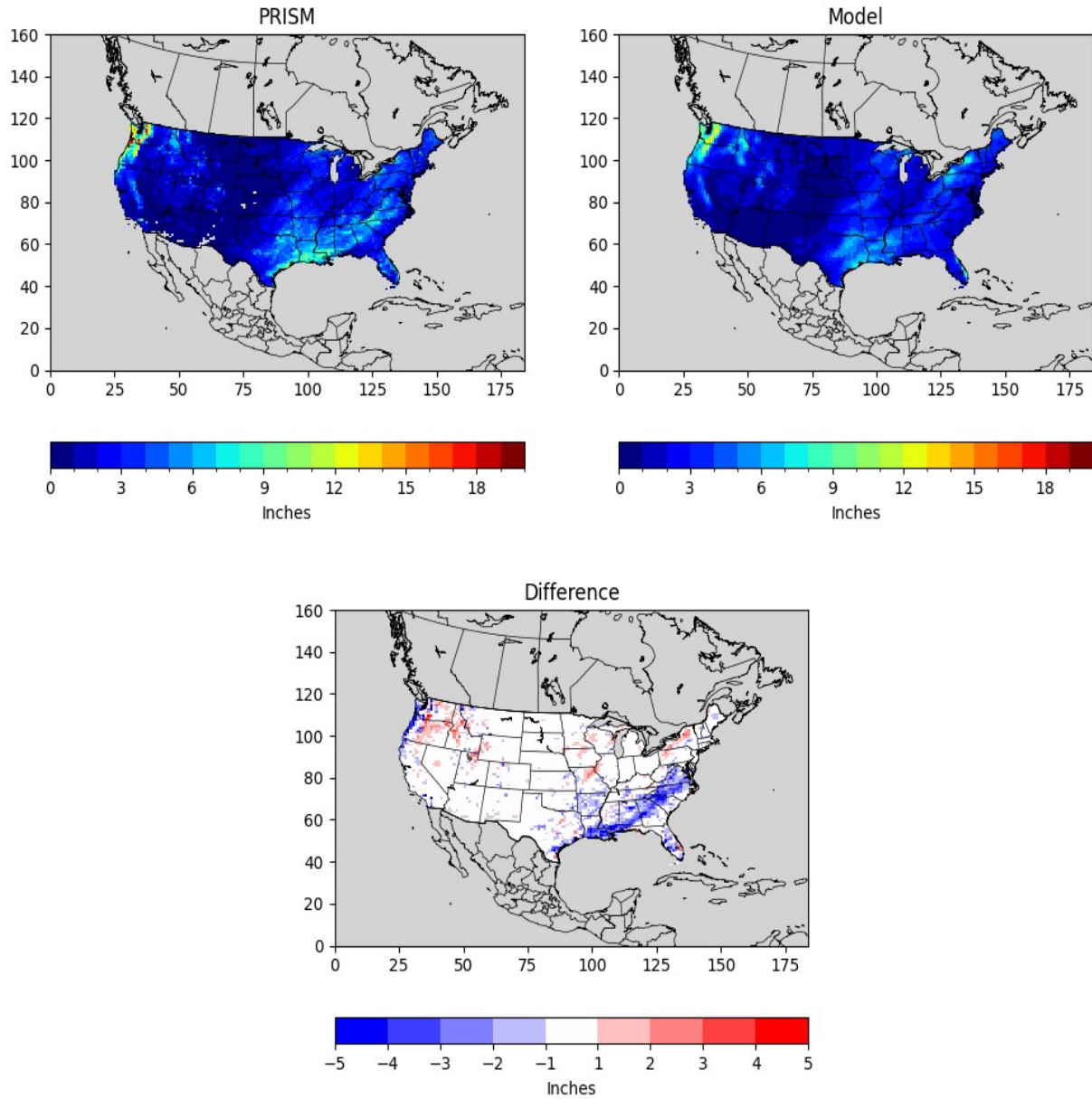


**Figure 3.4.11.** PRISM analysis (top left) and WRF (top right) estimated monthly total rainfall (in) and the difference (bottom) for November for the 36NOAM domain.

Precipitation, December 2022

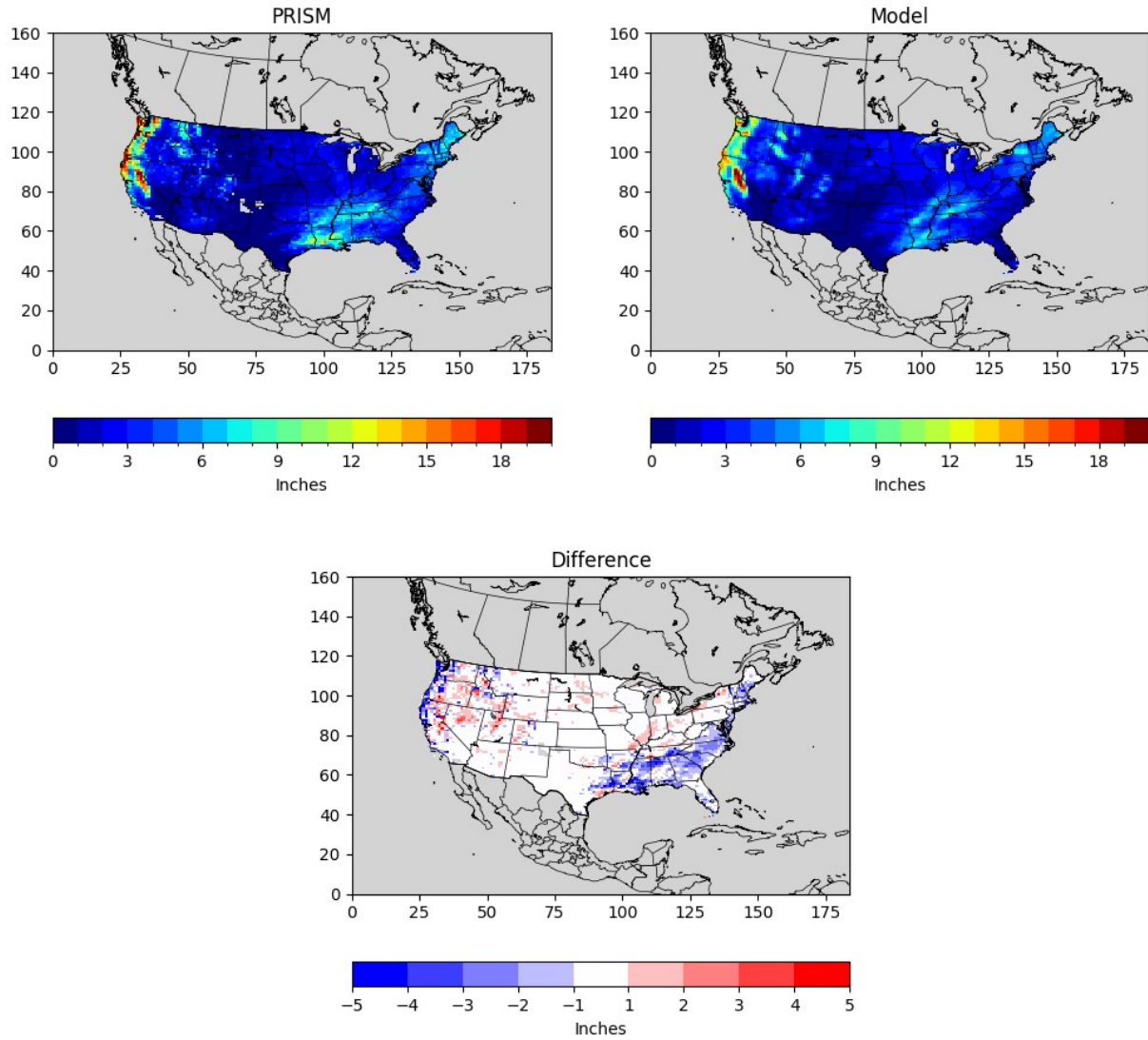


**Figure 3.4.12.** PRISM analysis (top left) and WRF (top right) estimated monthly total rainfall (in) and the difference (bottom) for December for the 36NOAM domain.

Precipitation, January 2022

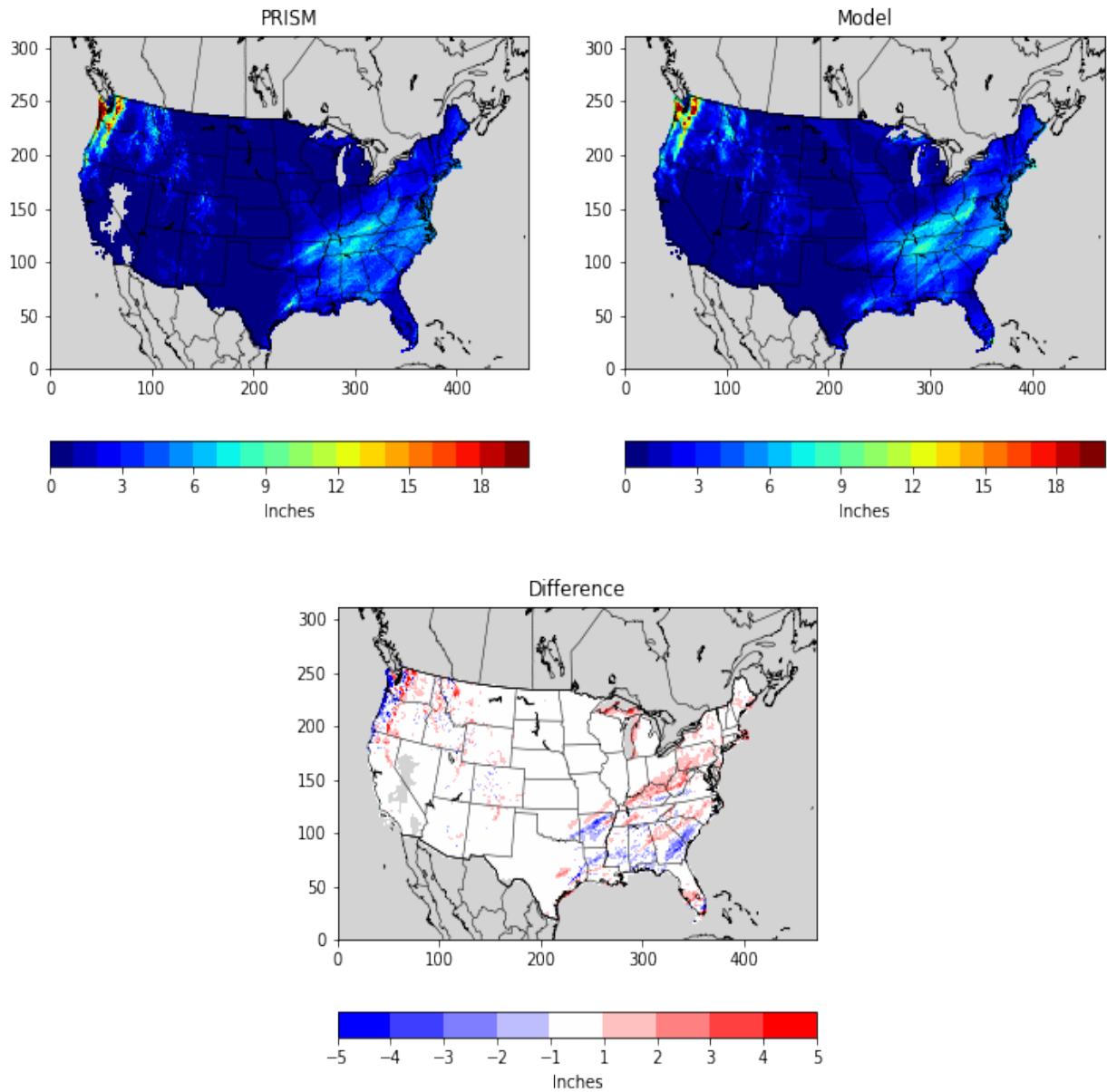


**Figure 3.4.13.** PRISM analysis (top left) and WRF (top right) estimated monthly total rainfall (in) and the difference (bottom) for January for the 12US domain.

Precipitation, February 2022

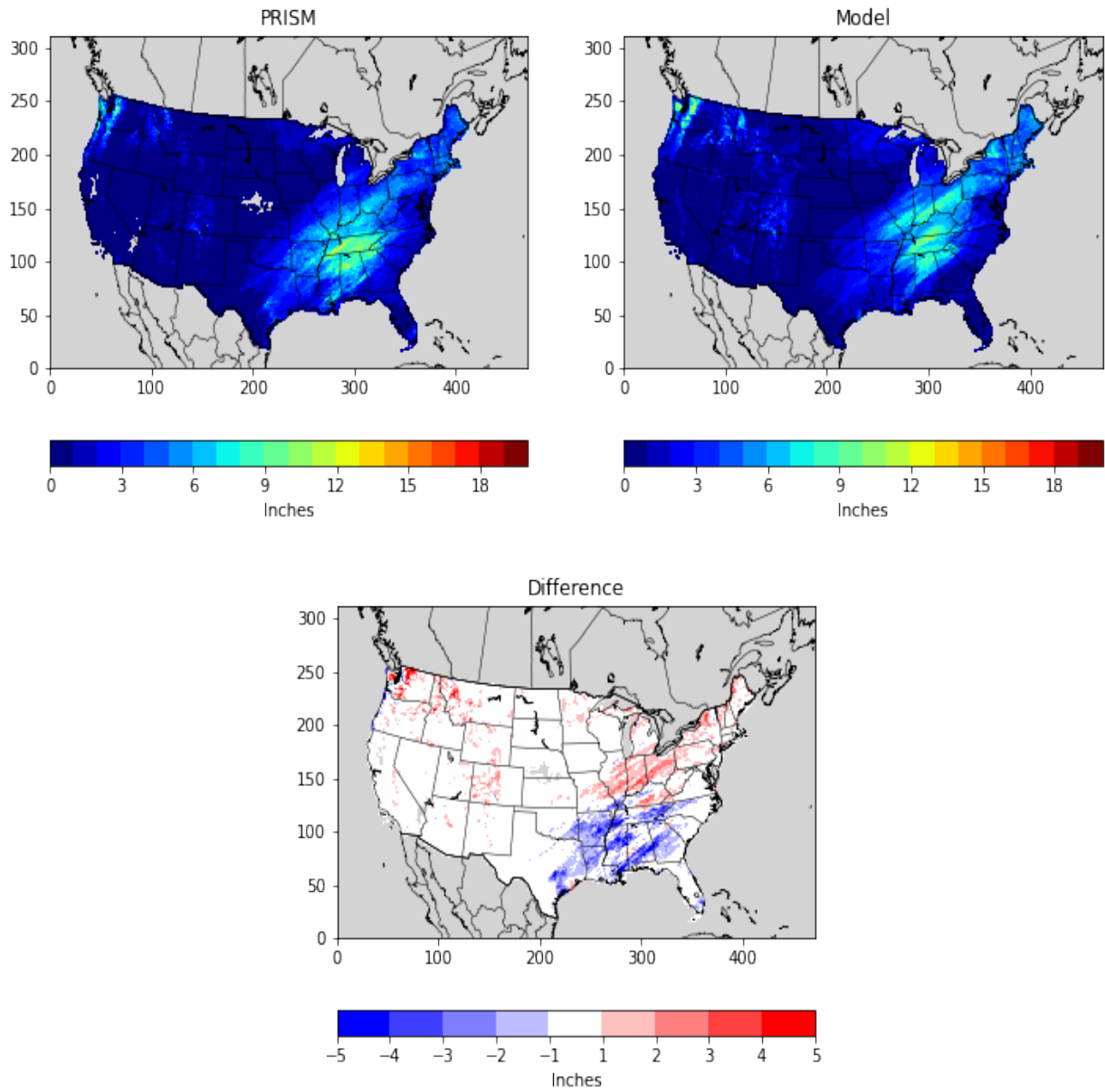


**Figure 3.4.14.** PRISM analysis (top left) and WRF (top right) estimated monthly total rainfall (in) and the difference (bottom) for February for the 12US domain.

Precipitation, March 2022

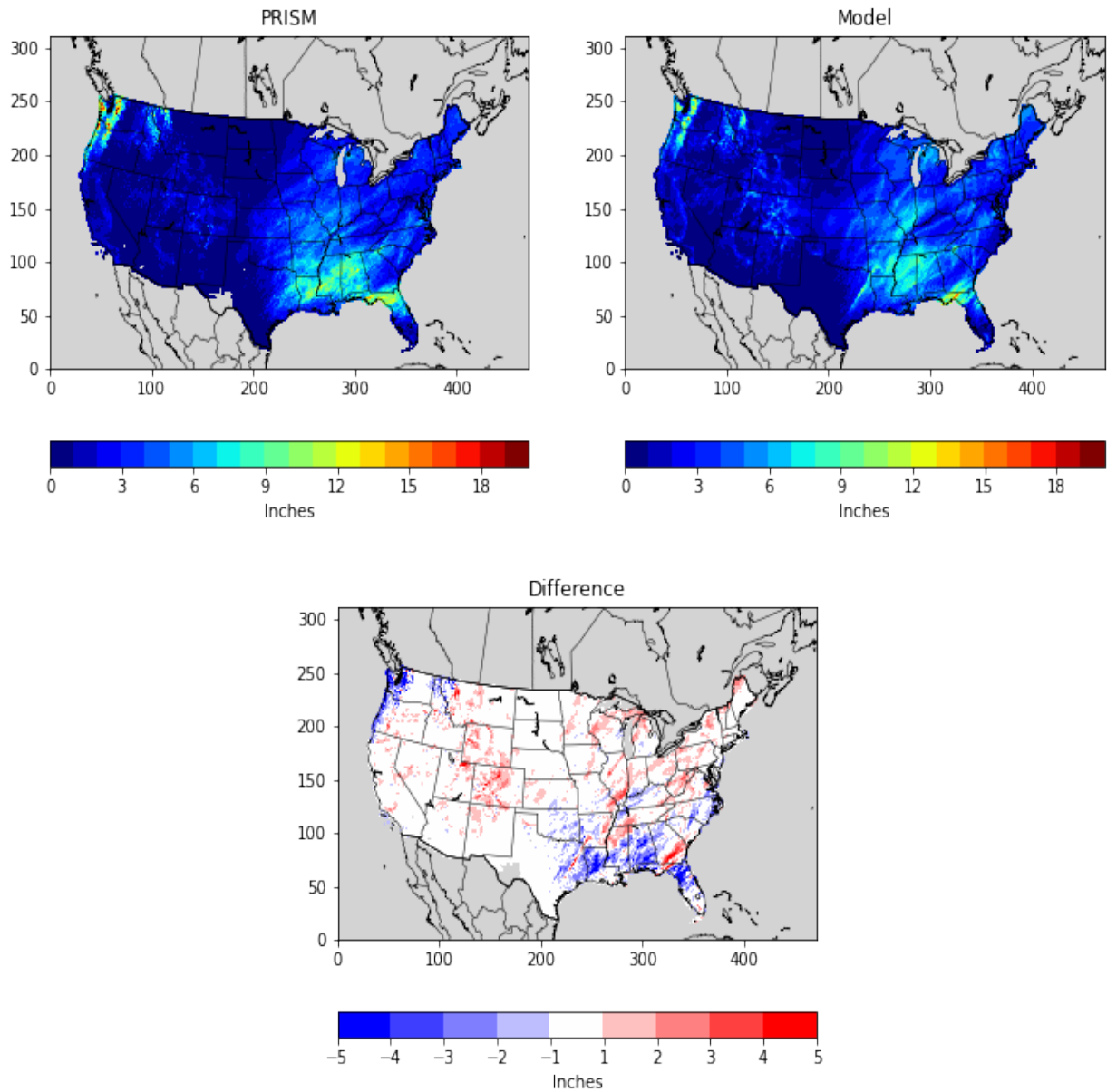


**Figure 3.4.15.** PRISM analysis (top left) and WRF (top right) estimated monthly total rainfall (in) and the difference (bottom) for March for the 12US domain.

Precipitation, April 2022

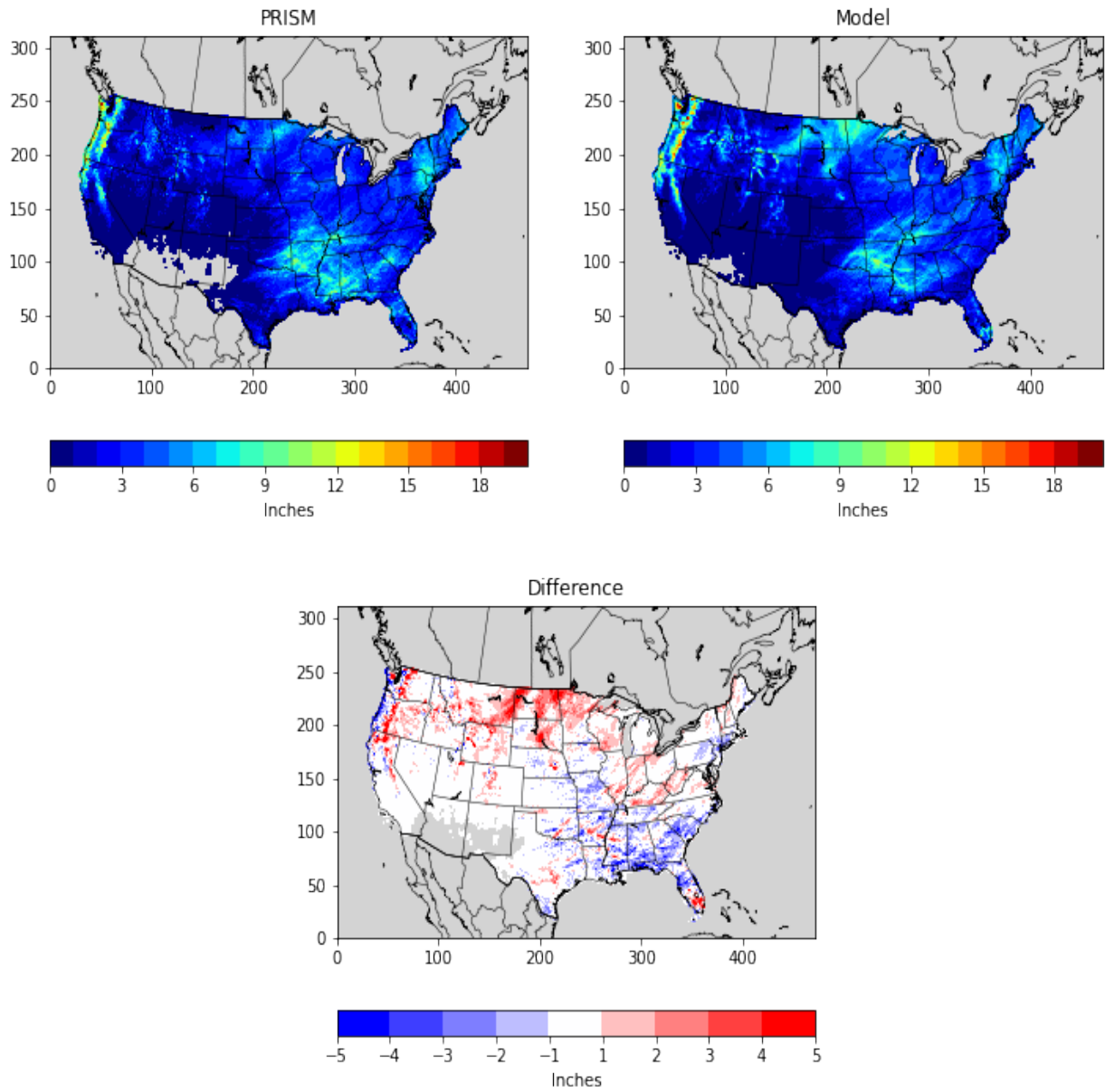


**Figure 3.4.16.** PRISM analysis (top left) and WRF (top right) estimated monthly total rainfall (in) and the difference (bottom) for April for the 12US domain.

Precipitation, May 2022

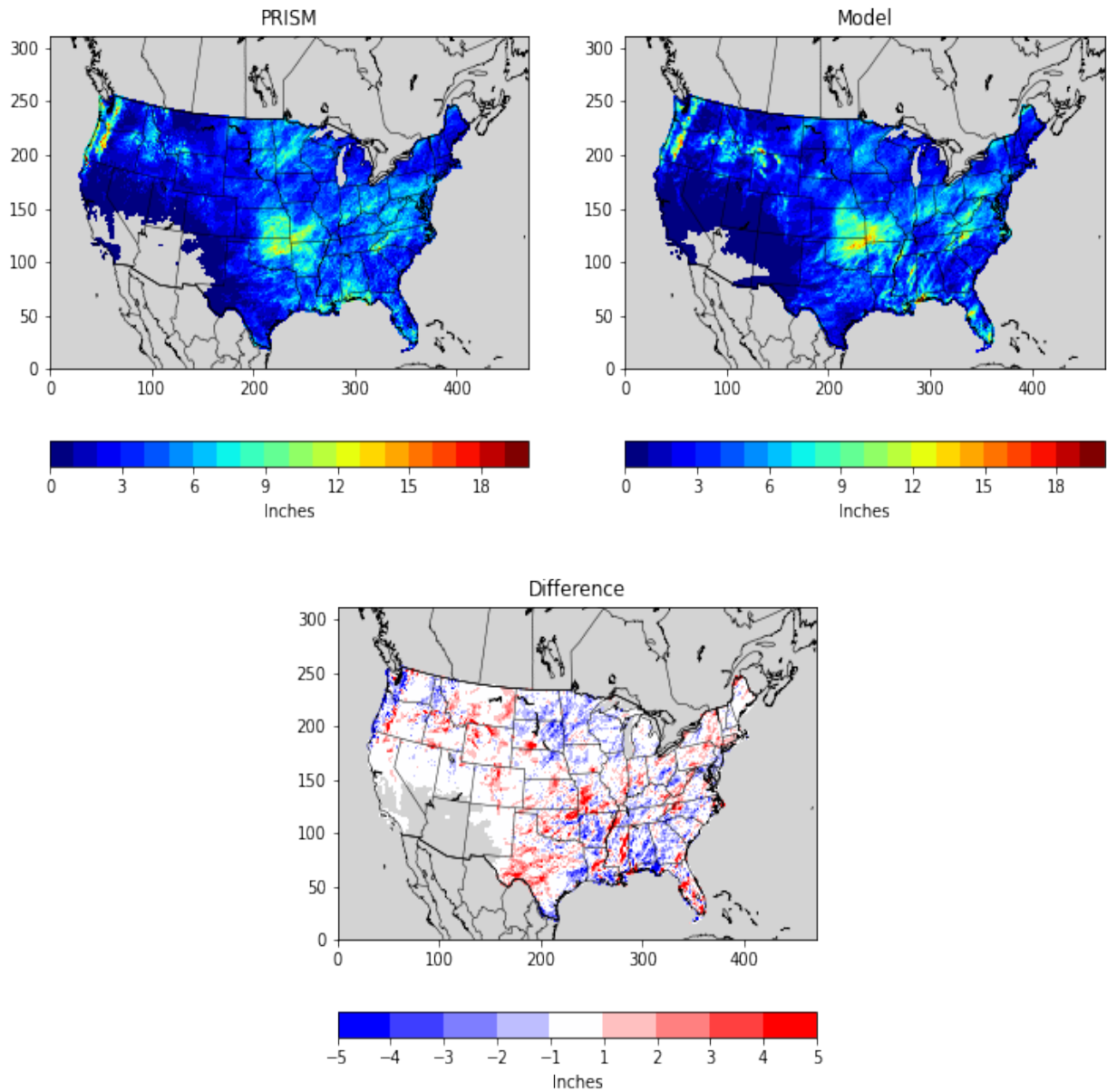


**Figure 3.4.17.** PRISM analysis (top left) and WRF (top right) estimated monthly total rainfall (in) and the difference (bottom) for May for the 12US domain.

Precipitation, June 2022

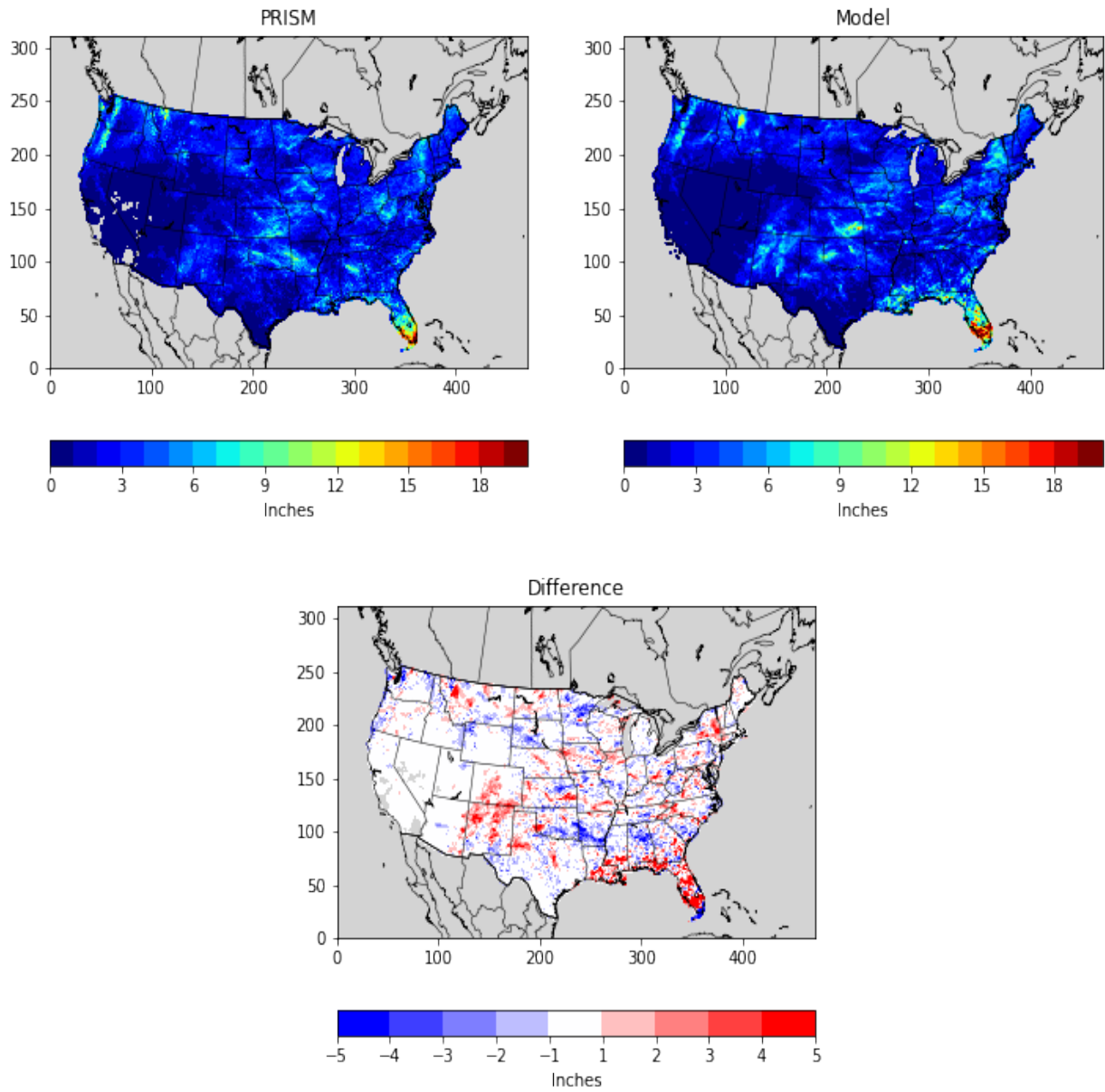


**Figure 3.4.18.** PRISM analysis (top left) and WRF (top right) estimated monthly total rainfall (in) and the difference (bottom) for June for the 12US domain.

Precipitation, July 2022

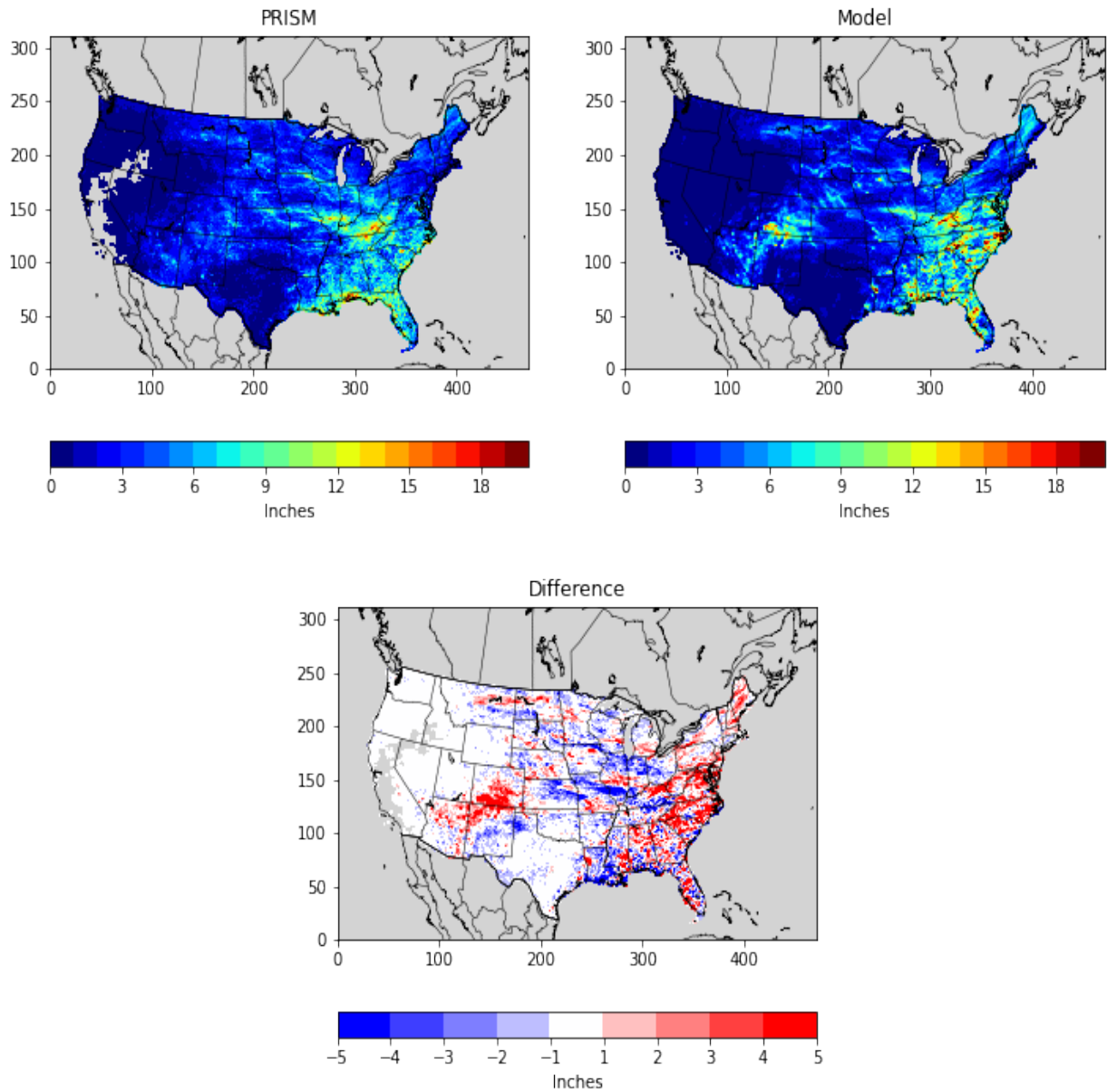


**Figure 3.4.19.** PRISM analysis (top left) and WRF (top right) estimated monthly total rainfall (in) and the difference (bottom) for July for the 12US domain.

Precipitation, August 2022

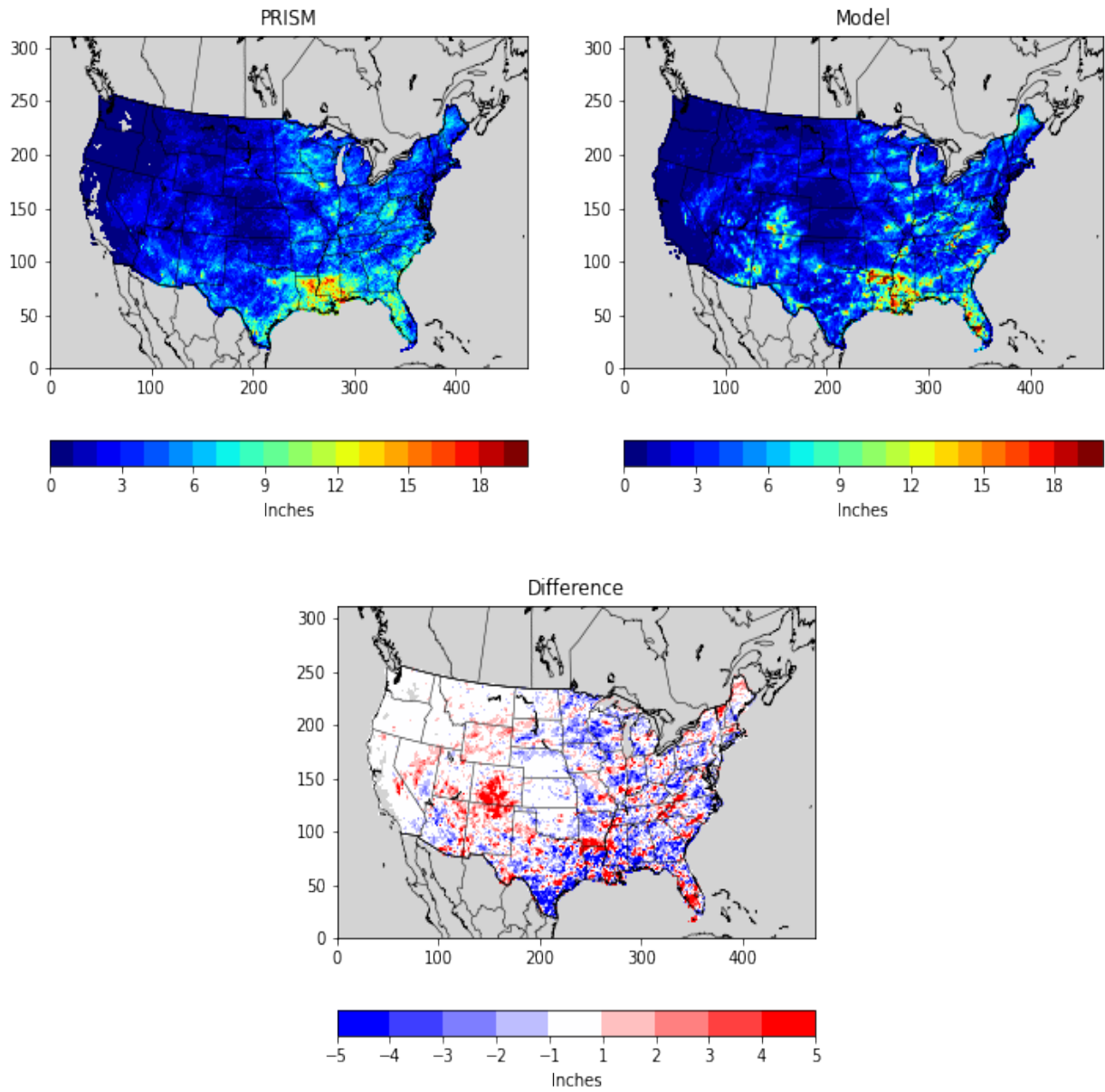


**Figure 3.4.20.** PRISM analysis (top left) and WRF (top right) estimated monthly total rainfall (in) and the difference (bottom) for August for the 12US domain.

Precipitation, September 2022

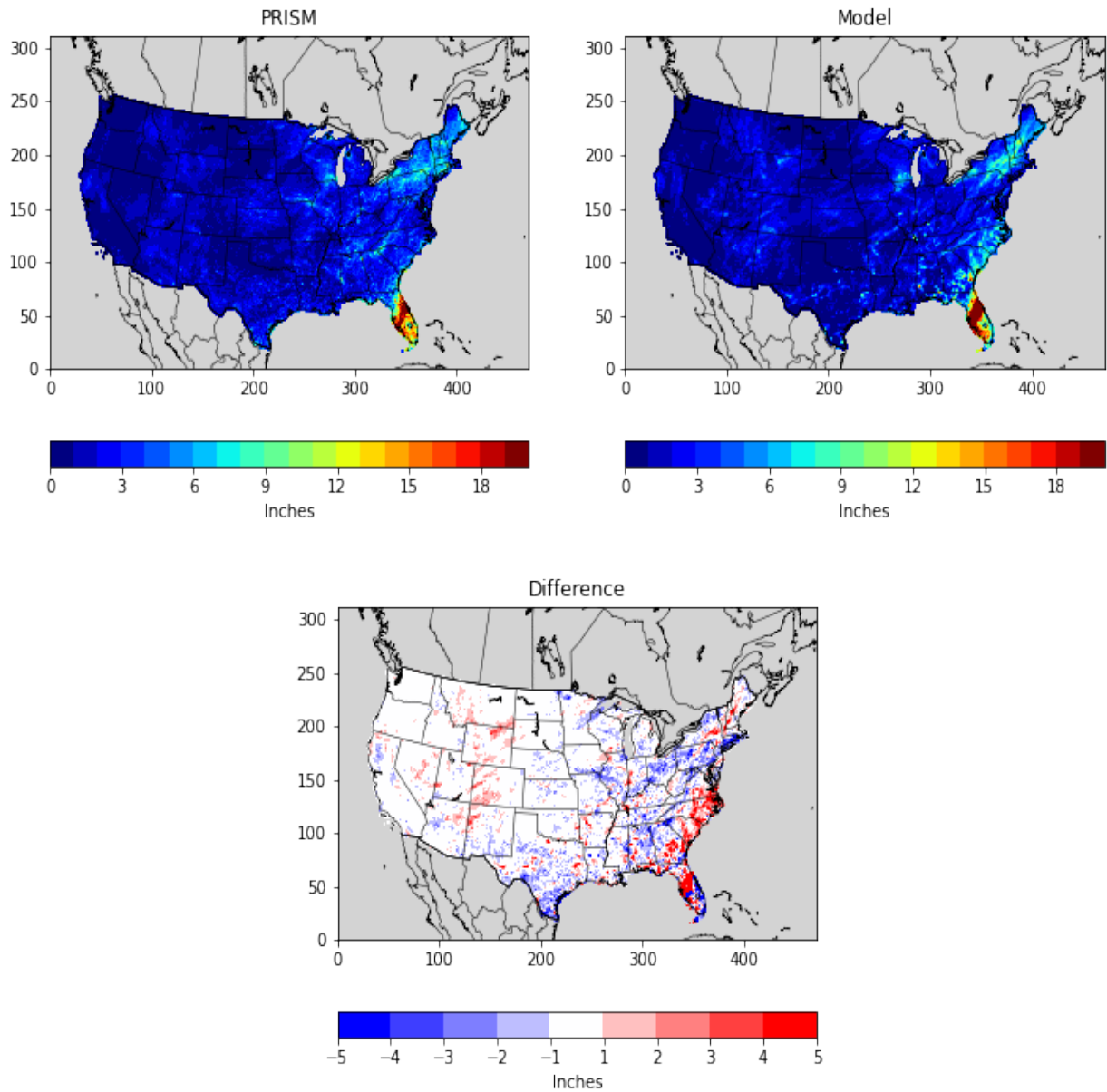


**Figure 3.4.21.** PRISM analysis (top left) and WRF (top right) estimated monthly total rainfall (in) and the difference (bottom) for September for the 12US domain.

Precipitation, October 2022

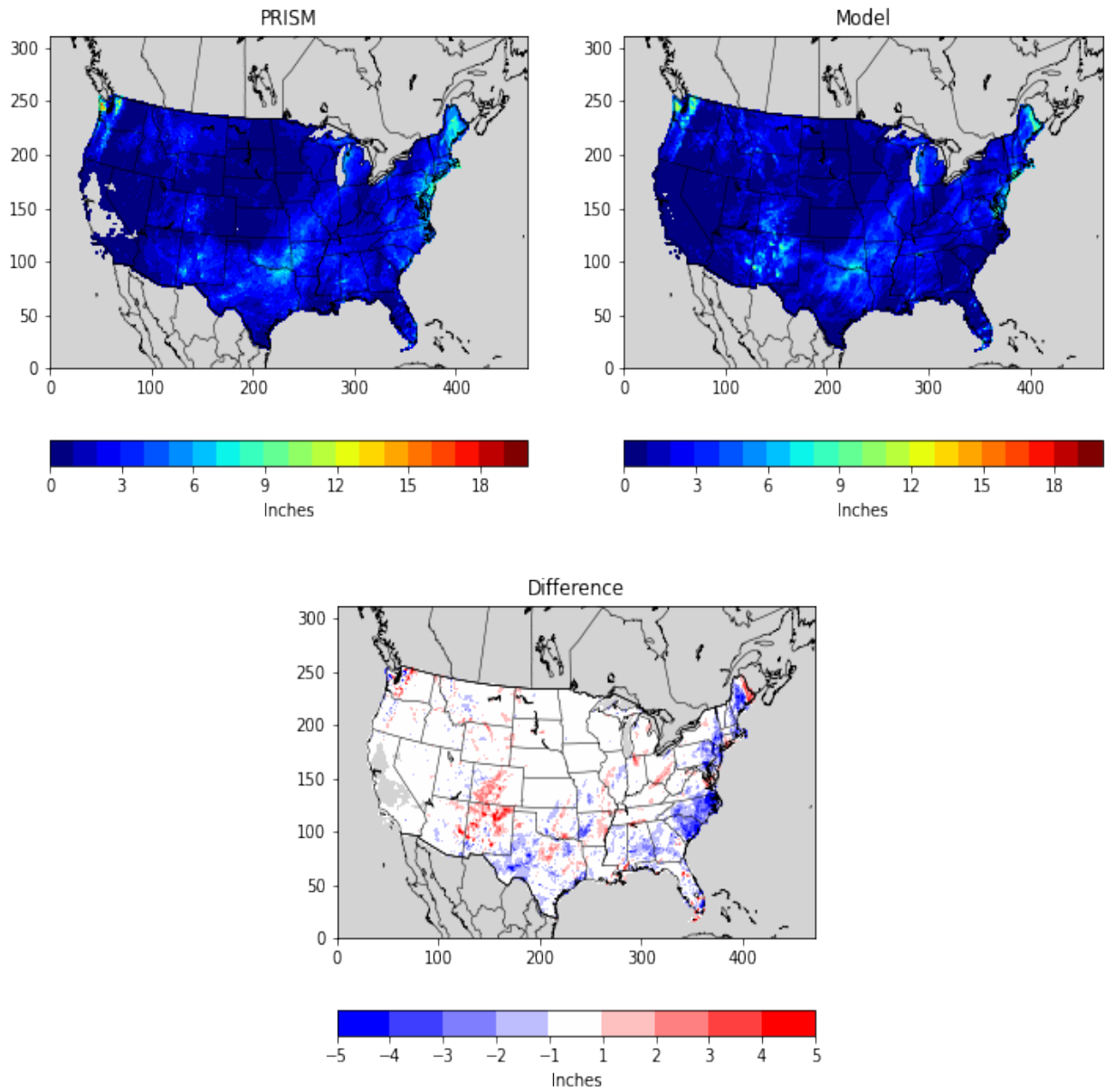


**Figure 3.4.22.** PRISM analysis (top left) and WRF (top right) estimated monthly total rainfall (in) and the difference (bottom) for October for the 12US domain.

Precipitation, November 2022

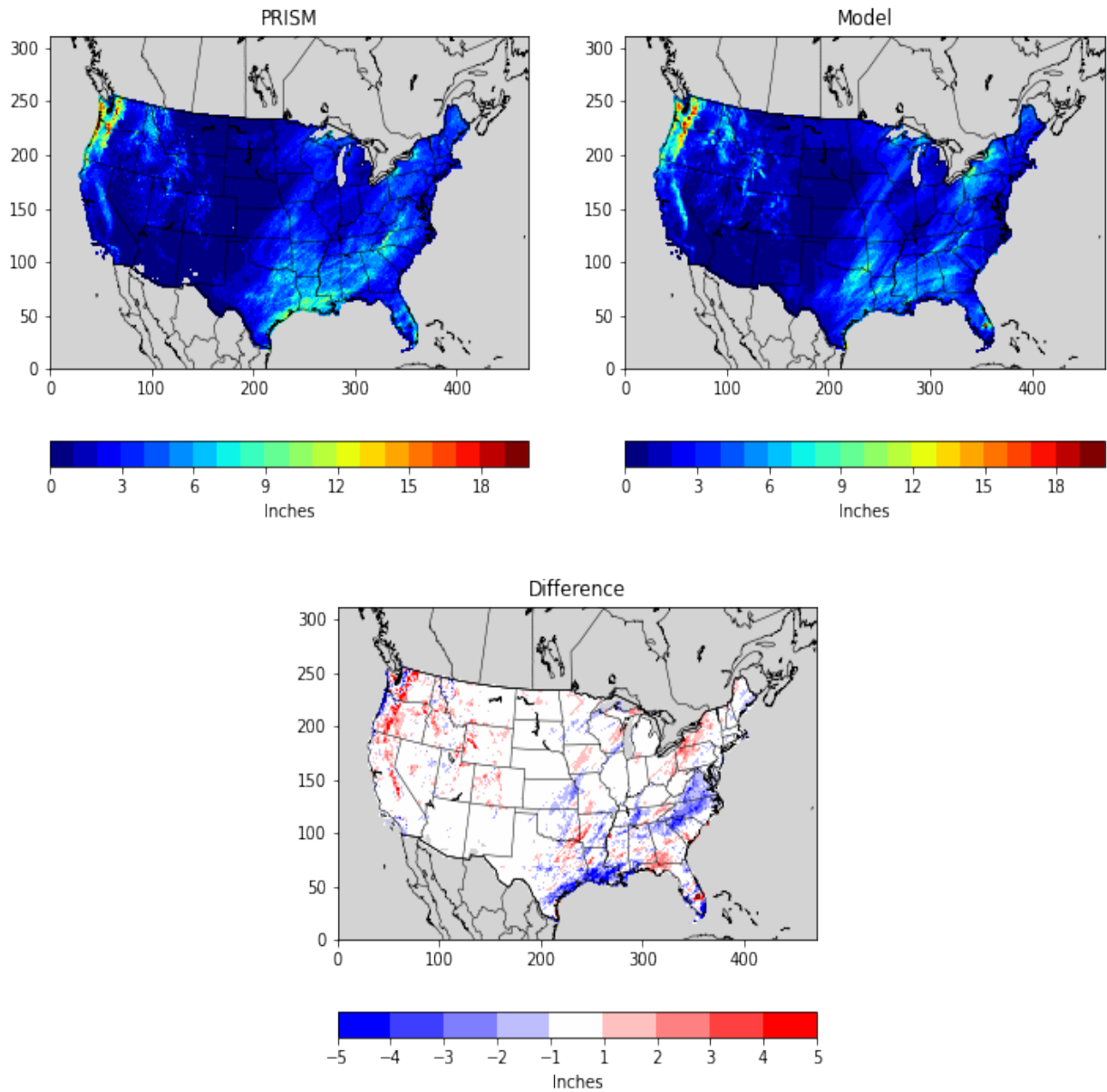


**Figure 3.4.23.** PRISM analysis (top left) and WRF (top right) estimated monthly total rainfall (in) and the difference (bottom) for November for the 12US domain.

Precipitation, December 2022

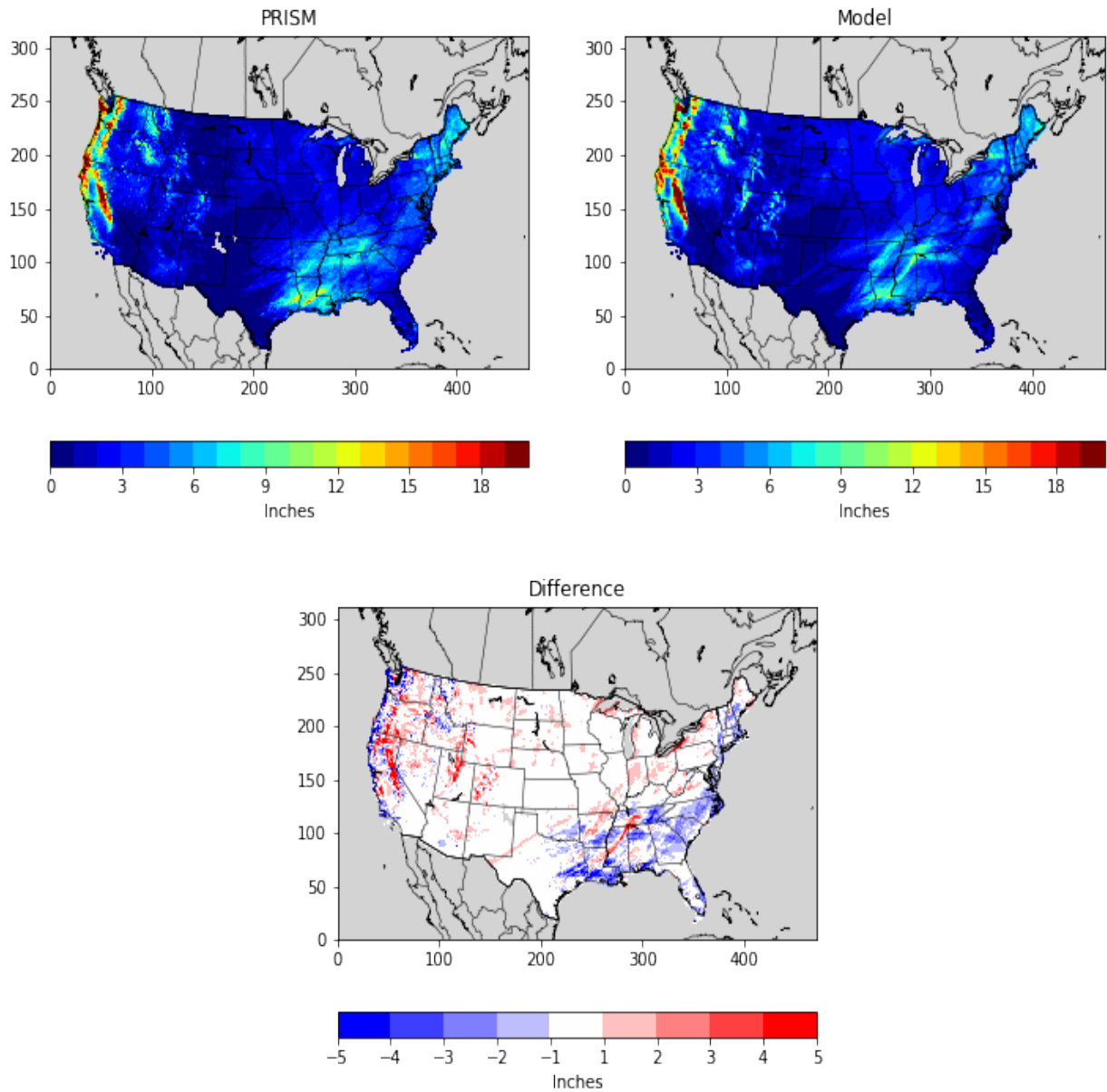


**Figure 3.4.24.** PRISM analysis (top left) and WRF (top right) estimated monthly total rainfall (in) and the difference (bottom) for December for the 12US domain.

Month	36NOAM	12US
January	0.12	0.19
February	0.09	0.13
March	0.15	0.13
April	0.31	0.16
May	0.24	0.02
June	0.25	0.01
July	0.55	0.02
August	0.56	-0.08
September	0.05	-0.07
October	-0.20	-0.15
November	-0.17	-0.03
December	-0.11	0.06

**Table 3.4.1.** Domain-wide biases (in inches) of total precipitation in the 36NOAM and 12US domains by month.

### 3.5 Model Performance for Solar Radiation

Photosynthetically activated radiation (PAR) is a fraction of shortwave downward radiation and is an important input for the biogenic emissions model for estimating isoprene (Carlton and Baker, 2011). Isoprene emissions are important for regional ozone chemistry and play a role in secondary organic aerosol formation. Radiation performance evaluation also gives an indirect assessment of how well the model captures cloud formation during daylight hours.

Shortwave downward radiation estimates are compared to surface-based measurements and shown below for the 36NOAM (Figure 3.5.1) and 12US (Figure 3.5.2) domains<sup>6</sup>.

In general, WRF slightly overpredicts shortwave radiation across all months of the year, showing a greater spread in the overprediction during the late Spring to early Fall months. Overall, the median bias in WRF for all months of the year is roughly 10-20 W/m<sup>2</sup>.

More variability is noted on an hourly basis as WRF overpredicts shortwave radiation across all daytime hours. The median bias during the hours of most downward shortwave radiation is less than 10-20 W/m<sup>2</sup>. A greater spread in the overprediction is noted during the afternoon to early evening hours when the sun is highest in the sky. The model's inability to accurately simulate sub grid clouds at both the 36km and 12km resolution is likely the cause of these errors.

---

<sup>6</sup> As noted above, the 12US WRF simulation used lightning data assimilation whereas the 36NOAM WRF simulation did not.

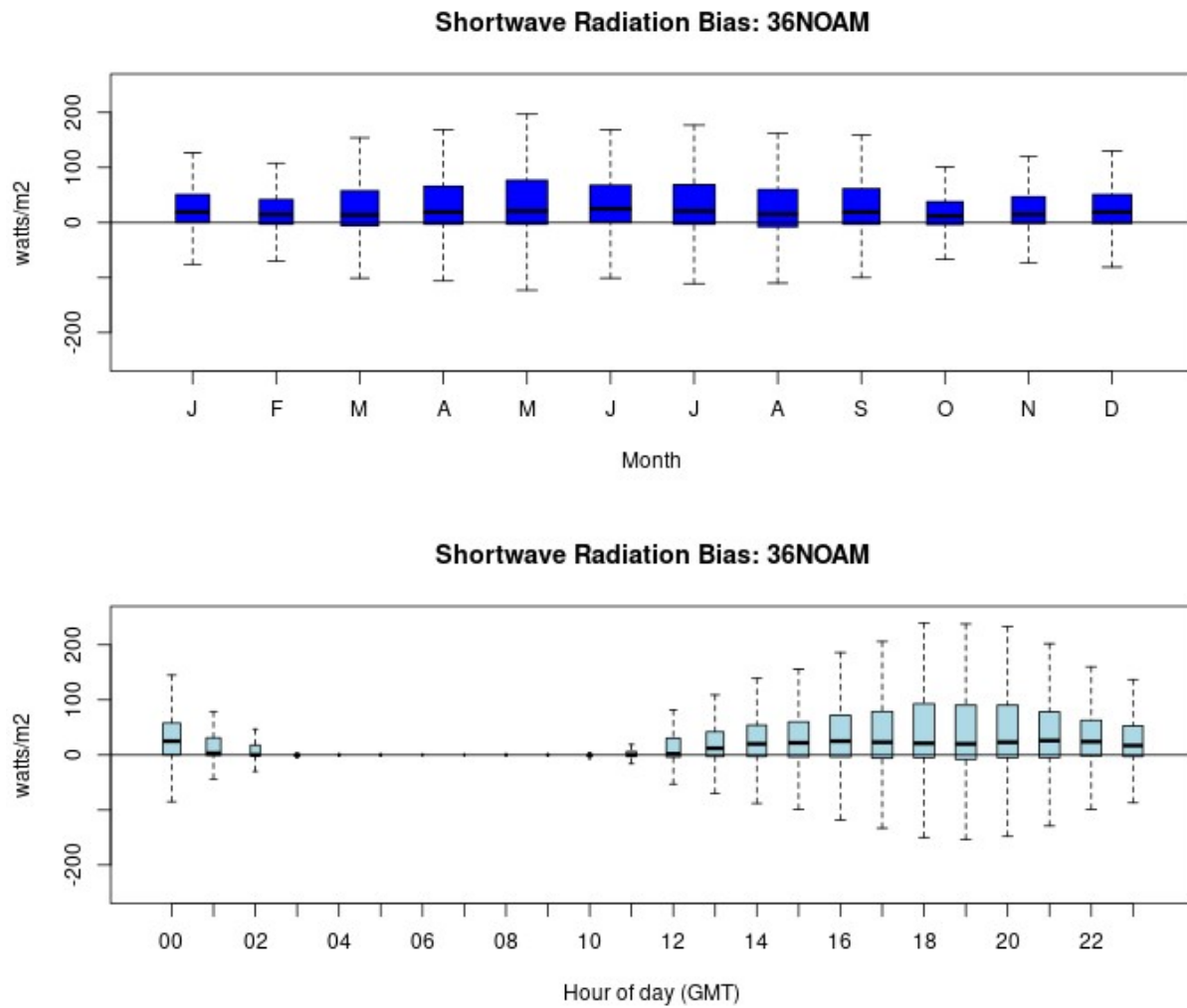


**Figure 3.5.1.** Distribution of hourly bias for shortwave radiation ( $W/m^2$ ) by month (top) and by hour of the day (bottom) for the 36NOAM domain.

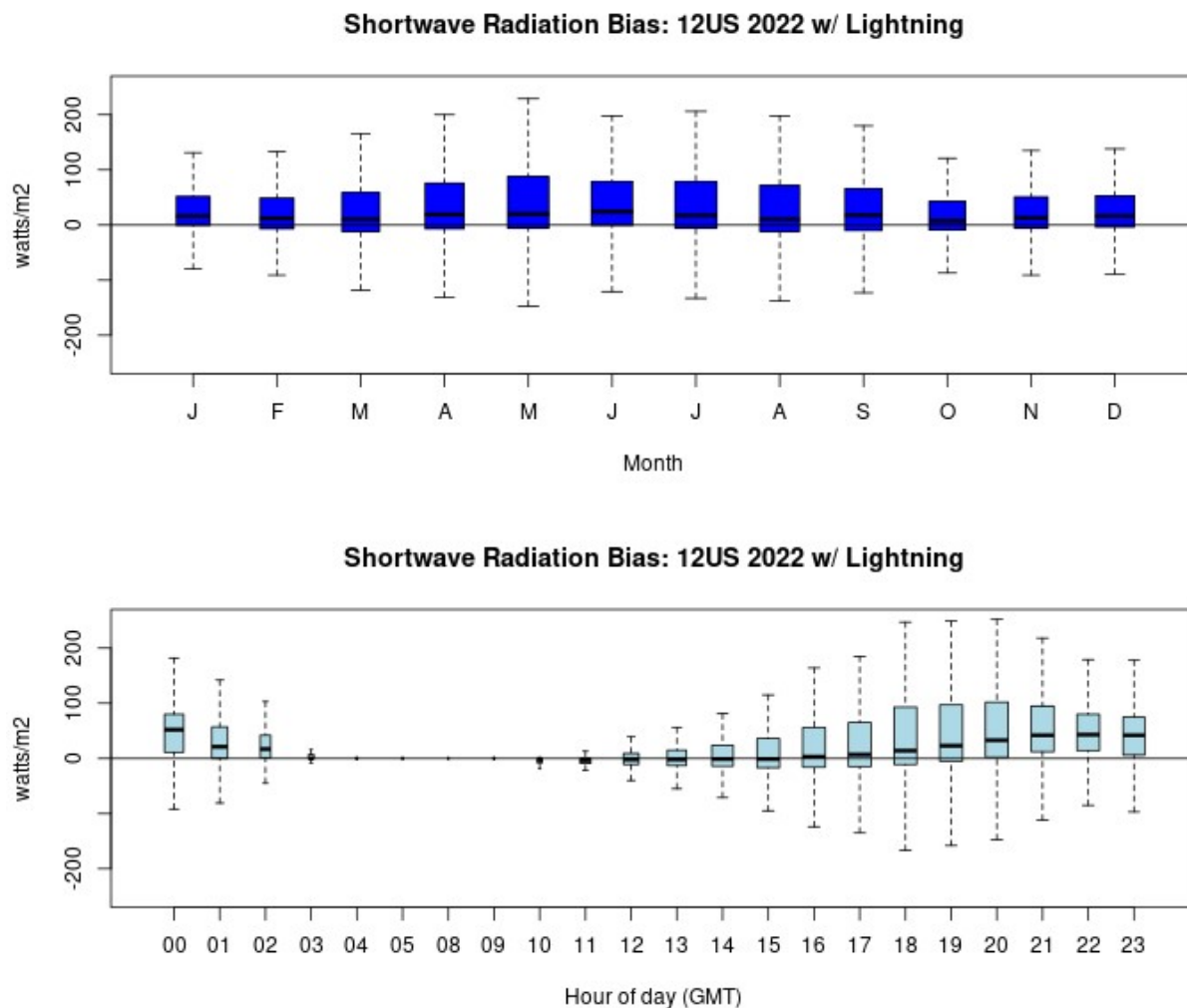


**Figure 3.5.2.** Distribution of hourly bias for shortwave radiation ( $W/m^2$ ) by month (top) and by hour of the day (bottom) for the 12US domain.

#### 4 CLIMATE REPRESENTATIVENESS OF 2022

Figures 4.1 and 4.2 show the divisional rankings for observed temperatures across the US for 2022. A climatic representation of the precipitation for 2022 is shown in Figures 4.3 and 4.4. These types of plots are used to determine whether the meteorological conditions in a specific year are near-normal or anomalous. Additionally, we can make determinations of their suitability for use in photochemical modeling in terms of a specific year's conduciveness for photochemical production of secondary pollutants.

In 2022, temperatures were average to above average for most months of the year. Much below average temperatures were noted in the Northwest and Northern Plains during April. Much above average temperatures were noted in the South in April through June. Record or

near-record warmth was observed in the Northeast in August, as well as various portions of the West, Northwest, and Southern Plains during July through October.

With regards to precipitation, 2022 was highly variable in terms of record to near-record drought or rainfall amounts. Much of the year, most of the country varied between below average to above average rainfall amounts, with no discernible pattern that persisted through any season or region. Record dry conditions were noted in California during January, May, and July. Record wet conditions were noted in the Northern Plains during December.

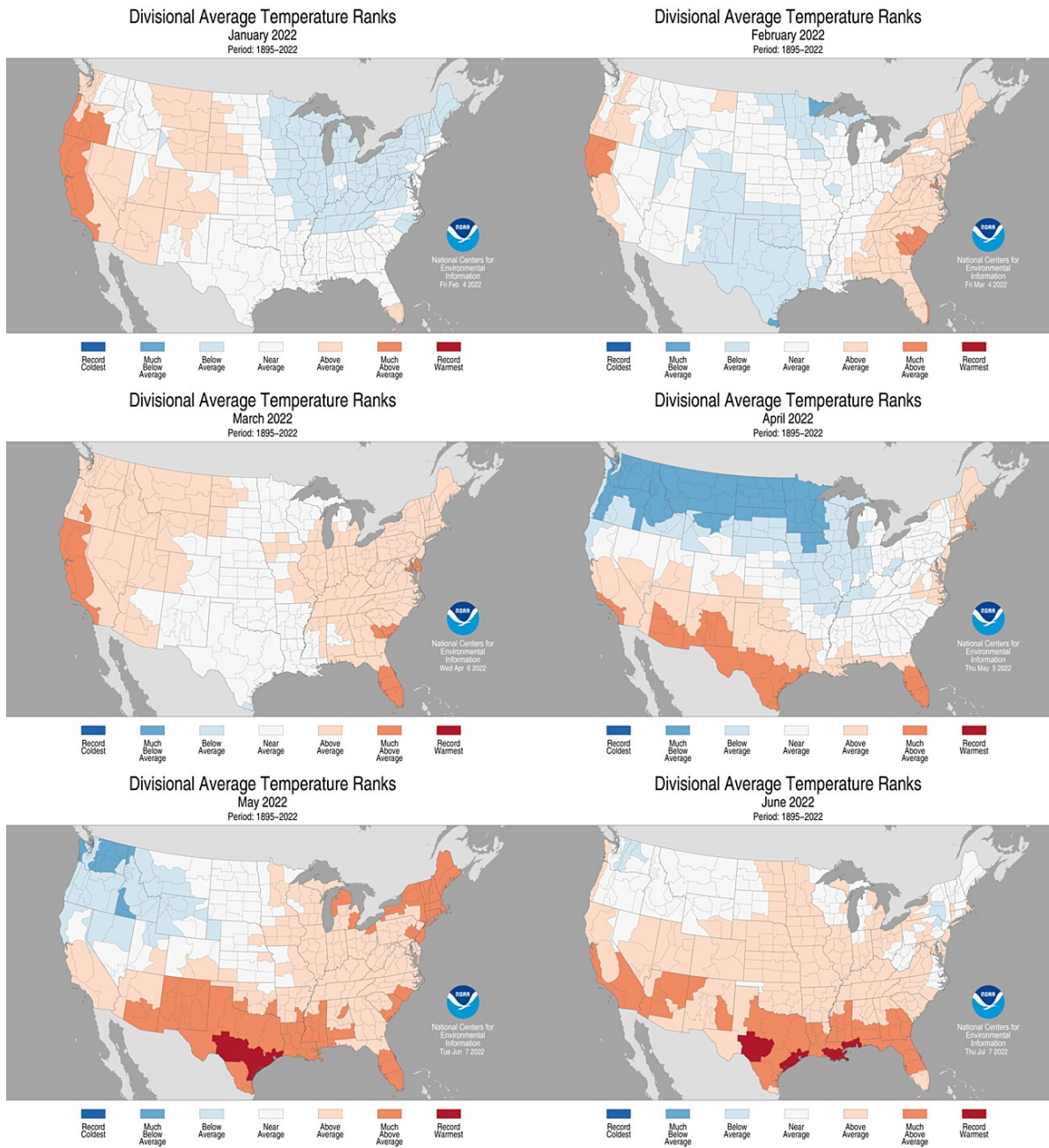


**Figure 4.1** Climatic temperature rankings by climate division: January to June 2022.  
<http://www.ncdc.noaa.gov/temp-and-precip/maps.php>

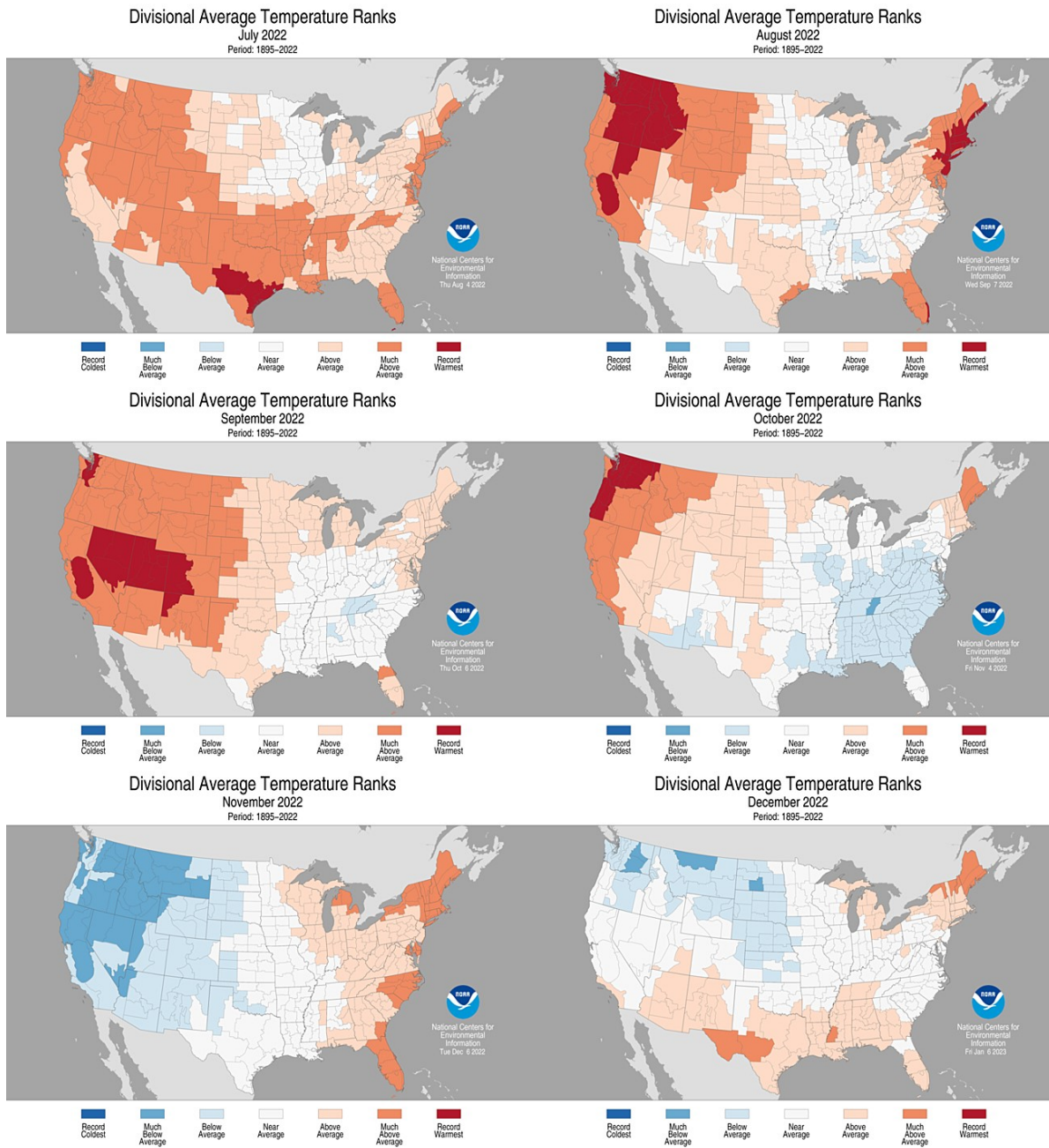


**Figure 4.2** Climatic temperature rankings by climate division: July to December 2022.  
<http://www.ncdc.noaa.gov/temp-and-precip/maps.php>

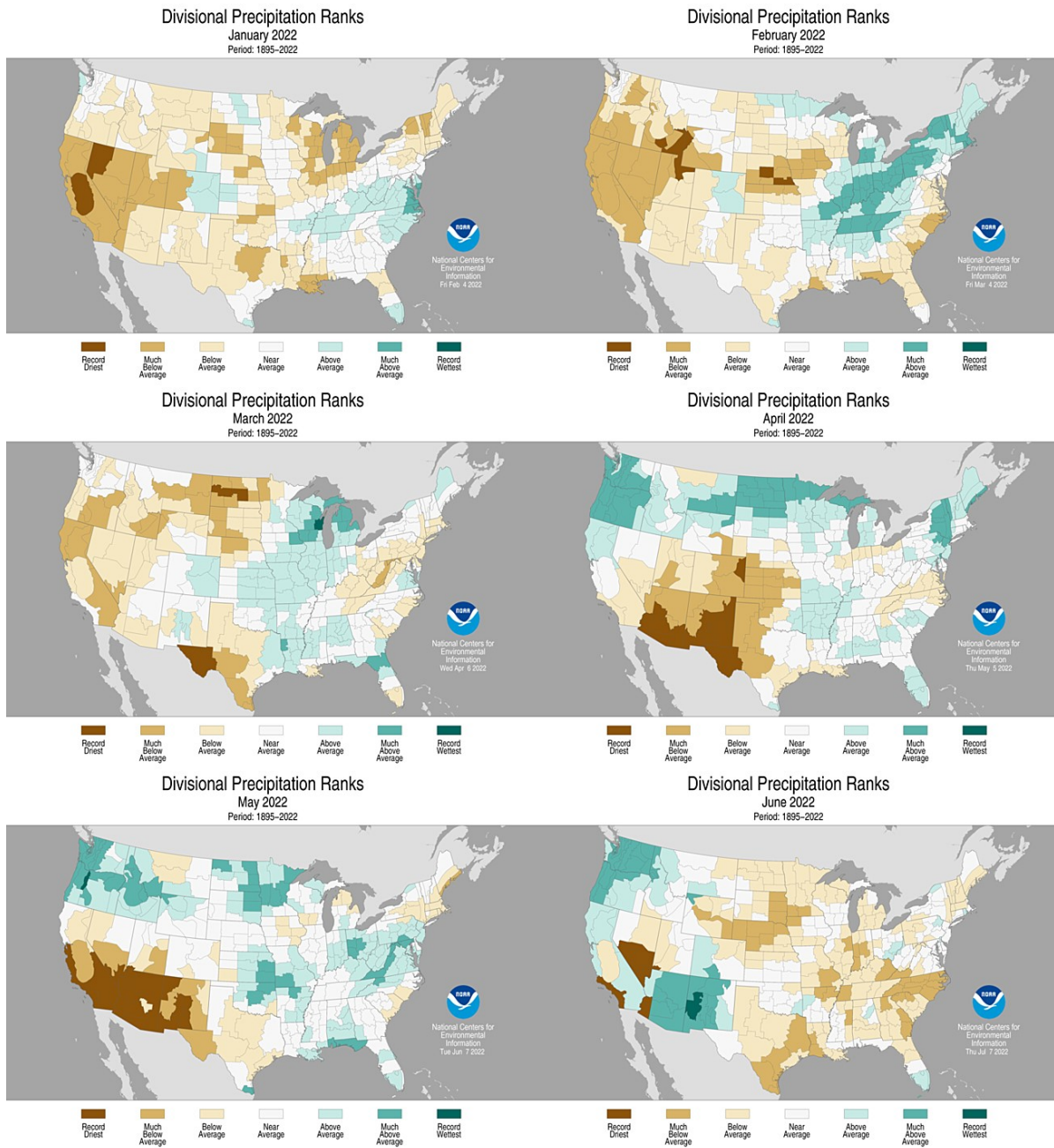


**Figure 4.3** Climatic rainfall rankings by climate division: January to June 2022.  
<http://www.ncdc.noaa.gov/temp-and-precip/maps.php>

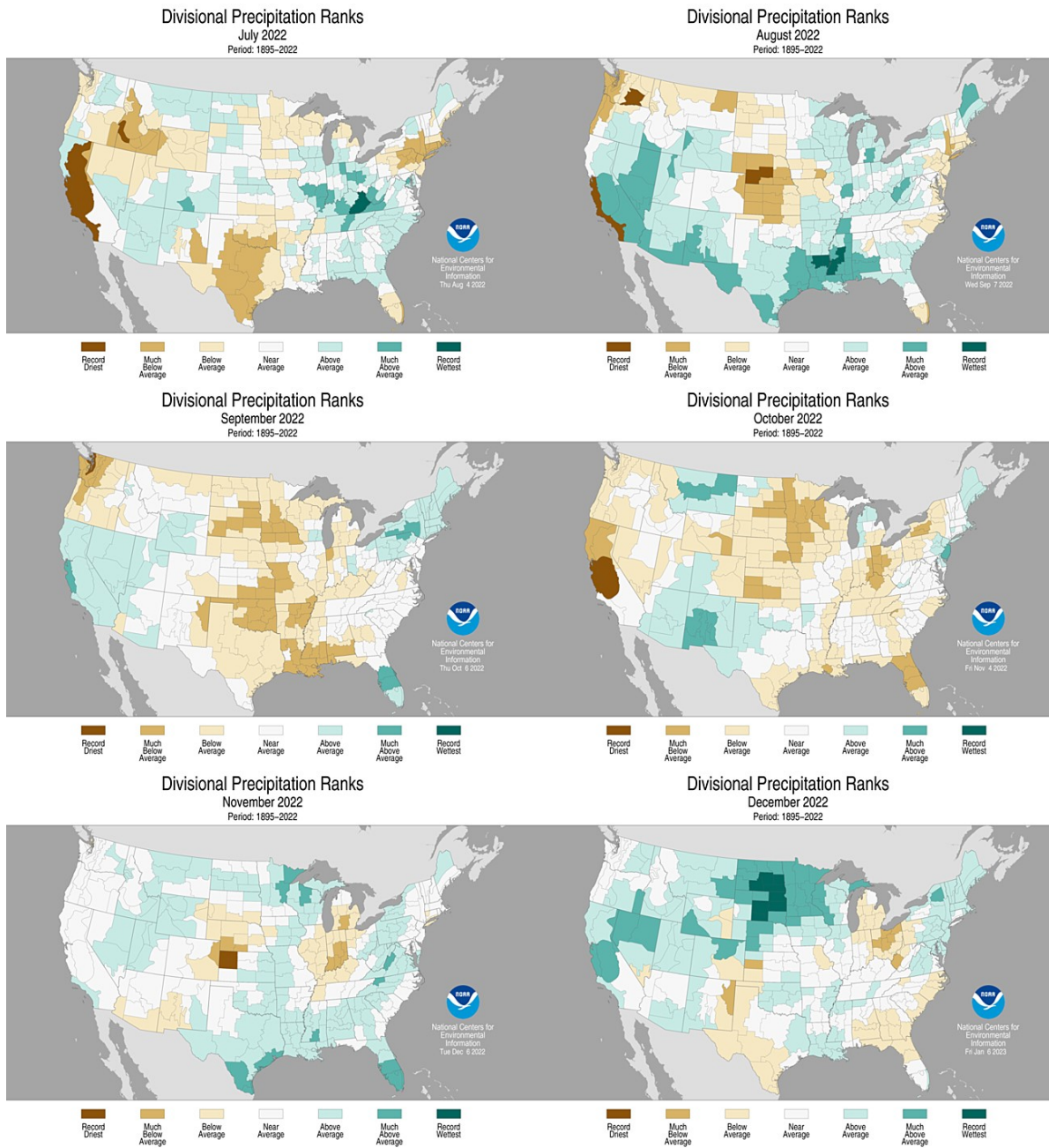


**Figure 4.4** Climatic rainfall rankings by climate division: July to December 2022.  
<https://www.ncdc.noaa.gov/sotc/>

## 5 REFERENCES

Boylan, J.W., Russell, A.G., 2006. PM and light extinction model performance metrics, goals, and criteria for three-dimensional air quality models. *Atmospheric Environment* 40, 4946-4959.

Carlton, A.G., Baker, K.R., 2011. Photochemical Modeling of the Ozark Isoprene Volcano: MEGAN, BEIS, and Their Impacts on Air Quality Predictions. *Environmental Science & Technology* 45, 4438-4445.

Cooper, O.R., Stohl, A., Hubler, G., Hsie, E.Y., Parrish, D.D., Tuck, A.F., Kiladis, G.N., Oltmans, S.J., Johnson, B.J., Shapiro, M., Moody, J.L., Lefohn, A.S., 2005. Direct Transport of Midlatitude Stratospheric Ozone into the Lower Troposphere and Marine Boundary Layer of the Pacific Ocean. *Journal of Geophysical Research – Atmospheres* 110, D23310, doi:10.1029/2005JD005783.

ENVIRON, 2008. User's Guide Comprehensive Air Quality Model with Extensions. ENVIRON International Corporation, Novato.

Gilliam, R.C., Pleim, J.E., 2010. Performance Assessment of New Land Surface and Planetary Boundary Layer Physics in the WRF-ARW. *Journal of Applied Meteorology and Climatology* 49, 760-774.

Heath, Nicholas K., Pleim, J.E., Gilliam, R., Kang, D., 2016. A simple lightning assimilation technique for improving retrospective WRF simulations. *Journal of Advances in Modeling Earth Systems*. 8. 10.1002/2016MS000735.

Langford, A.O., Reid, S.J., 1998. Dissipation and Mixing of a Small-Scale Stratospheric Intrusion in the Upper Troposphere. *Journal of Geophysical Research* 103, 31265-31276.

Otte, T.L., Pleim, J.E., 2010. The Meteorology-Chemistry Interface Processor (MCIP) for the CMAQ modeling system: updates through MCIPv3.4.1. *Geoscientific Model Development* 3, 243-256.

Skamarock, W.C., Klemp, J.B., Dudhia, J., Gill, D.O., Barker, D.M., Duda, M.G., Huang, X., Wang, W., Powers, J.G., 2008. A Description of the Advanced Research WRF Version 3.

Stammer, D., F.J. Wentz, and C.L. Gentemann, 2003, Validation of Microwave Sea Surface Temperature Measurements for Climate Purposes, *J. Climate*, 16, 73-87.

---

United States  
Environmental Protection  
Agency

Office of Air Quality Planning and Standards  
Air Quality Assessment Division  
Research Triangle Park, NC

Publication No. EPA-454/R-24-001  
March 2024

---